Tectonics

RESEARCH ARTICLE
10.1029/2024TC008368

Key Points:

- Strain compatibility demonstrates that the detachment displacement necessary to exhume footwall rocks from 21 to 30 km depths is not possible
- The 22°C/km gradient predicted by thermobarometry is incompatible with the Late Cretaceous thermal gradient of 46 ± 10°C/km that we calculate
- A non-lithostatic interpretation for pressure data from the Northern Snake Range is required, similar to other Cordilleran core complexes

Supporting Information:

Supporting Information may be found in the online version of this article.

Correspondence to:

S. P. Long,
sean.p.long@wsu.edu

Citation:

Long, S. P., Blackford, N. R., Lee, J., & Soignard, E. (2024). Crustal thermal architecture, structural reconstructions, field relationships, and geophysical data rule out deep structural burial of the footwall of the Northern Snake Range metamorphic core complex (Nevada, USA). *Tectonics*, *43*, e2024TC008368. https://doi.org/10.1029/2024TC008368

Received 9 APR 2024
Accepted 8 SEP 2024

Author Contributions:

Conceptualization: Sean P. Long
Formal analysis: Sean P. Long, Nolan R. Blackford, Emmanuel Soignard
Funding acquisition: Sean P. Long, Jeffrey Lee
Investigation: Sean P. Long, Nolan R. Blackford
Methodology: Sean P. Long, Emmanuel Soignard
Software: Emmanuel Soignard
Validation: Sean P. Long
Visualization: Sean P. Long
Writing – original draft: Sean P. Long

Crustal Thermal Architecture, Structural Reconstructions, Field Relationships, and Geophysical Data Rule Out Deep Structural Burial of the Footwall of the Northern Snake Range Metamorphic Core Complex (Nevada, USA)

Sean P. Long[1], Nolan R. Blackford[2], Jeffrey Lee[3], and Emmanuel Soignard[4]

[1]School of the Environment, Washington State University, Pullman, WA, USA, [2]Arizona Geological Survey, Tucson, AZ, USA, [3]Department of Geophysics, Colorado School of Mines, Golden, CO, USA, [4]Eyring Materials Center, Arizona State University, Tempe, AZ, USA

Abstract Thermobarometry in the Northern Snake Range metamorphic core complex (Nevada, USA) implies pre-extensional burial of footwall rocks to 21–30 km depths, while geologic field relationships support 7–13 km pre-extensional depths. This has fueled a 40-year-long debate, which has far-reaching implications for how pressure data are interpreted in orogenic settings. Here, we test published models for deep burial by integrating regional cross-section reconstructions with new (n = 95) and published (n = 132) peak temperature measurements, field relationships and published geophysical data. Burial of Neoproterozoic-Cambrian metasedimentary footwall rocks to 21–30 km depths is incompatible with a regional seismic reflection cross-section that interprets the top of Precambrian crystalline basement at 17–20 km depths. Two reconstructed cross-sections define 42 km and 50–65 km of displacement on the master detachment fault and demonstrate that the higher displacement ranges (>66–94 km and >76–102 km, respectively) necessary to exhume rocks from 21 to 30 km depths are not possible without spatially overlapping Cambrian rocks preserved in its footwall and hanging wall. The 22°C/km average Late Cretaceous thermal gradient predicted by thermobarometry is incompatible with the 46 ± 10°C/km Late Cretaceous peak thermal gradient that we calculate down to 15–20 km pre-extensional depths. Field relationships that rule out large-magnitude shortening invalidate models for deep footwall burial via thrust or reverse faulting. We conclude that there is no scenario for deep burial that is compatible with structural/geophysical constraints, crustal thermal architecture, and field relationships. This necessitates a non-lithostatic interpretation for pressures from the Northern Snake Range, similar to recent interpretations for other Cordilleran metamorphic core complexes.

1. Introduction

Cordilleran metamorphic core complexes in the western USA have been seminal field localities for investigating the processes that accommodate high-magnitude crustal extension (e.g., Coney & Harms, 1984; Crittenden et al., 1980; Dickinson, 2002, 2006; Platt et al., 2015; Whitney et al., 2013). The Northern Snake Range metamorphic core complex in east-central Nevada (Figure 1a) has been the site of decades of investigations (e.g., Coney, 1974; Cooper, Platt, Anczkiewicz, & Whitehouse, 2010; Cooper, Platt, Platzman, et al., 2010; Gans & Miller, 1983; Hoiland et al., 2022; J. Lee, 1995; J. Lee & Sutter, 1991; J. Lee et al., 1987, 2017; Lewis et al., 1999; Long, 2019; Long et al., 2022, 2023; E. L. Miller et al., 1983; Wrobel et al., 2021), and has inspired several classic models for the structural evolution of metamorphic core complexes (E. L. Miller et al., 1983; Wernicke, 1981). However, in the Northern Snake Range, as well as the Ruby East-Humboldt metamorphic core complex in northeastern Nevada (Figure 1a), disagreement over the pre-extensional burial depth of exhumed ductile footwall rocks has sparked an intriguing 40-year-long debate (e.g., Bartley & Wernicke, 1984; Camilleri & Chamberlain, 1997; Henry et al., 2011; Hoiland et al., 2022; Lewis et al., 1999; McGrew et al., 2000; E. L. Miller et al., 1983, E. L. Miller, Dumitru, et al., 1999; Wrobel et al., 2021; Zuza et al., 2020, 2022). Thermobarometry collected from footwall rocks in these metamorphic core complexes has yielded peak pressures between 6 and 11 kbar, corresponding to burial depths between 21 and 41 km assuming a lithostatic pressure gradient (Cooper, Platt, Anczkiewicz, & Whitehouse, 2010; Hallett & Spear, 2014; Hodges & Walker, 1992; Lewis et al., 1999; McGrew et al., 2000). These depths are 2–3 times greater than the restored stratigraphic depth range of these footwall rocks, which has led to the development of structural models that hypothesize large-displacement (25 km to >95 km), Jurassic-Cretaceous thrust faults as a burial mechanism (e.g., Bartley & Wernicke, 1984; Camilleri &

Writing – review & editing: Nolan R. Blackford, Jeffrey Lee, Emmanuel Soignard

Chamberlain, 1997; Lewis et al., 1999). However, field evidence for such large-scale thrust faults is lacking, and several predictions of these structural models are invalidated by regional field relationships that demonstrate minimal contractional deformation in this region of Nevada (e.g., Armstrong, 1972; Blackford et al., 2022; Gans & Miller, 1983; Henry et al., 2011; Long, 2012, 2015, 2019; Thorman et al., 1991; Zuza et al., 2020, 2022).

This debate is further compounded by thermometry that defines upper-crustal thermal gradients between ~35 and 60°C/km in the regions surrounding these metamorphic core complexes (Blackford et al., 2022; Hoiland et al., 2022; Long & Soignard, 2016; E. L. Miller & Gans, 1989; Vlaha et al., 2024; Zuza et al., 2020, 2022), which are 1.5–3 times higher than the ~20–25°C/km thermal gradients predicted by thermobarometry (Cooper, Platt, Anczkiewicz, & Whitehouse, 2010; Hallett & Spear, 2014; Lewis et al., 1999; McGrew et al., 2000). Resolution of this debate has regional implications for the magnitude of shortening and thickening accomplished during Jurassic-Paleogene Cordilleran orogenesis, as well as the magnitude of extension, exhumation, and crustal thinning accomplished by Cenozoic extensional tectonism. However, at the heart of this issue is a much more fundamental, far-reaching implication for how quantitative pressure data are interpreted in orogenic settings. For example, one possibility for reconciling this debate (though controversial) is that the footwall rocks in these metamorphic core complexes were not deeply buried, but instead experienced tectonic overpressure (e.g., Gerya, 2015; Petrini & Podladchikov, 2000; Schmalholz & Podladchikov, 2013), which has recently been proposed for the Ruby-East Humboldt metamorphic core complex (Zuza et al., 2022).

The richly detailed structural and stratigraphic framework of the Northern Snake Range and its surrounding region, which has been obtained through decades of mapping-based research (e.g., Dechert, 1967; Drewes, 1967; Gans, Miller, Huggins, & Lee, 1999; Gans, Miller, & Lee, 1999; Hintze, 1974a, 1974b; Hose, 1965, 1974; J. Lee et al., 1999a, 1999b, 2023; J. Lee, Miller, et al., 1993; E. L. Miller & Gans, 1999; E. L. Miller, Gans, et al., 1999; Rodgers, 1987; Whitebread, 1969; Young, 1960), make it a critically important field locality for investigating this problem. One important aspect of the Northern Snake Range, which is quite rare in metamorphic core complexes, is that its exhumed ductile footwall is comprised of metasedimentary rocks that can be placed in the detailed stratigraphic context of adjacent ranges (e.g., E. L. Miller et al., 1983; E. L. Miller, Dumitru, et al., 1999). This makes the Northern Snake Range the ideal testing ground for addressing the deep-versus-shallow footwall debate.

The purpose of this paper is to test the interpretations of thermobarometry data and associated structural models (Bartley & Wernicke, 1984; Cooper, Platt, Anczkiewicz, & Whitehouse, 2010; Lewis et al., 1999) that call for the deep (21–30 km) pre-extensional burial of footwall rocks in the Northern Snake Range metamorphic core complex. To achieve this goal, we undertook a regional-scale investigation that integrates cross section reconstructions, crustal thermal architecture, geologic field relationships, and published seismic reflection data. We present three regional-scale (120–130 km modern east-west length) cross sections across the Northern Snake Range and surrounding ranges, which we reconstruct to pre-extensional geometries. We also present Raman spectroscopy of carbonaceous material (RSCM) thermometry from 95 samples of Neoproterozoic-Paleozoic metasedimentary and sedimentary rocks, which we combine with 132 published peak temperature measurements from thermobarometry, RSCM thermometry, and conodont alteration indices. Integrating these temperature data with our restored cross sections provides an unprecedented view of the regional crustal thermal architecture. We then explore the implications of our structural and temperature data sets, invoking important regional geologic field relationships and interpretations of seismic reflection data, to make arguments that invalidate the predictions of published models for deep burial of footwall rocks, as well as ruling out other possible geometric scenarios for deep burial. Finally, we discuss regional implications for Cordilleran shortening and Cenozoic extensional tectonism, and more importantly, far-reaching implications for how pressure data are interpreted in orogenic settings.

2. Geologic Background of the Northern Snake Range and Surrounding Region

2.1. Tectonic Framework

The Northern Snake Range and surrounding ranges in east-central Nevada and west-central Utah (Figure 1b) record tectonic environments that progressed from Neoproterozoic-Paleozoic passive margin deposition to Mesozoic contractional orogenesis to Cenozoic extension (e.g., Dickinson, 2006). Following the Neoproterozoic rifting of the western margin of Laurentia (e.g., Yonkee et al., 2014), eastern Nevada and western Utah were the site of deposition of a thick package of shallow-marine sedimentary rocks between the late Neoproterozoic and the Triassic (Poole et al., 1992; Stewart, 1980; Stewart & Poole, 1974).

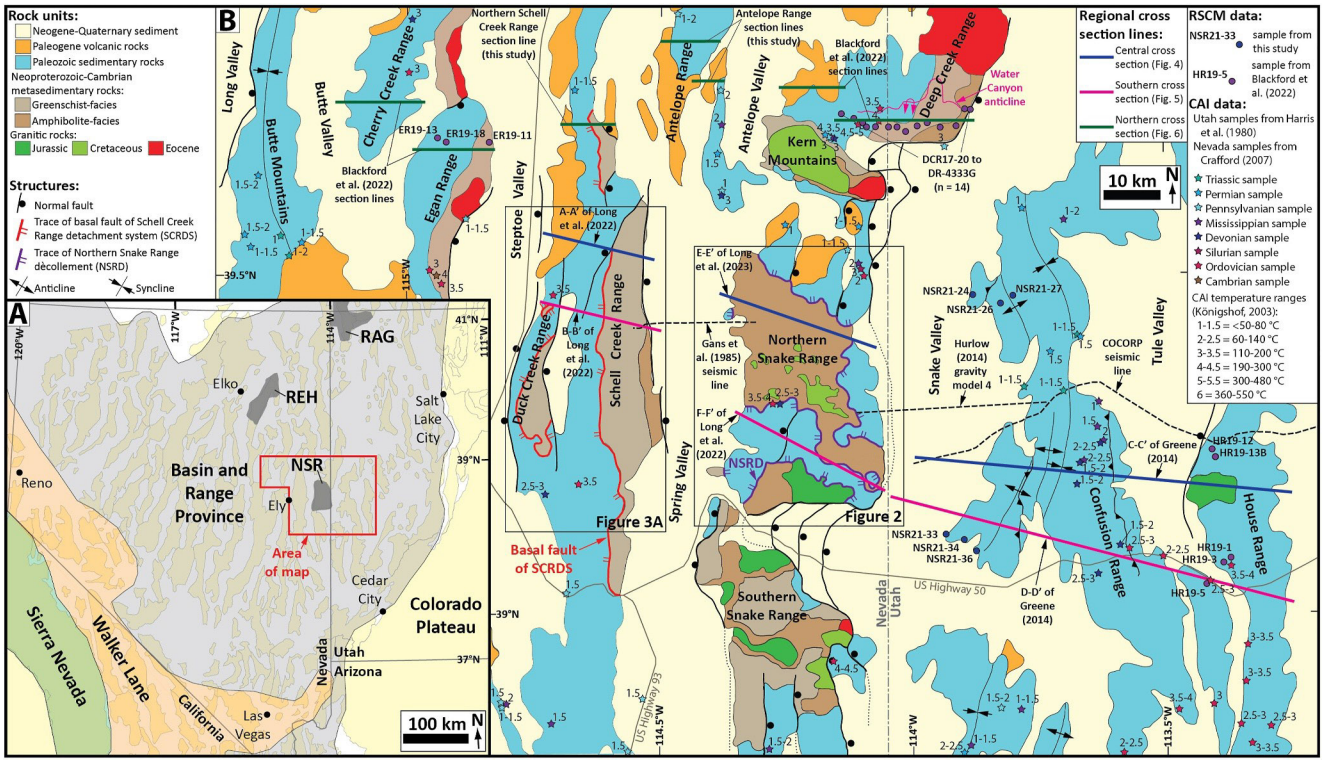

Figure 1. (a) Map of modern tectonic provinces in southeastern California, Nevada, and western Utah (modified from Long (2019)), showing locations of metamorphic core complexes (NSR, Northern Snake Range; REH, Ruby-East Humboldt; RAG, Raft River-Albion-Grouse Creek). (b) Simplified geologic map of the region of eastern Nevada and western Utah surrounding the Northern Snake Range metamorphic core complex (modified from J. Lee et al. (2017)), showing the areas of Figures 2 and 3a, lines of section for the central (Figure 4), southern (Figure 5), and northern (Figure 6) regional cross sections (shown in blue, pink, and green, respectively), the Consortium for Continental Reflection Profiling (COCORP) seismic line, locations and values of published conodont alteration index (CAI) samples, and locations of Raman spectroscopy of carbonaceous material (RSCM) samples that lie outside of the areas of Figures 2 and 3a.

During the Jurassic, Andean-style subduction along the western North American margin initiated construction of the Cordilleran orogenic belt (e.g., Burchfiel et al., 1992; DeCelles, 2004; Yonkee & Weil, 2015). Nevada and western Utah resided in a broad retroarc region in which a composite, east-vergent fold-thrust system was constructed (e.g., Di Fiori et al., 2021). The majority of crustal shortening (~220 km) was accommodated in the Sevier fold-thrust belt in western Utah between ~125 and 55 Ma (e.g., DeCelles & Coogan, 2006; Yonkee et al., 2019), with low-magnitude (~35–40 km total; Blackford et al., 2022) Jurassic(?)-Cretaceous shortening diffusely distributed within fold-thrust systems in western Utah (Greene, 2014), eastern Nevada (Long, 2015), and central Nevada (Di Fiori et al., 2020, 2021; Long et al., 2014; Taylor et al., 2000). As much as ~10–20 km of structural burial via Jurassic-Cretaceous thrust faulting has been interpreted on the basis of thermobarometry from metasedimentary rocks in the Northern Snake Range (e.g., Cooper, Platt, Anczkiewicz, & Whitehouse, 2010; Lewis et al., 1999). However, this has become a topic of vigorous debate, as no structures have been documented that could have accommodated such deep burial (e.g., Blackford et al., 2022; Hoiland et al., 2022; Wrobel et al., 2021). Eastern Nevada is interpreted as the site of a ~2.75–3.5 km-elevation, Late Cretaceous-Paleocene orogenic plateau, which was underlain by ~50–60 km-thick crust (Cassel et al., 2014, 2018; Chapman et al., 2015; Coney & Harms, 1984; DeCelles & Coogan, 2006; Long, 2019; Snell et al., 2014). Westward underthrusting of the thick North American craton beneath eastern Nevada was likely the dominant crustal thickening mechanism that constructed the plateau (Gottlieb et al., 2022; Long, 2019, 2023).

Between ~40 and 20 Ma, felsic volcanism swept southwestward across Nevada during the Great Basin ignimbrite flareup (e.g., Henry & John, 2013), which has been attributed to rollback of the subducting Farallon slab (e.g., Dickinson & Snyder, 1978; Humphreys, 1995). Over this time interval, a large region of eastern Nevada experienced high-magnitude extension, which included normal faulting and extensional ductile shearing in the Northern Snake Range (J. Lee, 1995; J. Lee & Sutter, 1991; J. Lee et al., 1987, 2017; E. L. Miller et al., 1983), and normal faulting in the Kern Mountains and Deep Creek Range to the north (Gans et al., 1989; Rodgers, 1987), the

Southern Snake Range to the south (Evans et al., 2015; McGrew, 1993; E. L. Miller, Dumitru, et al., 1999), and the Schell Creek, Duck Creek and Egan Ranges to the west (Druschke et al., 2009; Gans, 1982; Gans & Miller, 1983; Gans et al., 2001; Long et al., 2022; Wernicke, 1981) (Figure 1b). This early phase of extension has been attributed to the decrease in interplate coupling that accompanied slab rollback (e.g., Dickinson, 2002; Smith et al., 2014), or alternatively to crustal weakening during the ignimbrite flareup (e.g., Axen et al., 1993; Lund-Snee & Miller, 2022). This was followed by widespread high-angle normal faulting, which has progressively constructed the Basin and Range Province over the last ∼15–20 Myr (e.g., Dickinson, 2002). In east-central Nevada, Basin and Range normal faulting initiated no earlier than ∼22–17 Ma in most places (e.g., Evans et al., 2015; E. L. Miller, Dumitru, et al., 1999; Stockli, 1999).

2.2. Geologic Framework of the Northern Snake Range Metamorphic Core Complex

The bedrock stratigraphy in the Northern Snake Range and surrounding ranges consists of a >15-km-thick, conformable package of Neoproterozoic-Triassic marine sedimentary rocks (e.g., Fritz, 1968; Gans & Miller, 1983; Rodgers, 1987; Stewart, 1980; Young, 1960). The Neoproterozoic (our unit "Z") and Lower Cambrian (our unit "Cl") sections are dominated by clastic rocks, which in most ranges have been metamorphosed to quartzite interlayered with phyllite or schist (e.g., E. L. Miller & Gans, 1989; E. L. Miller et al., 1988). The overlying Middle Cambrian to Triassic section is dominated by un-metamorphosed limestone, with lesser dolomite and shale (e.g., Stewart, 1980). We group these rocks into Middle-Upper Cambrian (unit "Cu"), Ordovician-Silurian (unit "OS"), Devonian (unit "D"), Mississippian-Pennsylvanian (unit "MIP"), Permian (unit "P"), and Triassic (unit "Tr") units. This sedimentary package is unconformably overlain (typically at Mississippian-Permian erosion levels) by as much as ∼1 km of Paleogene volcanic and sedimentary rocks (our unit "Pg"), most of which were deposited during the late Eocene (∼36–35 Ma) (e.g., Druschke et al., 2009; Gans et al., 1989; Hintze & Davis, 2002).

Rocks in this region experienced magmatism, metamorphism, and shortening during Jurassic-Cretaceous Cordilleran orogenesis. Middle-Late Jurassic (∼160–169 Ma; U-Pb zircon; D. E. Lee et al., 1984; E. L. Miller et al., 1988) granites intruded Neoproterozoic-Cambrian rocks in the Northern Snake, Southern Snake, and House Ranges (Figure 1b). Neoproterozoic-Cambrian rocks in the Northern Snake Range experienced greenschist- to amphibolite-facies metamorphism at peak temperatures of ∼475–660°C and peak pressures of ∼6–8 kbar (Cooper, Platt, Anczkiewicz, & Whitehouse, 2010; Hoiland et al., 2022; Lewis et al., 1999) between ∼78 and 91 Ma, which is the timing range of metamorphic monazite (U-Pb), zircon (U-Pb) and garnet (Sm-Nd and Lu-Hf) growth (Cooper, Platt, Anczkiewicz, & Whitehouse, 2010; Huggins & Wright, 1989). Peak metamorphism temporally overlapped with intrusion of Late Cretaceous granites into Neoproterozoic-Cambrian rocks in the Northern Snake Range (Figure 2), which spanned from ∼101 to 75 Ma (U-Pb zircon; Gottlieb et al., 2022; Kenney, 2013; E. L. Miller et al., 1988; Womer, 2017). To the north in the Deep Creek Range and Kern Mountains (Figure 1b), Neoproterozoic rocks experienced greenschist- to amphibolite-facies metamorphism at peak temperatures of ∼515–625°C (Blackford et al., 2022; Rodgers, 1987). The minimum age for this metamorphism is dated by ∼73 Ma post-metamorphic cooling ($^{40}Ar/^{39}Ar$ amphibole; Rodgers, 1987), and metamorphism is interpreted to have been contemporaneous with 75 ± 9 Ma (U-Pb zircon; D. E. Lee et al., 1986) granite intrusion (E. L. Miller & Gans, 1989). To the west in the Schell Creek Range (Figure 1b), Neoproterozoic rocks experienced greenschist- and (locally) amphibolite-facies metamorphism at peak temperatures of ∼470–525°C (Blackford et al., 2022; E. L. Miller & Gans, 1989). The minimum age for this metamorphism is dated by ∼82 Ma post-metamorphic cooling ($^{40}Ar/^{39}Ar$ phlogopite; E. L. Miller et al., 1988). The spatial and temporal overlap of Late Cretaceous peak metamorphism and granitic magmatism across multiple ranges has led several researchers to conclude that magmatism was the primary heat source for peak metamorphism (Barton, 1990; Barton et al., 1988; Blackford et al., 2022; Gottlieb et al., 2022; C. F. Miller & Bradfish, 1980; E. L. Miller & Gans, 1989; E. L. Miller et al., 1988). Additionally, deeply exhumed rocks in the western parts of the Northern Snake Range and Kern Mountains and on the eastern flank of the Schell Creek Range yield cooling ages between ∼70 and 40 Ma (K-Ar and $^{40}Ar/^{39}Ar$ muscovite, biotite, and K-feldspar: Armstrong, 1970; Best et al., 1974; Gébelin et al., 2011; Hoiland, 2019; D. E. Lee et al., 1980; J. Lee, 1995; J. Lee & Sutter, 1991; E. L. Miller et al., 1988; zircon fission track: E. L. Miller, Dumitru, et al., 1999). These data define as much as ∼200–250°C of post-peak-metamorphic (i.e., <∼73–91 Ma) and post-magmatic (i.e., <∼75–101 Ma), but pre-extensional (i.e., >∼38 Ma; e.g., J. Lee et al., 2017) cooling, and demonstrate a lack of significant reheating during <∼38 Ma extension. This supports previous interpretations that peak crustal thermal conditions in this region

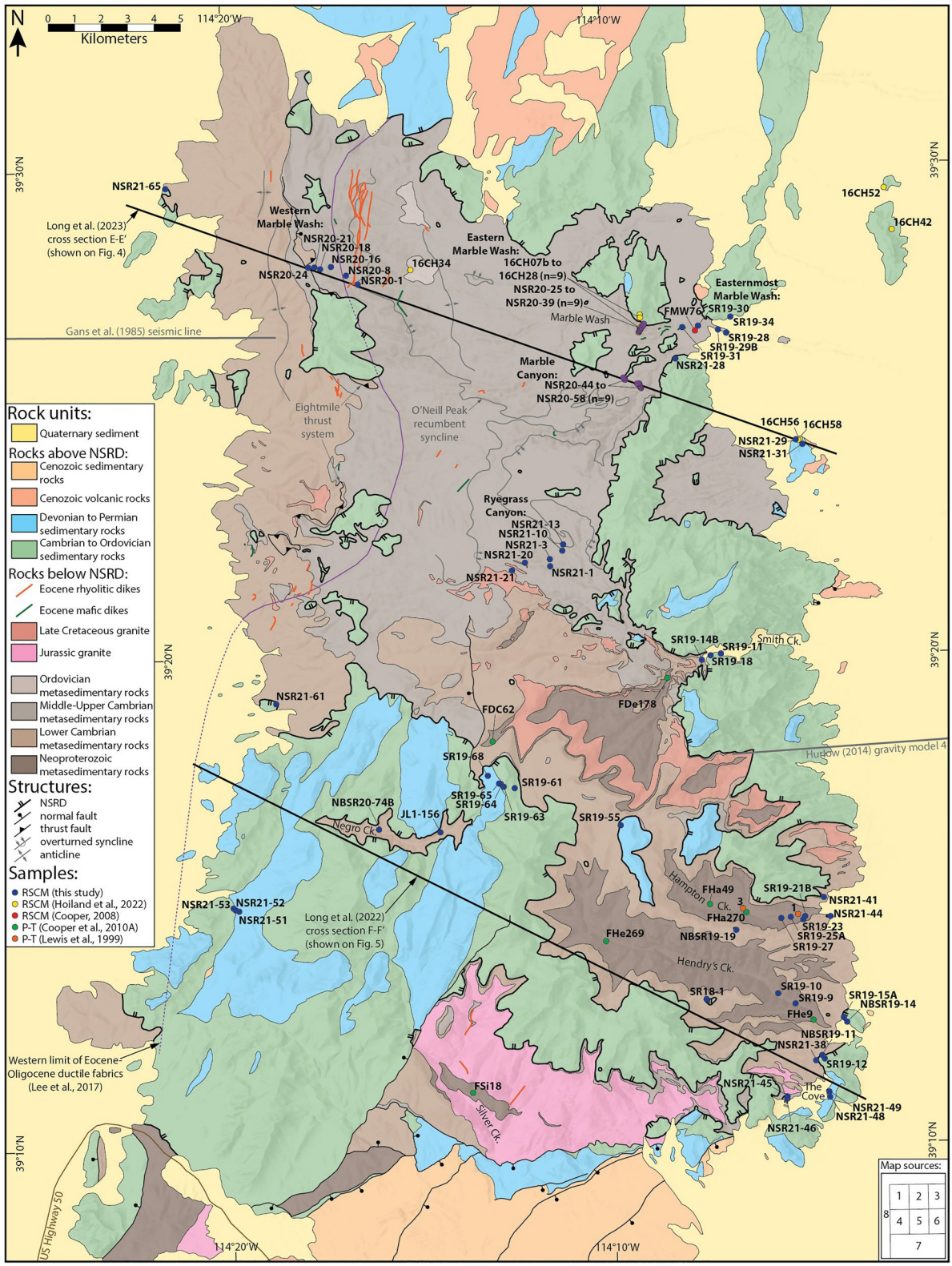

Figure 2.

were attained during the Late Cretaceous (e.g., Blackford et al., 2022; Hoiland et al., 2022; E. L. Miller & Gans, 1989; E. L. Miller et al., 1988), which is consistent with interpretations from several recent studies in other parts of eastern Nevada (Long & Soignard, 2016; Vlaha et al., 2024; Zuza et al., 2020, 2022).

Low-magnitude, diffusely distributed shortening of Jurassic(?)-Cretaceous age was accomplished at upper-crustal levels, including ~15 km of shortening accommodated by gentle to open folding across much of eastern Nevada (Blackford et al., 2022; Gans & Miller, 1983; Long, 2015) and ~10 km of shortening in the east-vergent Western Utah thrust belt in the Confusion Range (Figure 1b) (Greene, 2014). In the Northern Snake Range, contractional structures include the east-vergent O'Neill Peak recumbent syncline, which accomplished ~3 km of structural thickening, and the east-directed Eightmile thrust system, which has >1 km of displacement (J. Lee et al., 1999b; Wrobel et al., 2021) (Figure 2). Wrobel et al. (2021) interpreted that these structures were active during ~78–91 Ma peak metamorphism and that they are part of the western root zone of the Western Utah thrust belt. Large-displacement (25 km to >90 km), east- and west-vergent Jurassic-Cretaceous thrust and reverse faults have been hypothesized in this region, to account for thermobarometry from the Northern Snake Range that implies as much as ~20 km of structural burial (Bartley & Wernicke, 1984; Cooper, Platt, Anczkiewicz, & Whitehouse, 2010; Lewis et al., 1999). Testing the validity of these interpretations is one of the primary goals of this paper.

Following Cordilleran contractional deformation, high-magnitude Cenozoic extension constructed the Northern Snake Range metamorphic core complex (e.g., Gans et al., 1985; E. L. Miller et al., 1983). The Northern Snake Range dècollement (NSRD), which is the master extensional structure in the metamorphic core complex, is a low dip-angle (typically ≤10°), top-down-to-ESE, brittle-ductile detachment fault that is exposed across the full extent of the range (Figure 2) (e.g., E. L. Miller et al., 1983). The NSRD lies at the top of the Lower Cambrian Prospect Mountain Quartzite in the southern and western parts of the range and overlies Middle-Upper Cambrian carbonates in the northeastern part (Gans, Miller, Huggins, & Lee, 1999; Gans, Miller, & Lee, 1999; J. Lee et al., 1999a, 1999b, 2023; J. Lee, Miller, et al., 1993; E. L. Miller & Gans, 1999; E. L. Miller, Gans, et al., 1999). In the footwall of the NSRD, greenschist- to amphibolite-facies, Neoproterozoic-Cambrian metasedimentary rocks exhibit mylonitic, linear-planar ductile fabrics that accommodated subhorizontal stretching and subvertical thinning (J. Lee et al., 1987; E. L. Miller et al., 1983). Foliation planes exhibit prominent ESE-trending (~110–125°) mineral stretching lineations, which record the maximum extension direction (e.g., E. L. Miller et al., 1983). These ductile fabrics die out to the northwest and are not observed on the northwestern flank of the range (Figure 2) (J. Lee et al., 1999b, 2023). Finite strain studies from NSRD footwall rocks define a dramatic eastward increase in ductile extension and thinning, to values as high as ~1,200–1,400% and ~80–95%, respectively, at the eastern flank of the range (e.g., J. Lee et al., 1987; Long et al., 2022, 2023; E. L. Miller et al., 1983). The total ductile extension accommodated in the NSRD footwall is estimated at ~12–20 km (~220–250%) (J. Lee et al., 1987; Long et al., 2022, 2023). The timing of ductile extensional shearing is bracketed between ~38 and 22 Ma by U-Pb zircon dating of pre- and post-shearing rhyolitic dikes (J. Lee et al., 2017). The eastern portion of the NSRD footwall exhibits an overall eastward-younging trend of cooling ages (K-Ar muscovite, $^{40}Ar/^{39}Ar$ muscovite and K-feldspar, zircon fission track) from ~40 to ~24 Ma, which reflects the progressive migration of extensional unroofing during displacement on the NSRD (Gébelin et al., 2011, 2015; D. E. Lee et al., 1980; J. Lee, 1995; J. Lee & Sutter, 1991; E. L. Miller, Dumitru, et al., 1999).

In the hanging wall of the NSRD, unmetamorphosed Middle Cambrian-Permian carbonates have been extended by polyphase, top-down-to-ESE normal faulting, with faults soling or terminating downward into the NSRD (E. L. Miller et al., 1983). Cross section restorations yield estimates of 13–25 km of extension accommodated in the NSRD hanging wall (Long, 2019; Long et al., 2022; E. L. Miller et al., 1983). The timing of normal faulting is not well-constrained but tilting of syn-extensional volcanic and sedimentary rocks locally initiated as early as ~35 Ma (Gans et al., 1989) and continued until at least ~24–21 Ma (Martinez et al., 1998).

Figure 2. Simplified geologic map of the Northern Snake Range, compiled from (see lower-right inset): 1—J. Lee et al. (1999b); 2—J. Lee et al. (1999a); 3—Gans, Miller, and Lee (1999); 4—J. Lee et al. (2023); 5—J. Lee, Miller, et al. (1993); 6—Gans, Miller, Huggins, and Lee (1999); 7—Johnston (2000); 8—Hose and Blake (1976). For simplicity, normal faults within NSRD hanging wall exposures are not shown. The map pattern of the O'Neill Peak recumbent syncline is from Wrobel et al. (2021). Cross section line E-E′ from Long et al. (2023) (which is shown on Figure 4), cross section line F-F′ from Long et al. (2022) (which is shown on Figure 5), and the locations of the Gans et al. (1985) seismic line and the Hurlow (2014) gravity model are shown, as well as locations of Raman spectroscopy of carbonaceous material (RSCM) samples from this study, Hoiland et al. (2022), and Cooper (2008), and thermobarometry (*P-T*) samples from Cooper, Platt, Anczkiewicz, and Whitehouse (2010) and Lewis et al. (1999).

10.1029/2024TC008368

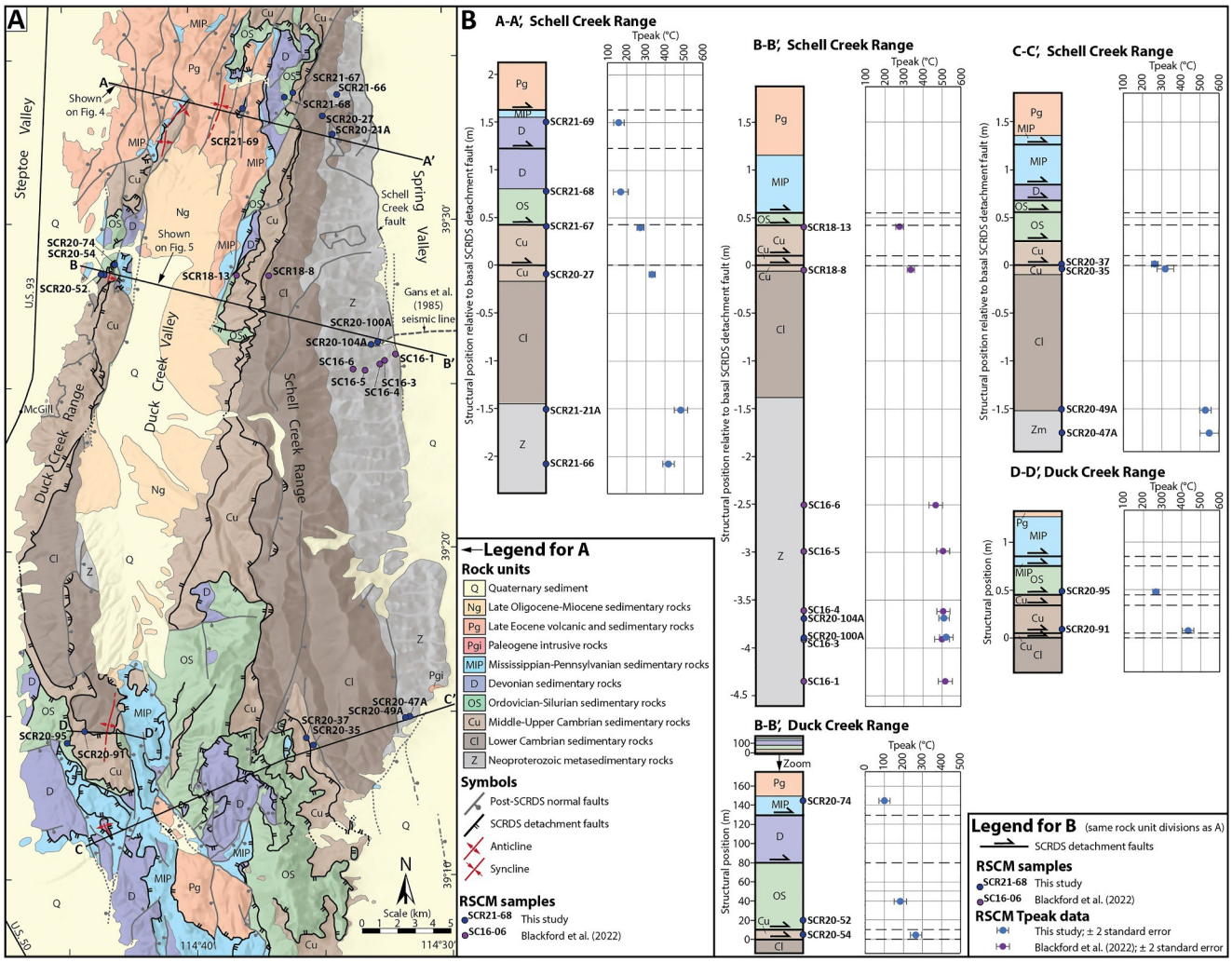

Figure 3. (a) Geologic map of the Schell Creek and Duck Creek Ranges (modified from Long et al. (2022)), showing lines of section for cross sections A-A′ (shown on Figure 4), B-B′ (shown on Figure 5), C-C′, and D-D′ from Long et al. (2022). Locations of Raman spectroscopy of carbonaceous material (RSCM) samples from this study (blue dots) and Blackford et al. (2022) (purple dots) are shown. (b) Columns plotting the present-day structural position (i.e., thicknesses on the corresponding cross sections from Long et al. (2022) measured normal to tectonic foliation in Neoproterozoic metasedimentary rocks, normal to bedding in unmetamorphosed Cambrian-Pennsylvanian sedimentary rocks, and normal to compaction and flow foliation in Paleogene volcanic rocks) of RSCM samples relative to the basal fault of the Schell Creek Range detachment system (SCRDS), with graphs of T_{peak} shown to the right of each column.

Displacement on the NSRD has been linked to the Schell Creek Range detachment system (SCRDS), a series of low dip-angle, low stratigraphic cutoff-angle, top-down-to-ESE, brittle detachment faults to the west in the Schell Creek and Duck Creek Ranges (Figures 1b and 3) (Long et al., 2022). The SCRDS is interpreted to represent the low-angle (~5–10°E initial dip) brittle breakaway zone for the NSRD, which rooted to a flat at the top of the Lower Cambrian section and fed at least 17–36 km of displacement eastward into the NSRD (Long et al., 2022). Displacement on the SCRDS is bracketed between ~37 and 26 Ma, based on SCRDS faults cutting 36.5–35.2 Ma volcanic and sedimentary rocks (Drewes, 1967; Druschke et al., 2009, 2011; Young, 1960) and SCRDS faults being cut by a high-angle normal fault with 28.7–26.1 Ma sediments deposited in a half-graben in its hanging wall (Anderson et al., 1983).

One of the longest outstanding questions is the magnitude of displacement on the NSRD, which is hindered by differing interpretations about the depths that NSRD footwall rocks were buried to prior to extension. Earlier studies (Gans & Miller, 1983; E. L. Miller et al., 1983) interpreted that NSRD footwall rocks were never buried deeper than their stratigraphic depth range of 7–13 km, and that the NSRD thus originated at a depth of ~7 km. Later thermobarometry studies (Cooper, Platt, Anczkiewicz, & Whitehouse, 2010; Lewis et al., 1999) interpreted

that NSRD footwall rocks were buried to depths of ~21–30 km via thrust faulting and were subsequently exhumed to ~15 km depths via mid-crustal spreading prior to displacement on the NSRD. Other structural reconstructions argue for more modest peak burial depths of ~15–20 km for NSRD footwall rocks (Bartley & Wernicke, 1984; Wrobel et al., 2021). These differing interpretations have resulted in NSRD displacement magnitudes varying between ~10 and 60 km (cf., Bartley & Wernicke, 1984; Lewis et al., 1999; Long et al., 2022; E. L. Miller et al., 1983; Wrobel et al., 2021).

3. Regional Cross Sections

To illustrate the post- and pre-extensional geometry of the Northern Snake Range and surrounding ranges, we present three 1:100,000-scale regional cross sections (Figures 4–6; lines of section shown on Figure 1b). Full-sized versions of these three cross section figures are available in Figures S6–S8. The central (Figure 4) and southern (Figure 5) cross sections are constrained by published cross sections of the Duck Creek and Schell Creek Ranges (Long et al., 2022), Northern Snake Range (Long et al., 2022, 2023), and Confusion and House Ranges (Greene, 2014). On the central and southern cross sections, the subsurface geology beneath Spring Valley is constrained by a seismic reflection cross section from Gans et al. (1985) and the subsurface geometry of the valley fill-bedrock contact beneath Snake Valley is constrained by a gravity model from Hurlow (2014) (locations on Figure 1b). Additional constraints include the 25°E average dip of the NSRD beneath Snake Valley interpreted on the Consortium for Continental Reflection Profiling (COCORP) seismic line (Allmendinger et al., 1983; their Figure 3, Event H), which can be traced to a depth of 8 km, and two prominent reflectors (their Event C) at depths of 12–18 km beneath the House and Confusion Ranges, which have been interpreted as the lowest thrust dècollements of the Sevier fold-thrust belt (Allmendinger et al., 1983; DeCelles & Coogan, 2006). The central and southern cross sections are shown with two phases of retro-deformation, the first in which displacement on post-SCRDS-NSRD normal faults has been restored (Figures 4b and 5b), and the second in which displacement on the SCRDS-NSRD system (as well as ductile stretching of the NSRD footwall) has been restored (Figures 4c and 5c).

3.1. Central Cross Section

The central cross section (Figure 4) is supported by cross section A-A′ of Long et al. (2022) across the Duck Creek and Schell Creek Ranges, which was drafted normal to the 015° average strike direction of SCRDS detachment faults, cross section E-E′ of Long et al. (2023) across the Northern Snake Range, which was drafted parallel to the 115° mean trend of mineral stretching lineations in the NSRD footwall, and cross section C-C′ of Greene (2014) across the Confusion and House Ranges, which was drafted normal to the 005° mean trend of fold axes at this latitude.

3.1.1. Cordilleran Contractional Structures

In the western part of the Northern Snake Range, unit Cu in the NSRD footwall is deformed by the eastward-opening O'Neill Peak recumbent syncline (Figures 2 and 4), which has been transposed to a near-isoclinal geometry by Eocene-Oligocene ductile shearing (J. Lee, 1990; J. Lee et al., 1999a, 1999b; Wrobel et al., 2021). Construction of the syncline is interpreted to be genetically related to displacement on the east-directed Eightmile thrust system, which is discontinuously mapped in the western part of the range and deforms the top of unit Cl and base of unit Cu (J. Lee et al., 1999b, 2023; Wrobel et al., 2021) (Figures 2 and 4c). Wrobel et al. (2021) interpreted that these contractional structures were active during the Late Cretaceous (~78–91 Ma), contemporaneous with peak metamorphism. In the Confusion Range, the Western Utah thrust belt consists of four thrust faults (and related folds) that deform Ordovician-Triassic rocks and have a cumulative displacement of 7.1 km, including (from structurally high to low) the Brown's Wash thrust, an unnamed thrust within unit D, the Payson Canyon thrust, and the Eureka detachment (Greene, 2014). At the western edge of the Confusion Range, the lowest two thrusts merge westward to a flat at the base of unit OS and the upper two thrusts occupy flats within the middle and top of unit D, respectively (Figures 4a and 4b). On Figure 4c, in the region between the western edge of the Confusion Range and the easternmost restored rocks in the Schell Creek Range, we interpret a geometry in which these thrusts ramp downward to the west to merge into a flat at the Cl-Cu contact, which produces a composite fault-bend-fold anticline. Although this geometry is speculative, it: (a) satisfies geometric constraints in the Confusion Range that require these thrust faults to root westward; (b) is consistent with the lack of mapped older-

10.1029/2024TC008368

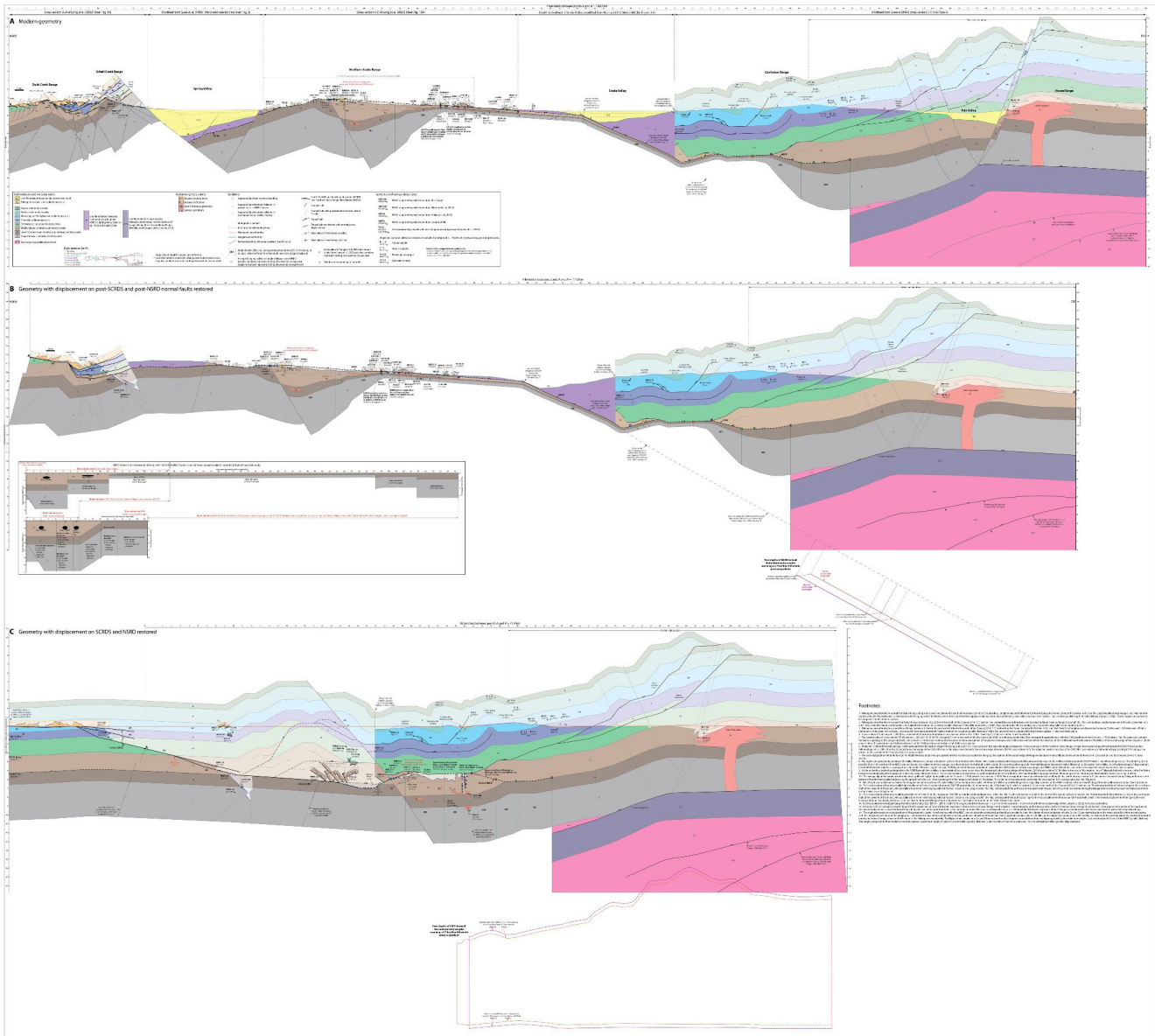

Figure 4. Central cross section across the Duck Creek, Schell Creek, Northern Snake, Confusion, and House Ranges (supporting lines of section shown on Figure 1b), showing present-day (a) and restored (b–c) geometries (a full-sized version of this figure is available in Figure S6). RSCM, CAI, and thermobarometry samples that lie proximal to the section lines (typically within 3 km to the NNE or SSW of the section lines, but thermobarometry samples were projected from 10 to 15 km to the SSW and some CAI and RSCM samples from the Confusion Range were projected from as far as 20 km to the north of the section line) are projected to their corresponding east-west position and sampled stratigraphic level. Late Cretaceous granites in the Northern Snake Range were projected from 7 to 10 km to the SSW of the section line (Figure 2). On B, the Northern Snake Range dècollement (NSRD) is projected eastward at the 29°E average dip defined at its deepest traceable depth of 8 km on the COCORP seismic line (Allmendinger et al., 1983). On (b and c), the permissible restored burial depth range of two thermobarometry samples from Cooper, Platt, Anczkiewicz, and Whitehouse (2010) are projected in the subsurface assuming that their peak pressures correspond to burial under a 3.7 km/kbar lithostatic gradient. The inset diagram on the left-hand side below (b) shows a strain model for the NSRD footwall; strain domains 3–5 are from Long et al. (2023) and hypothesized strain domains 6–8 represent a mirror image of strain domains 3–5 (see text for further discussion).

over-younger thrust faults in the Schell Creek Range (Young, 1960); and (c) provides a thrust dècollement at the Cu-Cl contact that was ripe for later exploitation as a flat by the SCRDS-NSRD system (e.g., Long et al., 2022; E. L. Miller et al., 1983). Beneath the House Range and Tule Valley, prominent reflectors on the COCORP seismic cross section are interpreted as thrust faults of the western root zone of the Sevier fold-thrust belt. The shallowest (6–12 km depth) is Event F of Allmendinger et al. (1983), which was later interpreted as the Canyon Range thrust by DeCelles and Coogan (2006) (Figure 4). The Canyon Range thrust is the highest-displacement structure

10.1029/2024TC008368

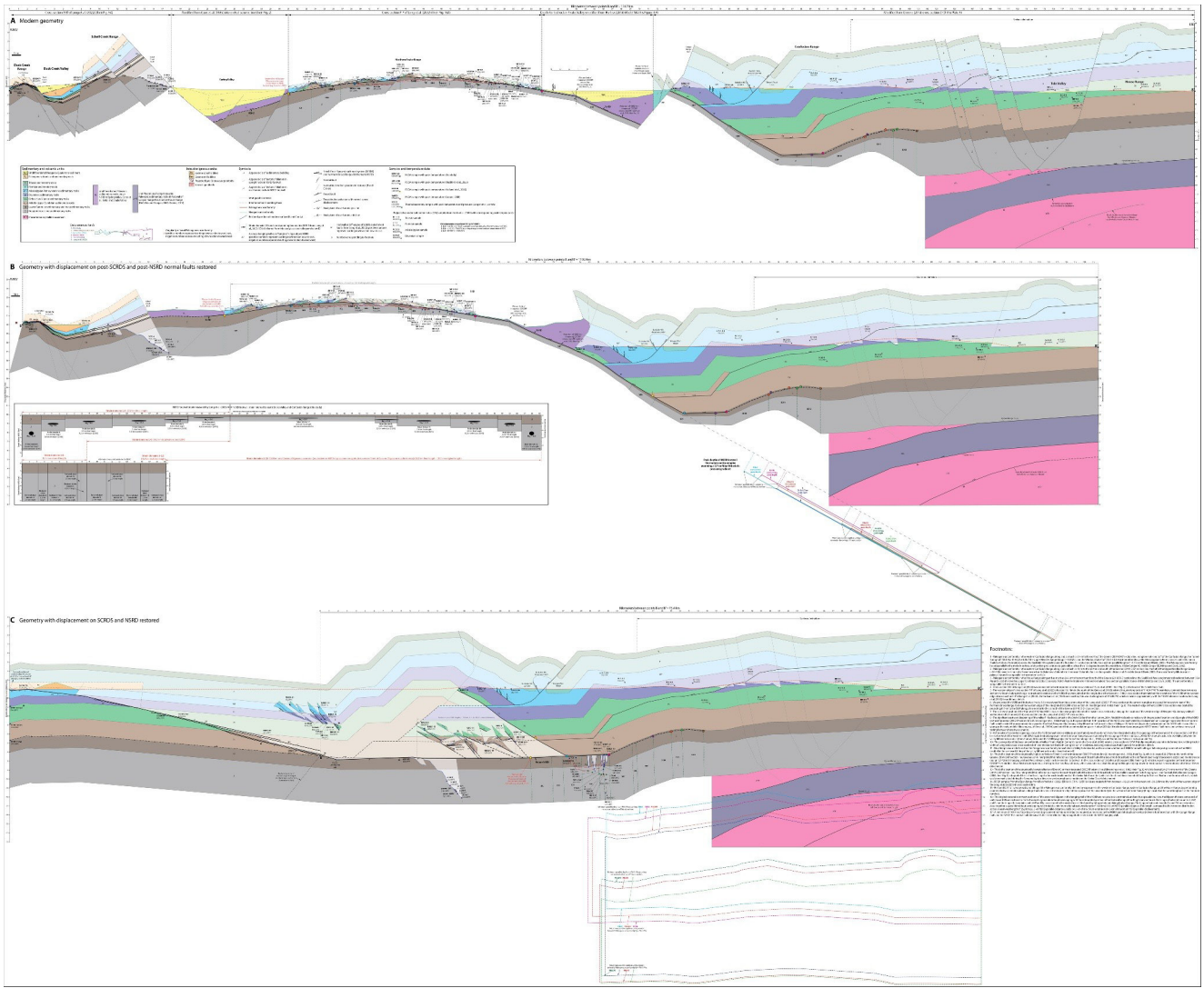

Figure 5. Southern cross section across the Duck Creek, Schell Creek, Northern Snake, Confusion, and House Ranges (supporting lines of section shown on Figure 1b), showing present-day (a) and restored (b–c) geometries (a full-sized version of this figure is available in Figure S7). RSCM, CAI, and thermobarometry samples that lie proximal to the section lines (typically within 5 km to the NNE or SSW of the section lines, but some CAI samples from the Confusion Range were projected from as far as 25 km SSW of the section line) are projected to their corresponding east-west position and sampled stratigraphic level. Late Cretaceous granites in the Northern Snake Range were projected from 6 to 8 km to the NNE of the section line (Figure 2). On (b), the Northern Snake Range dècollement (NSRD) is projected eastward at the 29°E average dip defined at its deepest traceable depth of 8 km on the COCORP seismic line (Allmendinger et al., 1983). On (b and c), the permissible restored depth range of seven thermobarometry samples from Lewis et al. (1999) and Cooper, Platt, Anczkiewicz, and Whitehouse (2010) are projected in the subsurface assuming that their peak pressures correspond to burial under a 3.7 km/kbar lithostatic gradient. The inset diagram on the left-hand side below (b) shows a strain model for the NSRD footwall; strain domains 1–6 are from Long et al. (2022) and hypothesized strain domains 7–12 represent a mirror image of strain domains 1–6 (see text for further discussion).

(~107 km) of the Sevier fold-thrust belt, and places the thick Neoproterozoic-Triassic passive margin basin section over the markedly thinner cratonic section that was deposited to the east (DeCelles & Coogan, 2006) (unit "Z-Pz" on Figure 4). Below the Canyon Range thrust, upper (12–16 km depth) and lower (13–18 km depth) reflectors of Event C of Allmendinger et al. (1983) are interpreted as the Pavant thrust and the Paxton/Gunnison thrust, respectively, the latter being the basal dècollement of the Sevier fold-thrust belt (DeCelles & Coogan, 2006). Both thrusts are interpreted to carry Precambrian crystalline basement (Allmendinger et al., 1983; DeCelles & Coogan, 2006).

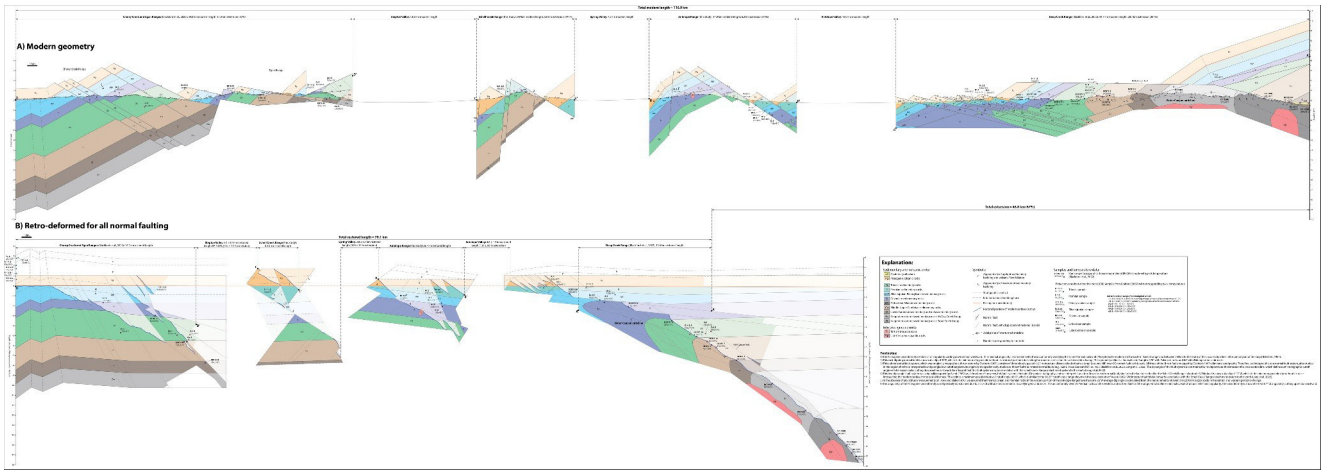

Figure 6. Northern regional cross section across the Cherry Creek, Egan, Schell Creek, Antelope, and Deep Creek Ranges (supporting lines of section shown on Figure 1b), showing (a) the present-day geometry and (b) a geometry restored for all normal faulting and associated tilting (a full-sized version of this figure is available in Figure S8). The cross sections of the Cherry Creek/Egan Ranges and Deep Creek Range are modified from Blackford et al. (2022). The cross sections of the Schell Creek Range and Antelope Range are from this study and are supported by the mapping of Dechert (1967) and Avent (1962), respectively. The cross sections were restored using methods defined in Long (2019), in which the geometries of modern valleys are not interpreted and their pre-extensional widths are restored using percent shortening estimates in the ranges bounding either side. RSCM samples from Blackford et al. (2022) that fall within 2 km to the north or south of the section lines and CAI samples from Crafford (2007) that fall within 25 km to the south and 15 km to the north of the section lines are projected to their corresponding east-west position and sampled stratigraphic level. Late Cretaceous granites in the Deep Creek Range are projected from within 5 km to the north of the section line (Blackford et al., 2022).

3.1.2. Paleogene Unconformity

In the Duck Creek and Schell Creek Ranges, the Paleogene unconformity overlies unit MIP with minimal angularity (0–4°) (Long et al., 2022; Young, 1960) and underlies sedimentary and volcanic rocks that were deposited between ~36.5 and 35.2 Ma (Druschke et al., 2009, 2011; Gans et al., 1989). The unconformity is exposed in one klippen above the NSRD on the eastern flank of the Northern Snake Range, overlying unit MIP and underlying ~35 Ma dacite (Gans et al., 1989; Gans, Miller, & Lee, 1999). In the Confusion and House Ranges, the unconformity underlies volcanic and sedimentary rocks that are as old as ~35.4 Ma (Hintze & Davis, 2002) and defines ~4° of average post-unconformity eastward tilting (Figures 4a and 4b). The unconformity cuts down-section eastward from unit P to unit Cu, which defines the Sevier culmination, a structural dome with its crest in the House Range (Harris, 1959; Hintze & Davis, 2003; Long, 2012) (Figure 4). Construction of the culmination is attributed to duplexing of underlying thrust sheets of Precambrian crystalline basement (Allmendinger et al., 1983, 1987).

3.1.3. SCRDS-NSRD System and Ductile Extension in the NSRD Footwall

On Figure 4, the SCRDS consists of four top-down-to-ESE faults, which cut down-section eastward at 2–11° stratigraphic cutoff-angles and root to a flat at the Cu-Cl contact. At this latitude, the SCRDS fed at least 16.8 km of total displacement eastward into the NSRD (Long et al., 2022) (Figure 4). The NSRD is gently domed, with a 15°W average dip at the western flank of the range and a 4°E average dip across the eastern half (Long et al., 2023). The NSRD lies at the top of unit Cl at the western flank of the range, and cuts upsection eastward through unit Cu as it crosses an open anticline and a pre-NSRD normal fault. The NSRD exhibits a footwall flat at the top of unit Cu across the eastern half of the range (Gans, Miller, & Lee, 1999; J. Lee et al., 1999a; Long et al., 2023). Unmetamorphosed carbonates of unit Cu in NSRD hanging wall klippe overlie their metamorphosed stratigraphic equivalents in the footwall across a 17.5 km NSRD-parallel distance, which provides a minimum displacement estimate for the NSRD (Long et al., 2023).

In the western part of the range, NSRD footwall rocks locally exhibit ductile fabrics with NNW-trending intersection and stretching lineations, which record low-magnitude strain during Late Cretaceous shortening (J. Lee et al., 1999b, 2023; Wrobel et al., 2021). NSRD footwall rocks in the central and eastern parts of the range exhibit ubiquitous mylonitic ductile fabrics with strongly developed, ESE-trending stretching lineations, which record Eocene-Oligocene ductile extensional shearing (Gans, Miller, & Lee, 1999; J. Lee et al., 1999a). Ductile

thinning increases from ~15% to ~95% between the western limit of Eocene-Oligocene ductile fabrics and the eastern flank of the range (Long et al., 2023) (Figure 4). Long et al. (2023) presented a strain model for the NSRD footwall on this cross section and calculated that lineation-parallel extension increases eastward to ~1,035%, with 12.1 km of total Eocene-Oligocene ductile extension (Figure 4b inset).

Beneath Snake Valley, we projected the NSRD at the 25°E average dip angle interpreted on the COCORP line (Allmendinger et al., 1983; their Event H) (Figure 4). We suggest that Event H, which consists of as many as 3–5 closely spaced reflectors, corresponds to the fabric anisotropy of stretched footwall rocks, as opposed to just the upper surface that represents the NSRD itself. Event H cannot be correlated beyond 8 km depth and projecting it downward at the 29°E dip that it exhibits at its deepest traceable levels would result in it being truncated by the west-dipping Canyon Range thrust reflector (Event F) at a depth of ~15 km (Allmendinger et al., 1983). On Figure 4a, we projected the NSRD and its footwall rocks to a depth of 6–6.5 km, and then show them flattening out eastward. This geometry is consistent with the footwall flat at the top of unit Cu that is observed across the eastern half of the NSRD footwall (Gans, Miller, & Lee, 1999; J. Lee et al., 1999a; Long et al., 2023) as well as the subsurface geometry of the western part of the Confusion Range interpreted on the Greene (2014) C-C′ cross section.

3.1.4. Post-SCRDS-NSRD Normal Faulting

Several high-angle normal faults with 100's of m displacement cut SCRDS faults in the Duck Creek and Schell Creek Ranges (Long et al., 2022). The Schell Creek fault accommodated 10.5 km of top-down-to-east displacement, which generated the westward tilting (15° total) that created the Neogene-Quaternary Spring Valley half-graben (Gans et al., 1985; Long et al., 2022). The Northern Snake and Confusion Ranges lack high-displacement, post-NSRD normal faults at the latitude of Figure 4 (Gans, Miller, & Lee, 1999; Greene, 2014; J. Lee et al., 1999a, 1999b). The normal fault system on the eastern side of Tule Valley accommodated 3.1 km of top-down-to-west displacement. Retro-deformation of post-SCRDS-NSRD normal faults restores the cross section from a modern length of 128.1 km (Figure 4a) to a restored length of 117.8 km (Figure 4b), defining 10.3 km (8.7%) of extension.

3.1.5. Restoration of SCRDS-NSRD Extension

At least 16.8 km of total SCRDS displacement was fed into the NSRD on Figure 4 (Long et al., 2022). NSRD hanging wall klippe that contain unit Cu are distributed over a modern NSRD-parallel length of 24.5 km (Figure 4a). Restoration of these klippe as close together as possible without overlapping yields a minimum NSRD-parallel length of 5.6 km (Figure 4c), which defines a maximum of 18.9 km of displacement fed into the NSRD via hanging wall normal faulting. We show a geometry in which the structural elevation accomplished by the O'Neill Peak recumbent syncline constructed the overlying Knoll Hill anticline in the western Confusion Range (Figure 4c). Though our interpreted geometries differ in detail, this was inspired by Wrobel et al. (2021), who interpreted the O'Neill Peak recumbent syncline as part of the root zone of the Western Utah thrust belt. We show the O'Neill Peak recumbent syncline as the lower kink axis of a fault-propagation fold that was constructed by displacement fed in from the Eightmile thrust system to the west (Figure 4c). Our interpreted geometry provides piercing points, including the footwall and hanging wall positions of a pre-NSRD normal fault (blue hexagon on Figure 4) and the western limit of Eocene-Oligocene ductile fabrics (yellow hexagon), which define 41.9 km of cumulative displacement on the NSRD. This is consistent with the displacement fed into the NSRD from the SCRDS and from hanging wall normal faulting in the Northern Snake Range, which total to 35.7 km. The remaining 6.2 km of displacement was likely accommodated by normal faulting within the undifferentiated Paleozoic rocks above the NSRD in Spring Valley and Snake Valley (Figure 4a). Restoration of SCRDS-NSRD displacement yields an initial length of 77.9 km (Figure 4c). When compared to the post-SCRDS-NSRD length of 117.8 km (Figure 4b), this corresponds to 39.9 km of total ESE-directed extension (51%).

Eocene-Oligocene ductile stretching of the NSRD footwall has the net effect of progressively decreasing NSRD displacement eastward. At the eastern edge of the Northern Snake Range (pink hexagon on Figure 4), 12.1 km of cumulative ductile extension of the NSRD footwall (Long et al., 2023) has decreased net displacement on the NSRD from its maximum of 41.9 km (measured at the western limit of Eocene-Oligocene ductile fabrics) to 29.8 km, a 29% decrease. We hypothesize that ductile stretching of NSRD footwall rocks continues in the subsurface, based on event H on the COCORP line that can be traced continuously to 8 km depth (Allmendinger

et al., 1983). On Figures 4a and 4b, we show a geometry in which the magnitude of ductile stretching of the NSRD footwall matches the 41.9 km of cumulative displacement on the NSRD. To approximate the geometry of this ductile stretching, we used a mirror image of the strain model presented in Long et al. (2023), with hypothesized strain domains 6–8 at depth mirroring the stretching measured in strain domains 3–5 (Figure 4b inset). This geometry results in NSRD displacement progressively decreasing eastward (pink, orange, and green hexagons on Figure 4) and terminating beneath the Confusion Range (brown hexagon). This footwall geometry is speculative, and it is possible that some NSRD displacement was fed further eastward. If this were the case, the most likely scenario would be that this displacement was fed eastward to reactivate the Canyon Range thrust beneath the House Range, because: (a) there is no geophysical evidence for the NSRD or its stretched footwall rocks extending below 8 km depth (Allmendinger et al., 1983); (b) eastward projection of the NSRD reflector would result in its truncation by the Canyon Range thrust reflector (Allmendinger et al., 1983); and (c) the Canyon Range thrust would be an ideal mechanically weak contact that was ripe for reactivation.

3.1.6. Structural Arguments Invalidating Deep NSRD Footwall Burial

Burial of NSRD footwall rocks to the depths implied by thermobarometry is incompatible with published seismic reflection data and with geometric constraints on Figure 4. Two thermobarometry samples from Cooper, Platt, Anczkiewicz, and Whitehouse (2010) are projected onto Figure 4 (FDC62 and FDe178). These samples yielded peak pressures of 8.2 ± 0.9 and 8.2 ± 1.0 kbar, respectively, corresponding to lithostatic burial depths between ~26.5 and 34 km. Burial of these Neoproterozoic metasedimentary rocks to such depths is incompatible with the ~17–20 km maximum restored depth of the upper contact of Precambrian crystalline basement interpreted below the Confusion and House Ranges on the COCORP line (Allmendinger et al., 1983; DeCelles & Coogan, 2006) (Figure 4b). Assuming that these samples actually attained ~26.5–34 km peak depths, and projecting the NSRD at the 29°E dip defined at its deepest traceable levels on the COCORP line, it would require a minimum of 66–77 km of displacement on the NSRD (assuming no erosion beneath the top of the Triassic section at the time of Late Cretaceous peak burial) and a maximum of 75–94 km of displacement on the NSRD (assuming erosion to the level of the Paleogene unconformity at the time of Late Cretaceous peak burial) to exhume these samples. Strain compatibility demonstrates that such high displacements are not possible for the SCRDS-NSRD system. Rocks of unit Cu preserved in the SCRDS footwall in the eastern Schell Creek Range (Long et al., 2022), in NSRD hanging wall klippe in the Northern Snake Range (Long et al., 2023), and in the NSRD hanging wall in the subsurface of the western Confusion Range (which have been drilled; see Greene, 2014, cross section B-B′) cannot spatially overlap after restoration, which provides a firm limit on the maximum displacement possible on the SCRDS-NSRD system. On Figure 4c, only an additional 12.6 km of NSRD displacement beyond the 41.9 km that we already show is possible without spatially overlapping rocks of unit Cu preserved in the Schell Creek Range, Northern Snake Range, and Confusion Range.

3.2. Southern Cross Section

The southern cross section (Figure 5) is supported by cross sections B-B′ of Long et al. (2022) across the Duck Creek and Schell Creek Ranges, F-F′ of Long et al. (2022) across the Northern Snake Range, and D-D′ of Greene (2014) across the Confusion and House Ranges (Figure 1b). Similar procedures were followed to construct and restore Figure 5 as described above for Figure 4. Therefore, below we present a comparatively abbreviated discussion of Figure 5.

3.2.1. Cordilleran Contractional Structures

No evidence for folding or thrust faulting is observed in the NSRD footwall on Figure 5 (Johnston, 2000; J. Lee et al., 2023; J. Lee, Miller, et al., 1993). In the Confusion Range, the Western Utah thrust belt consists of the King's Canyon and Brown's Wash thrust faults (and related folds), which accommodated 10.1 km of total displacement (Greene, 2014). Similar to Figure 4c, we interpret that these thrust faults ramp downward to the west to root into a flat at the Cl-Cu contact, which generated a hypothesized fault-bend-fold anticline.

3.2.2. Paleogene Unconformity

In the Duck Creek and Schell Creek Ranges, the Paleogene unconformity lies within unit MIP and underlies ~35.2 Ma volcanic rocks (Gans et al., 1989; Young, 1960). In the Confusion and House Ranges, the unconformity

underlies rocks as old as ~35.4 Ma (Hintze & Davis, 2002), cuts down-section eastward from unit P to the top of unit Cu, and defines <1° of post-unconformity eastward tilting (Figures 5a and 5b).

3.2.3. SCRDS-NSRD System and Ductile Extension in the NSRD Footwall

At the latitude of Figure 5, the SCRDS consists of five faults, which cut down-section eastward at an average stratigraphic cutoff-angle of 8°, root eastward to a flat at the Cu-Cl contact, and fed at least 36.0 km of total displacement into the NSRD (Long et al., 2022). The NSRD occupies a footwall flat at the top of unit Cu across the full width of the Northern Snake Range (Johnston, 2000; J. Lee et al., 2023; J. Lee, Miller, et al., 1993), and most NSRD hanging wall klippe carry units Cu and OS (Figure 5). NSRD footwall rocks exhibit Eocene-Oligocene extensional ductile fabrics with ESE-WNW-trending stretching lineations across the full width of the range (Figure 5) (J. Lee et al., 1987). These fabrics die out westward at localities 6 km to the NNE and 9 km to the SSW of the western edge of the cross section line (Figure 2), which constrains the approximate western limit of Eocene-Oligocene fabrics (J. Lee et al., 2017). Long et al. (2022) presented a strain model for the NSRD footwall on this cross section and documented that horizontal extension and vertical thinning increase from 8% to 86% and 17%–647%, respectively, between the western and eastern flanks of the range, with 19.1 km of total Eocene-Oligocene ductile extension (Figure 5b inset).

3.2.4. Post-SCRDS-NSRD Normal Faulting

Several normal faults cut the SCRDS in the Duck Creek and Schell Creek Ranges, including the Duck Creek and Schell Creek faults, which each generated ~15°W-tilted half-grabens (Gans et al., 1985). One top-down-to-west, post-NSRD normal fault is mapped in the Northern Snake Range (Johnston, 2000; J. Lee et al., 2023; J. Lee, Miller, et al., 1993). The top-down-to-west Conger Range fault on the western side of the Confusion Range accommodated 5 km of displacement, and normal faults with 100's of m of displacement deform the eastern Confusion Range and western House Range (Greene, 2014). Retro-deformation of post-SCRDS-NSRD normal faults restores the cross section from a modern length of 131.7 km (Figure 5a) to a length of 119.5 km (Figure 5b), defining 12.2 km of extension (10%).

3.2.5. Restoration of SCRDS-NSRD Extension

Figure 5 lacks a piercing point between the hanging wall and footwall of the NSRD. Constraints on the displacement magnitude on the NSRD include: (a) At least 36.0 km of displacement on the SCRDS was fed eastward into the NSRD (Long et al., 2022); (b) NSRD hanging wall klippe that carry units Cu and OS are distributed over a modern NSRD-parallel length of 25.5 km (Figure 5b) and restore to a minimum NSRD-parallel length of 11.0 km (Figure 5c), defining 14.5 km of maximum displacement fed into the NSRD by normal faulting in its hanging wall; and (c) At least 14.0 km of displacement was fed into the NSRD by an east-dipping normal fault that presently underlies the western Confusion Range, which cuts downward through units D, OS, and Cu. These constraints define 50.0 km (which is shown on Figure 5b) to 64.6 km of displacement on the NSRD. Restoration of SCRDS-NSRD displacement restores the cross section from a final length of 119.5 km (Figure 5b) to an initial length of 73.4 km (Figure 5c), defining 46.1 km of minimum extension (63%).

On Figure 5, 19.1 km of Eocene-Oligocene ductile stretching of the NSRD footwall (Long et al., 2022) decreases net displacement on the NSRD to 30.9 km at the eastern edge of the range (a 38% decrease) (pink hexagon). Similar to Figure 4, we show ductile stretching of the NSRD footwall continuing in the subsurface beneath Snake Valley and the Confusion Range, eventually matching the 50.0 km of cumulative displacement that we show on the NSRD (Figure 5b), using a mirror image of the strain model presented in Long et al. (2022) (Figure 5b inset).

3.2.6. Structural Arguments Invalidating Deep NSRD Footwall Burial

Thermobarometry samples from Cooper, Platt, Anczkiewicz, and Whitehouse (2010) ($n = 5$) and Lewis et al. (1999) ($n = 2$) projected onto Figure 5 yielded pressures between 5.7 ± 0.9 and 8.1 ± 0.7 kbar. Projection of these Neoproterozoic metasedimentary samples to the ~21–30 km depth range implied by thermobarometry is incompatible with the ~17–20 km maximum restored depth of the upper contact of Precambrian crystalline basement interpreted on the COCORP line (Allmendinger et al., 1983; DeCelles & Coogan, 2006; Greene, 2014) (Figure 5b). Assuming that the thermobarometry samples did attain ~21–30 km peak depths, and projecting the NSRD at its dip angle interpreted on the COCORP line, it would require 65–90 km of minimum displacement on

the NSRD (assuming no erosion beneath the top of the Triassic section at the time of Late Cretaceous peak burial), and 73–102 km of maximum displacement on the NSRD (assuming erosion to the level of the Paleogene unconformity at the time of Late Cretaceous peak burial). Such high displacements are not possible without resulting in spatial overlap of rocks from unit Cu preserved in the SCRDS footwall in the Schell Creek Range and preserved in the NSRD hanging wall in the Northern Snake and Confusion Ranges (Figure 5c). A maximum additional 17.9 km of NSRD displacement beyond the 50.0 km shown in Figure 5c is possible without overlapping rocks of units Cu, yielding an upper limit of 67.9 km of displacement. This falls short of the 76–102 km displacement range required to exhume the three highest-pressure samples (Figure 5b).

3.3. Northern Cross Section

We present a northern regional cross section (Figure 6; section lines shown on Figure 1b) that is supported by cross sections across the Cherry Creek/Egan (Blackford et al., 2022), Schell Creek (this study; supported by mapping from Dechert, 1967), Antelope (this study; supported by mapping from Avent (1962); Hose and Blake (1976)), and Deep Creek Ranges (Blackford et al., 2022). Figure 6 was restored using methods defined in Long (2019), in which the bedrock geometries of modern valleys are not interpreted and their pre-extensional widths are restored using percent extension estimates in the ranges bounding either side. Though the NSRD is not exposed at the latitude of Figure 6, this cross section is important for testing interpretations of deep structural burial via thrust and reverse faulting (Bartley & Wernicke, 1984; Lewis et al., 1999), for comparison with the extension magnitude measured on Figures 4 and 5, and for providing a third regional view of the structural and thermal architecture of the crust.

The Cherry Creek Range contains the western breakaway zone for top-down-to-east, domino-style normal faulting (Figure 6a), which is the dominant structural style observed in all ranges to the east (Blackford et al., 2022; Gans, 1982; Gans & Miller, 1983; Rodgers, 1987). The magnitude of westward tilting accommodated by domino-style normal faulting, as defined by the Paleogene subvolcanic unconformity, is typically 35–45°. Restoration of all normal faulting (Figure 6b) yields 46.8 km of total extension (67%; 116.9 km modern length and 70.1 km pre-extensional length). This is similar to the 50.2 km total extension (39.9 km SCRDS-NSRD extension and 10.3 km post-SCRDS-NSRD extension) measured on Figure 4, which is only 20–40 km to the south of Figure 6. This similarity provides a strain compatibility argument against deep NSRD footwall burial. For example, increasing displacement on the NSRD on Figure 4 to the 66–94 km displacement required to exhume 30 km-deep footwall rocks would result in approximately doubling the regional extension magnitude across a 20–40 km north-south distance, which would generate significant strain incompatibility.

Figure 6b demonstrates that the Paleogene unconformity overlies Pennsylvanian-Permian rocks with a typical angularity ≤10°, which defines minimal pre-Paleogene deformation. Exposure levels in the Egan and Schell Creek Ranges restore as deep as 13 and 9 km, respectively, below the top of the Triassic section, and define gentle folding and no evidence for thrust faulting. The Deep Creek Range exposes rocks that restore as deep as 20 km below the top of the Triassic section, including Neoproterozoic rocks that are stratigraphically deeper than those exposed in the NSRD footwall (Rodgers, 1987). The Deep Creek Range provides no evidence for thrust faulting down to a restored depth of 20 km, which is at odds with a regional, top-to-east thrust fault hypothesized at 10–12 km depth as a mechanism to bury NSRD footwall rocks (Bartley & Wernicke, 1984). The Deep Creek Range is deformed by the west-vergent Water Canyon anticline (Figure 6), which Lewis et al. (1999) proposed was involved in accommodating deep burial of NSRD footwall rocks; we discuss this in detail below.

4. Thermal Architecture of the Northern Snake Range and Surrounding Region

Here, we present peak temperatures (T_{peak}) from 95 samples from the Northern Snake Range and surrounding ranges, which we combine with 132 published T_{peak} measurements. We integrate these T_{peak} data with stratigraphic thicknesses and our reconstructed cross sections to provide a detailed view of the pre-extensional thermal architecture of the crust in this region, which provides support for several arguments against the deep burial of NSRD footwall rocks.

4.1. Peak Metamorphic Temperatures From RSCM Thermometry

The RSCM thermometer (e.g., Aoya et al., 2010; Beyssac et al., 2002, 2003; Kouketsu et al., 2014; Lünsdorf et al., 2017; Rahl et al., 2005) quantifies the T_{peak} attained by metasedimentary rocks that contain metamorphosed

organic matter. We utilized the RSCM calibrations of Rahl et al. (2005) and Kouketsu et al. (2014) to measure T_{peak} from 95 samples, consisting of 17 from the Duck Creek and Schell Creek Ranges, 72 from the Northern Snake Range, and 6 from the Confusion Range (Table 1; sample locations shown on Figures 1–3). Examples of Raman spectra from representative samples and photomicrographs of analyzed grains of carbonaceous material are shown on Figure 7. Analytical methods, supporting data, and examples of Raman spectra from all 95 samples are included in Supporting Information S1.

We followed procedures described in Rahl et al. (2005) and Kouketsu et al. (2014), which involved fitting as many as five Raman peaks (G, D1, D2, D3, D4) in the wavenumber range of 1,000–1,800 cm^{-1}. We used Equation 3 of Rahl et al. (2005), which is calibrated to the peak height ratio of D1/G (their parameter R1) and the peak area ratio of D1/(G + D1 + D2) (their parameter R2) to calculate T_{peak} for grain analyses >400°C, and we used Equation 1 (calibrated to the full width at half maximum of the D1 peak) and Equation 2 (calibrated to the full width at half maximum of the D2 peak) of Kouketsu et al. (2014) to calculate T_{peak} for grain analyses between 200–400°C and 150–200°C, respectively. T_{peak} values reported for our samples represent the mean of multiple analyzed grains of carbonaceous material (typically between 12 and 16 grains per sample; Table 1). T_{peak} values are reported with two standard errors of the mean (Table 1, footnote 3), which typically ranges between ±~20–50°C for our samples.

4.2. Compilation of Published RSCM and CAI Data

We combined the T_{peak} data from our 95 RSCM samples with published T_{peak} data (Table 2; sample locations shown on Figures 1–3), including 29 RSCM samples from Blackford et al. (2022) (3 from the Egan Range, 7 from the Schell Creek Range, 14 from the Deep Creek Range, and 5 from the House Range), 15 RSCM samples from the Northern Snake Range (14 from Hoiland et al. (2022); 1 from Cooper (2008)), and 9 thermobarometry samples from the Northern Snake Range (7 from Cooper, Platt, Anczkiewicz, and Whitehouse (2010); 2 from Lewis et al. (1999)).

We combined these 148 total T_{peak} measurements with published conodont alteration index (CAI) values from Cambrian to Triassic sedimentary rock samples in east-central Nevada (Crafford, 2007) and west-central Utah (Harris et al., 1980) (sample locations and CAI values shown on Figure 1b). The CAI, which is based on the color change that occurs as conodonts attain progressively higher temperatures, provides a semi-quantitative estimate of T_{peak} (e.g., Epstein et al., 1977). We used the T_{peak} ranges reported in Königshof (2003), in which CAI values of 1–1.5 = <50–80°C, 2–2.5 = 60–140°C, 3–3.5 = 110–200°C, 4–4.5 = 190–300°C, and 5–5.5 = 300–480°C. We compiled CAI values from 79 samples that fall on the area of Figure 1b, yielding a combined data set of 227 total T_{peak} measurements. Below, we discuss T_{peak} patterns as a function of stratigraphic depth, restored structural depth, and west-to-east distance (for simplicity, in the following sections we list T_{peak} values without their accompanying error ranges).

4.3. Results of Combined RSCM, Thermobarometry, and CAI Data Sets

Overall, T_{peak} values increase as a function of stratigraphic depth (Figures 8 and 9). Most Triassic and Permian samples (12 out of 18) yielded CAI values of 1, indicating T_{peak} <50–80°C (Figure 8a). Most Mississippian-Pennsylvanian samples also attained low T_{peak} values; out of 26 total CAI samples, 13 yielded values of 1 (<50–80°C) and 10 were between 1 and 2 (<50–80°C to 60–140°C) (Figure 8b). RSCM temperatures from 9 Mississippian-Pennsylvanian samples yielded T_{peak} values between 74 and 193°C. Seven of these samples yielded T_{peak} values that fall below the 150°C minimum calibration temperature of Kouketsu et al. (2014) Equation 2, and therefore can only be constrained as <150°C. Devonian samples yielded CAI values between 1 and 3 (n = 10), without a dominant value, and RSCM temperatures typically between ~150 and 200°C (n = 11) (Figure 8c). Ordovician-Silurian rocks yielded CAI values with a mode of 3 (11 out of 24 total) (110–200°C) and RSCM temperatures typically between ~180 and 280°C (n = 16) (Figure 8c).

Excluding NSRD footwall samples, Middle-Upper Cambrian rocks yielded RSCM temperatures typically between ~250 and 370°C (n = 33) (Figure 8d), with samples in the Schell Creek Range, Deep Creek Range, NSRD hanging wall, and House Range yielding similar average temperatures of 314 ± 54°C (n = 8), 367 ± 5°C (n = 3), 305 ± 40°C (n = 18), and 351 ± 80°C (n = 3), respectively (errors for average T_{peak} values listed at 1σ level) (Figure 8g). Middle-Upper Cambrian metasedimentary rocks in the NSRD footwall are hotter, typically ranging between ~470 and 580°C, with an average of 528 ± 39°C (n = 42) (Figures 8d and 8g). Lower Cambrian rocks

Table 1

Summary of RSCM Thermometry Results for Samples From This Study From the Duck Creek, Schell Creek, Northern Snake, and Confusion Ranges

Sample	Latitude (°N)	Longitude (°W)	Transect	Structural position (m)[a]	Map unit	Formation	Lithology	Relative to NSRD	Temperature Calibration[b]	D1 FWHM Mean	D1 FWHM 1σ	D2 FWHM Mean	D2 FWHM 1σ	R1 Mean	R1 1σ	R2 Mean	R2 1σ	T_{peak} (°C) Mean	T_{peak} (°C) 1σ	T_{peak} (°C) 2 SEM[c]	*n*
SCR21-69	39.55814	114.63156	Schell Creek Range, cross section A-A′	1,500	D	Guilmette Formation	Limestone	–	Kouketsu et al. (2014) Equation 2	–	–	55.3	3.4	–	–	–	–	160	23	28	15
SCR21-68	39.56353	114.60386	Schell Creek Range, cross section A-A′	775	OS	Laketown Dolomite	Dolomite	–	Kouketsu et al. (2014) Equation 2	–	–	53.8	8.3	–	–	–	–	170	56	39	15
SCR21-67	39.56569	114.59900	Schell Creek Range, cross section A-A′	400	Cu	Raiff Limestone	Limestone	–	Kouketsu et al. (2014) Equation 1	95.3	7.2	–	–	–	–	–	–	273	15	18	14
SCR20-27	39.55419	114.57861	Schell Creek Range, cross section A-A′	−90	Cu	Eldorado Limestone	Limestone	–	Kouketsu et al. (2014) Equation 1	66.7	2.7	–	–	–	–	–	–	335	6	16	15
SCR20-21A	39.54489	114.57225	Schell Creek Range, cross section A-A′	−1,510	Z	McCoy Creek Group, Unit A	Argillite	–	Rahl et al. (2005) Equation 3	–	–	–	–	0.177	0.034	0.288	0.039	485	36	35	12
SCR21-66	39.56475	114.56942	Schell Creek Range, cross section A-A′	−2,075	Z	McCoy Creek Group, Unit C	Argillite	–	Rahl et al. (2005) Equation 3	–	–	–	–	0.709	0.234	0.469	0.051	420	20	30	13
SCR20-104A	39.43703	114.54861	Schell Creek Range, cross section B-B′	−3,510	Z	McCoy Creek Group, Unit H	Schist	–	Rahl et al. (2005) Equation 3	–	–	–	–	0.179	0.027	0.259	0.028	516	22	28	15
SCR20-100A	39.43833	114.54433	Schell Creek Range, cross section B-B′	−3,720	Z	McCoy Creek Group, Unit H	Schist	–	Rahl et al. (2005) Equation 3	–	–	–	–	0.169	0.061	0.245	0.059	528	47	36	15
SCR20-74	39.47861	114.71528	Duck Creek Range, cross section B-B′	145	MIP	Ely Limestone	Limestone	–	Kouketsu et al. (2014) Equation 2	–	–	63.8	3.9	–	–	–	–	102	27	29	15
SCR20-52	39.47375	114.72428	Duck Creek Range, cross section B-B′	40	OS	Laketown Dolomite	Dolomite	–	Kouketsu et al. (2014) Equation 2	–	–	51.7	3.7	–	–	–	–	185	25	32	12
SCR20-54	39.47347	114.72219	Duck Creek Range, cross section B-B′	5	Cu	Eldorado Limestone	Limestone	–	Kouketsu et al. (2014) Equation 1	98.2	9.0	–	–	–	–	–	–	267	19	29	6
SCR20-37	39.23778	114.59400	Schell Creek Range, cross section C-C′	20	Cu	Lincoln Peak Formation	Limestone	–	Kouketsu et al. (2014) Equation 1	98.6	6.2	–	–	–	–	–	–	266	13	17	15
SCR20-35	39.23408	114.58939	Schell Creek Range, cross section C-C′	−30	Cu	Pole Canyon Limestone	Limestone	–	Kouketsu et al. (2014) Equation 1	73.0	4.0	–	–	–	–	–	–	321	9	44	2
SCR20-49A	39.24756	114.52897	Schell Creek Range, cross section C-C′	−1,510	Cl	Prospect Mountain Quartzite	Argillite	–	Rahl et al. (2005) Equation 3	–	–	–	–	0.194	0.017	0.249	0.018	531	15	30	12
SCR20-47A	39.24814	114.52614	Schell Creek Range, cross section C-C′	−1,750	Z	McCoy Creek Group, undifferentiated	Argillite	–	Rahl et al. (2005) Equation 3	–	–	–	–	0.152	0.122	0.217	0.114	551	88	49	17
SCR20-95	39.23558	114.75153	Duck Creek Range, cross section D-D′	480	OS	Late Cambrian-Early Ordovician, undiff.	Limestone	–	Kouketsu et al. (2014) Equation 1	112.7	9.1	–	–	–	–	–	–	236	19	18	15

Tectonics
10.1029/2024TC008368

Table 1
Continued

Sample	Latitude (°N)	Longitude (°W)	Transect	Structural position (m)[a]	Map unit	Formation	Lithology	Relative to NSRD	Temperature Calibration[b]	D1 FWHM		D2 FWHM		R1		R2		T_{peak} (°C)			
										Mean	1σ	Mean	1σ	Mean	1σ	Mean	1σ	Mean	1σ	2 SEM[c]	*n*
SCR20-91	39.24186	114.73869	Duck Creek Range, cross section D-D′	80	Cu	Pole Canyon Limestone	Limestone	–	Rahl et al. (2005) Equation 3	–	–	–	–	0.517	0.112	0.417	0.040	436	21	30	13
NSR21-65	39.49350	114.35808	Northern Snake Range, Third Butte	10	Cu	Middle Cambrian limestone, undiff.	Limestone	Hanging wall	Kouketsu et al. (2014) Equation 1	75.0	9.1	–	–	–	–	–	–	317	20	21	12
NSR20-24	39.46653	114.29617	Northern Snake Range, Western Marble Wash	−85	Cu	Eldorado Limestone	Marble	Footwall	Rahl et al. (2005) Equation 3	–	–	–	–	0.415	0.152	0.421	0.081	406	50	34	17
NSR20-21	39.46664	114.29297	Northern Snake Range, Western Marble Wash	−250	Cu	Raiff Limestone	Marble	Footwall	Rahl et al. (2005) Equation 3	–	–	–	–	0.133	0.080	0.199	0.089	566	72	45	15
NSR20-18	39.46614	114.28942	Northern Snake Range, Western Marble Wash	−415	Cu	Raiff Limestone	Marble	Footwall	Rahl et al. (2005) Equation 3	–	–	–	–	0.115	0.057	0.181	0.071	580	60	42	14
NSR20-16	39.46692	114.28597	Northern Snake Range, Western Marble Wash	−605	Cu	Raiff Limestone	Marble	Footwall	Rahl et al. (2005) Equation 3	–	–	–	–	0.325	0.243	0.320	0.119	487	69	44	15
NSR20-8	39.46389	114.27908	Northern Snake Range, Western Marble Wash	−925	Cu	Raiff Limestone	Marble	Footwall	Rahl et al. (2005) Equation 3	–	–	–	–	0.256	0.203	0.274	0.136	518	95	68	10
NSR20-1	39.46092	114.27419	Northern Snake Range, Western Marble Wash	−1,170	Cu	Notch Peak Formation	Marble	Footwall	Rahl et al. (2005) Equation 3	–	–	–	–	0.259	0.117	0.301	0.093	493	68	49	12
NSR21-13	39.37161	114.18567	Northern Snake Range, Ryegrass Canyon	−10	Cu	Notch Peak Formation	Marble	Footwall	Rahl et al. (2005) Equation 3	–	–	–	–	0.153	0.147	0.209	0.124	560	93	64	11
NSR21-10	39.36947	114.18617	Northern Snake Range, Ryegrass Canyon	−75	Cu	Dunderberg Shale	Marble	Footwall	Rahl et al. (2005) Equation 3	–	–	–	–	0.247	0.300	0.239	0.170	549	107	68	12
NSR21-3	39.36642	114.19156	Northern Snake Range, Ryegrass Canyon	−280	Cu	Raiff Limestone	Marble	Footwall	Rahl et al. (2005) Equation 3	–	–	–	–	0.219	0.185	0.264	0.148	519	110	70	12
NSR21-1	39.36394	114.19169	Northern Snake Range, Ryegrass Canyon	−420	Cu	Raiff Limestone	Marble	Footwall	Rahl et al. (2005) Equation 3	–	–	–	–	0.134	0.112	0.191	0.108	574	84	54	13
NSR21-20	39.36531	114.20261	Northern Snake Range, Ryegrass Canyon	−605	Cu	Raiff Limestone	Marble	Footwall	Rahl et al. (2005) Equation 3	–	–	–	–	0.156	0.051	0.232	0.066	538	56	43	12

Tectonics
10.1029/2024TC008368

Table 1
Continued

Sample	Latitude (°N)	Longitude (°W)	Transect	Structural position (m)[a]	Map unit	Formation	Lithology	Relative to NSRD	Temperature Calibration[b]	D1 FWHM		D2 FWHM		R1		R2		T_{peak} (°C)			
										Mean	1σ	Mean	1σ	Mean	1σ	Mean	1σ	Mean	1σ	2 SEM[c]	*n*
NSR21-21	39.36278	114.20836	Northern Snake Range, Ryegrass Canyon	−750	Cu	Eldorado Limestone	Marble	Footwall	Rahl et al. (2005) Equation 3	–	–	–	–	0.113	0.129	0.165	0.125	596	98	53	17
NSR20-39	39.44556	114.14928	Northern Snake Range, Eastern Marble Wash	10	Cu	Middle Cambrian limestone, undiff.	Dolomite	Hanging wall	Kouketsu et al. (2014) Equation 1	70.0	6.3	–	–	–	–	–	–	328	13	17	15
NSR20-38	39.44525	114.14964	Northern Snake Range, Eastern Marble Wash	−7	Cu	Notch Peak Formation	Marble	Footwall	Rahl et al. (2005) Equation 3	–	–	–	–	0.247	0.087	0.320	0.086	470	68	47	13
NSR20-37	39.44508	114.14992	Northern Snake Range, Eastern Marble Wash	−17	Cu	Notch Peak Formation	Marble	Footwall	Rahl et al. (2005) Equation 3	–	–	–	–	0.215	0.078	0.263	0.080	522	63	42	15
NSR20-36	39.44506	114.15011	Northern Snake Range, Eastern Marble Wash	−26	Cu	Notch Peak Formation	Marble	Footwall	Rahl et al. (2005) Equation 3	–	–	–	–	0.185	0.159	0.213	0.110	564	77	75	6
NSR20-35	39.44472	114.15011	Northern Snake Range, Eastern Marble Wash	−32	Cu	Dunderberg Shale	Marble	Footwall	Rahl et al. (2005) Equation 3	–	–	–	–	0.211	0.120	0.264	0.104	519	79	48	15
NSR20-31	39.44431	114.15031	Northern Snake Range, Eastern Marble Wash	−60	Cu	Raiff Limestone	Marble	Footwall	Rahl et al. (2005) Equation 3	–	–	–	–	0.207	0.144	0.230	0.112	553	82	46	17
NSR20-29	39.44425	114.15056	Northern Snake Range, Eastern Marble Wash	−71	Cu	Raiff Limestone	Marble	Footwall	Rahl et al. (2005) Equation 3	–	–	–	–	0.309	0.287	0.306	0.151	496	99	55	16
NSR20-26	39.44397	114.15058	Northern Snake Range, Eastern Marble Wash	−91	Cu	Eldorado Limestone	Marble	Footwall	Rahl et al. (2005) Equation 3	–	–	–	–	0.187	0.218	0.214	0.152	562	107	57	17
NSR20-25	39.44378	114.15078	Northern Snake Range, Eastern Marble Wash	−107	Cu	Eldorado Limestone	Marble	Footwall	Rahl et al. (2005) Equation 3	–	–	–	–	0.265	0.217	0.290	0.148	503	105	56	17
NSR20-58	39.42783	114.15847	Northern Snake Range, Marble Canyon	3	Cu	Middle Cambrian limestone, undiff.	Dolomite	Hanging wall	Kouketsu et al. (2014) Equation 1	72.2	5.1	–	–	–	–	–	–	323	11	16	15
NSR20-57	39.42764	114.15786	Northern Snake Range, Marble Canyon	1	Cu	Middle Cambrian limestone, undiff.	Dolomite	Hanging wall	Kouketsu et al. (2014) Equation 1	65.8	5.9	–	–	–	–	–	–	336	13	18	13
NSR20-56	39.42733	114.15772	Northern Snake Range, Marble Canyon	−4	Cu	Notch Peak Formation	Marble	Footwall	Rahl et al. (2005) Equation 3	–	–	–	–	0.196	0.092	0.251	0.085	529	66	39	18
NSR20-52	39.42586	114.15289	Northern Snake Range, Marble Canyon	−23	Cu	Notch Peak Formation	Marble	Footwall	Rahl et al. (2005) Equation 3	–	–	–	–	0.107	0.068	0.158	0.077	601	63	43	14
NSR20-49	39.42581	114.15167	Northern Snake Range, Marble Canyon	−31	Cu	Dunderberg Shale	Marble	Footwall	Rahl et al. (2005) Equation 3	–	–	–	–	0.349	0.267	0.325	0.167	486	113	75	11
NSR20-48	39.42569	114.15128	Northern Snake Range, Marble Canyon	−49	Cu	Dunderberg Shale	Marble	Footwall	Rahl et al. (2005) Equation 3	–	–	–	–	0.234	0.217	0.248	0.145	540	101	56	16

Tectonics
10.1029/2024TC008368

Table 1
Continued

Sample	Latitude (°N)	Longitude (°W)	Transect	Structural position (m)[a]	Map unit	Formation	Lithology	Relative to NSRD	Temperature Calibration[b]	D1 FWHM Mean	D1 FWHM 1σ	D2 FWHM Mean	D2 FWHM 1σ	R1 Mean	R1 1σ	R2 Mean	R2 1σ	T_{peak} (°C) Mean	T_{peak} (°C) 1σ	T_{peak} (°C) 2 SEM[c]	*n*
NSR20-46	39.42533	114.15133	Northern Snake Range, Marble Canyon	−69	Cu	Raiff Limestone	Marble	Footwall	Rahl et al. (2005) Equation 3	–	–	–	–	0.261	0.244	0.271	0.131	521	85	48	17
NSR20-44	39.42492	114.15133	Northern Snake Range, Marble Canyon	−87	Cu	Raiff Limestone	Marble	Footwall	Rahl et al. (2005) Equation 3	–	–	–	–	0.192	0.134	0.246	0.120	532	92	51	17
NSR21-28	39.43419	114.13539	Northern Snake Range, Easternmost Marble Canyon	190	OS	Ordovician-Silurian dolomite, undiff.	Dolomite	Hanging wall	Kouketsu et al. (2014) Equation 1*	135.3	11.5	–	–	–	–	–	–	187	25	20	15
SR19-34	39.44760	114.11067	Northern Snake Range, Easternmost Marble Wash	10	Cu	Middle Cambrian limestone, undiff.	Dolomite	Hanging wall	Kouketsu et al. (2014) Equation 1	94.1	11.6	–	–	–	–	–	–	276	25	20	15
SR19-28	39.44223	114.11308	Northern Snake Range, Easternmost Marble Wash	−20	Cu	Notch Peak Formation	Marble	Footwall	Rahl et al. (2005) Equation 3	–	–	–	–	0.311	0.224	0.317	0.111	487	71	45	15
SR19-29B	39.44386	114.11655	Northern Snake Range, Easternmost Marble Wash	−50	Cu	Dunderberg Shale	Marble	Footwall	Rahl et al. (2005) Equation 3	–	–	–	–	0.207	0.172	0.250	0.137	531	100	62	13
SR19-30	39.44523	114.12516	Northern Snake Range, Easternmost Marble Wash	−90	Cu	Raiff Limestone	Marble	Footwall	Rahl et al. (2005) Equation 3	–	–	–	–	0.217	0.144	0.274	0.082	510	52	37	15
SR19-31	39.44492	114.13211	Northern Snake Range, Easternmost Marble Wash	−120	Cu	Monte Neva Formation	Marble	Footwall	Rahl et al. (2005) Equation 3	–	–	–	–	0.292	0.183	0.298	0.138	503	98	73	9
NSR21-31	39.40450	114.08033	Northern Snake Range, Pete's Knoll	70	MIP	Ely Limestone	Limestone	Hanging wall	Kouketsu et al. (2014) Equation 2	–	–	61.7	8.6	–	–	–	–	116	58	40	15
NSR21-29	39.40664	114.08286	Northern Snake Range, Pete's Knoll	60	D	Guilmette Formation	Limestone	Hanging wall	Kouketsu et al. (2014) Equation 2	–	–	52.9	6.8	–	–	–	–	177	46	35	15
NSR21-61	39.31858	114.31256	Northern Snake Range, Fourmile Canyon	10	OS	Ordovician-Silurian dolomite, undiff.	Dolomite	Hanging wall	Kouketsu et al. (2014) Equation 1*	135.9	7.8	–	–	–	–	–	–	186	17	18	15
SR19-11	39.33390	114.11734	Northern Snake Range, Smith Creek	~100	Cu	Middle Cambrian limestone, undiff.	Dolomite	Hanging wall	Kouketsu et al. (2014) Equation 1	63.5	10.7	–	–	–	–	–	–	341	23	22	12
SR19-18	39.33311	114.12173	Northern Snake Range, Smith Creek	~50	Cu	Middle Cambrian limestone, undiff.	Dolomite	Hanging wall	Kouketsu et al. (2014) Equation 1	66.1	7.7	–	–	–	–	–	–	336	17	18	15
SR19-14B	39.33142	114.12598	Northern Snake Range, Smith Creek	−20	Cl	Prospect Mountain Quartzite	Schist	Footwall	Rahl et al. (2005) Equation 3	–	–	–	–	0.038	0.015	0.074	0.025	671	22	29	14

AGU ADVANCING EARTH AND SPACE SCIENCES
Tectonics
10.1029/2024TC008368

Table 1
Continued

Sample	Latitude (°N)	Longitude (°W)	Transect	Structural position (m)[a]	Map unit	Formation	Lithology	Relative to NSRD	Temperature Calibration[b]	D1 FWHM Mean	D1 FWHM 1σ	D2 FWHM Mean	D2 FWHM 1σ	R1 Mean	R1 1σ	R2 Mean	R2 1σ	T_{peak} (°C) Mean	T_{peak} (°C) 1σ	T_{peak} (°C) 2 SEM[c]	*n*
SR19-55	39.27561	114.16264	Northern Snake Range, Hampton Creek	10	D	Guilmette Formation	Limestone	Hanging wall	Kouketsu et al. (2014) Equation 1*	150.5	2.2	–	–	–	–	–	–	154	5	16	15
NBSR19-19	39.23933	114.11267	Northern Snake Range, Hampton Creek	10	Cu	Pole Canyon Limestone	Limestone	Hanging wall	Kouketsu et al. (2014) Equation 1	65.4	12.2	–	–	–	–	–	–	337	26	21	14
NSR21-44	39.24333	114.07175	Northern Snake Range, Hampton Creek	−10	Cu	Pole Canyon Limestone	Marble	Footwall	Rahl et al. (2005) Equation 3	–	–	–	–	0.147	0.070	0.196	0.071	573	56	40	14
NSR21-41	39.24908	114.07297	Northern Snake Range, Hampton Creek	−10	Cu	Pole Canyon Limestone	Marble	Footwall	Rahl et al. (2005) Equation 3	–	–	–	–	0.180	0.104	0.104	0.094	534	71	50	12
SR19-23	39.24261	114.08345	Northern Snake Range, Hampton Creek	−120	Z	McCoy Creek Group, Unit o	Schist	Footwall	Rahl et al. (2005) Equation 3	–	–	–	–	0.125	0.013	0.191	0.016	567	22	29	14
SR19-21B	39.24351	114.08260	Northern Snake Range, Hampton Creek	−110	Z	McCoy Creek Group, Unit o	Schist	Footwall	Rahl et al. (2005) Equation 3	–	–	–	–	0.059	0.018	0.102	0.029	647	26	29	15
SR19-25A	39.24342	114.08868	Northern Snake Range, Hampton Creek	−220	Z	McCoy Creek Group, Unit 2	Schist	Footwall	Rahl et al. (2005) Equation 3	–	–	–	–	0.253	0.022	0.302	0.017	491	14	29	13
SR19-27	39.24313	114.09280	Northern Snake Range, Hampton Creek	−250	Z	McCoy Creek Group, Unit 2	Schist	Footwall	Rahl et al. (2005) Equation 3	–	–	–	–	0.048	0.011	0.086	0.020	660	18	29	13
SR19-12	39.19506	114.07489	Northern Snake Range, Hendry's Creek	80	OS	Ordovician-Silurian dolomite, undiff.	Limestone	Hanging wall	Kouketsu et al. (2014) Equation 1	129.1	9.7	–	–	–	–	–	–	201	21	19	15
NBSR19-11	39.19625	114.07594	Northern Snake Range, Hendry's Creek	10	OS	Pogonip Group	Dolomite	Hanging wall	Kouketsu et al. (2014) Equation 1*	131.3	2.9	–	–	–	–	–	–	196	6	16	15
SR18-1	39.21583	114.12611	Northern Snake Range, Hendry's Creek	20	Cu	Notch Peak Formation	Limestone	Hanging wall	Kouketsu et al. (2014) Equation 1	119.4	12.3	–	–	–	–	–	–	221	27	19	17
SR19-15A	39.20897	114.06686	Northern Snake Range, Hendry's Creek	10	Cu	Notch Peak Formation	Limestone	Hanging wall	Kouketsu et al. (2014) Equation 1	80.4	4.5	–	–	–	–	–	–	305	10	17	14
NBSR19-14	39.20739	114.06525	Northern Snake Range, Hendry's Creek	20	Cu	Pole Canyon Limestone	Dolomite	Hanging wall	Kouketsu et al. (2014) Equation 1	42.6	2.7	–	–	–	–	–	–	386	6	16	15
NSR21-38	39.19475	114.07847	Northern Snake Range, Hendry's Creek	−10	Cu	Pole Canyon Limestone	Marble	Footwall	Rahl et al. (2005) Equation 3	–	–	–	–	0.192	0.173	0.221	0.124	558	88	52	15

Table 1
Continued

Sample	Latitude (°N)	Longitude (°W)	Transect	Structural position (m)[a]	Map unit	Formation	Lithology	Relative to NSRD	Temperature Calibration[b]	D1 FWHM Mean	D1 FWHM 1σ	D2 FWHM Mean	D2 FWHM 1σ	R1 Mean	R1 1σ	R2 Mean	R2 1σ	T_{peak} (°C) Mean	T_{peak} (°C) 1σ	T_{peak} (°C) 2 SEM[c]	*n*
SR19-9	39.21395	114.08732	Northern Snake Range, Hendry's Creek	−250	Z	McCoy Creek Group, Unit 2	Schist	Footwall	Rahl et al. (2005) Equation 3	–	–	–	–	0.060	0.016	0.098	0.024	651	21	28	15
SR19-10	39.21741	114.09483	Northern Snake Range, Hendry's Creek	−390	Z	McCoy Creek Group, Unit 5	Schist	Footwall	Rahl et al. (2005) Equation 3	–	–	–	–	0.165	0.062	0.245	0.061	527	48	40	12
NSR21-49	39.18372	114.07317	Northern Snake Range, The Cove	~250	MIP	Ely Limestone	Limestone	Hanging wall	Kouketsu et al. (2014) Equation 2	–	–	65.3	5.1	–	–	–	–	92	34	31	15
NSR21-48	39.18211	114.07283	Northern Snake Range, The Cove	30	D	Simonson Dolomite	Dolomite	Hanging wall	Kouketsu et al. (2014) Equation 2	–	–	49.8	2.1	–	–	–	–	197	14	27	15
NSR21-46	39.18158	114.09161	Northern Snake Range, The Cove	10	Cu	Notch Peak Formation	Limestone	Hanging wall	Kouketsu et al. (2014) Equation 1	112.1	4.3	–	–	–	–	–		237	9	16	15
NSR21-45	39.18231	114.09142	Northern Snake Range, The Cove	−10	Cu	Pole Canyon Limestone	Marble	Footwall	Rahl et al. (2005) Equation 3	–	–	–	–	0.136	0.064	0.196	0.074	570	60	42	14
SR19-68	39.29331	114.22003	Northern Snake Range, The Table	~220	D	Guilmette Formation	Limestone	Hanging wall	Kouketsu et al. (2014) Equation 2	–	–	53.3	2.4	–	–	–	–	174	16	27	15
SR19-65	39.29053	114.21550	Northern Snake Range, The Table	~340	D	Sevy Dolomite	Dolomite	Hanging wall	Kouketsu et al. (2014) Equation 1*	131.3	12.0	–	–	–	–	–	–	196	26	20	15
SR19-64	39.29028	114.21447	Northern Snake Range, The Table	~330	OS	Ordovician-Silurian dolomite, undiff.	Limestone	Hanging wall	Kouketsu et al. (2014) Equation 1	103.5	4.8	–	–	–	–	–	–	255	10	20	15
SR19-63	39.28933	114.21358	Northern Snake Range, The Table	~320	OS	Ordovician-Silurian dolomite, undiff.	Limestone	Hanging wall	Kouketsu et al. (2014) Equation 2	–	–	49.8	6.2	–	–	–	–	197	42	34	15
SR19-61	39.28867	114.20850	Northern Snake Range, The Table	~450	Cu	Lincoln Peak Formation	Limestone	Hanging wall	Kouketsu et al. (2014) Equation 1	83.1	4.0	–	–	–	–	–	–	299	9	16	16
NSR21-51	39.24806	114.33006	Northern Snake Range, Negro Creek	~300	MIP	Ely Limestone	Limestone	Hanging wall	Kouketsu et al. (2014) Equation 2	–	–	67.8	4.7	–	–	–	–	75	32	31	15
NSR21-52	39.24836	114.33058	Northern Snake Range, Negro Creek	~550	OS	Pogonip Group	Limestone	Hanging wall	Kouketsu et al. (2014) Equation 1	90.4	8.0	–	–	–	–	–	–	284	17	18	15
NSR21-53	39.24908	114.33222	Northern Snake Range, Negro Creek	~200	Cu	Lincoln Peak Formation	Limestone	Hanging wall	Kouketsu et al. (2014) Equation 1	101.3	10.0	–	–	–	–	–	–	260	22	22	11
NBSR20-74B	39.27542	114.26828	Northern Snake Range, Negro Creek	−90	Cl	Prospect Mountain Quartzite	Schist	Footwall	Rahl et al. (2005) Equation 3	–	–	–	–	0.112	0.044	0.197	0.065	561	57	39	15
JL1-156	39.27407	114.24127	Northern Snake Range, Negro Creek	−80	Cl	Prospect Mountain Quartzite	Quartzite	Footwall	Rahl et al. (2005) Equation 3	–	–	–	–	0.868	0.086	0.500	0.035	421	28	33	12

AGU ADVANCING EARTH AND SPACE SCIENCES
Tectonics
10.1029/2024TC008368

10.1029/2024TC008368

Table 1
Continued

Sample	Latitude (°N)	Longitude (°W)	Transect	Structural position (m)[a]	Map unit	Formation	Lithology	Relative to NSRD	Temperature Calibration[b]	D1 FWHM Mean	D1 FWHM 1σ	D2 FWHM Mean	D2 FWHM 1σ	R1 Mean	R1 1σ	R2 Mean	R2 1σ	T_{peak} (°C) Mean	T_{peak} (°C) 1σ	T_{peak} (°C) 2 SEM[c]	n
NSR21-26	39.45575	113.82867	Northwestern Confusion Range	–	MIP	Ely Limestone	Limestone	Hanging wall	Kouketsu et al. (2014) Equation 1*	188.1	5.8	–	–	–	–	–	–	74	13	17	15
NSR21-27	39.46597	113.80214	Northwestern Confusion Range	–	MIP	Joana Limestone	Limestone	Hanging wall	Kouketsu et al. (2014) Equation 2	–	–	58.7	4.1	–	–	–	–	137	28	29	15
NSR21-24	39.46658	113.88294	Northwestern Confusion Range	–	D	Simonson Dolomite	Dolomite	Hanging wall	Kouketsu et al. (2014) Equation 2	–	–	54.7	3.3	–	–	–	–	164	22	28	15
NSR21-36	39.08897	113.87681	West-central Confusion Range	–	MIP	Ely Limestone	Limestone	Hanging wall	Kouketsu et al. (2014) Equation 2	–	–	66.2	5.6	–	–	–	–	86	38	32	15
NSR21-34	39.10664	113.90081	West-central Confusion Range	–	D	Guilmette Formation	Limestone	Hanging wall	Kouketsu et al. (2014) Equation 2	–	–	53.9	3.5	–	–	–	–	169	24	28	16
NSR21-33	39.11508	113.93667	West-central Confusion Range	–	OS	Laketown Dolomite	Dolomite	Hanging wall	Kouketsu et al. (2014) Equation 1*	130.3	8.1	–	–	–	–	–	–	198	17	18	15

Note. NSRD, Northern Snake Range décollement; FWHM, full width at half-maximum; T_{peak}, peak temperature; SEM, standard error of the mean; *n*, number of grain spot analyses that support T_{peak}. [a]Structural position was measured as foliation- or bedding-normal distance below or above the structurally lowest Schell Creek Range detachment fault for Duck Creek and Schell Creek Range samples, and foliation-normal distance below or detachment-normal distance above the NSRD for Northern Snake Range samples. [b]T_{peak} values >400°C were determined using Equation 3 of Rahl et al. (2005), T_{peak} values between 200 and 400°C were determined using Equation 1 of Kouketsu et al. (2014), and T_{peak} values <200°C were determined using Equation 2 of Kouketsu et al. (2014). Equation 1 of Kouketsu et al. (2014) was utilized for seven samples (marked with asterisks) that yielded mean T_{peak} values below the 200°C calibration threshold for this equation, because mean T_{peak} values yielded by Kouketsu et al. (2014) Equation 2 for these samples were even further out of its 150–200°C calibration range. [c]After Cooper et al. (2013), T_{peak} values are reported with 2 standard errors of the mean (SEM), calculated from quadratic addition of 1σ internal error and the external error of ±50°C from Rahl et al. (2005) Equation 3, ±30°C from Kouketsu et al. (2014) Equation 1, or ±50°C from Kouketsu et al. (2014) Equation 2, divided by the square root of the number of individual grain spot analyses (*n*).

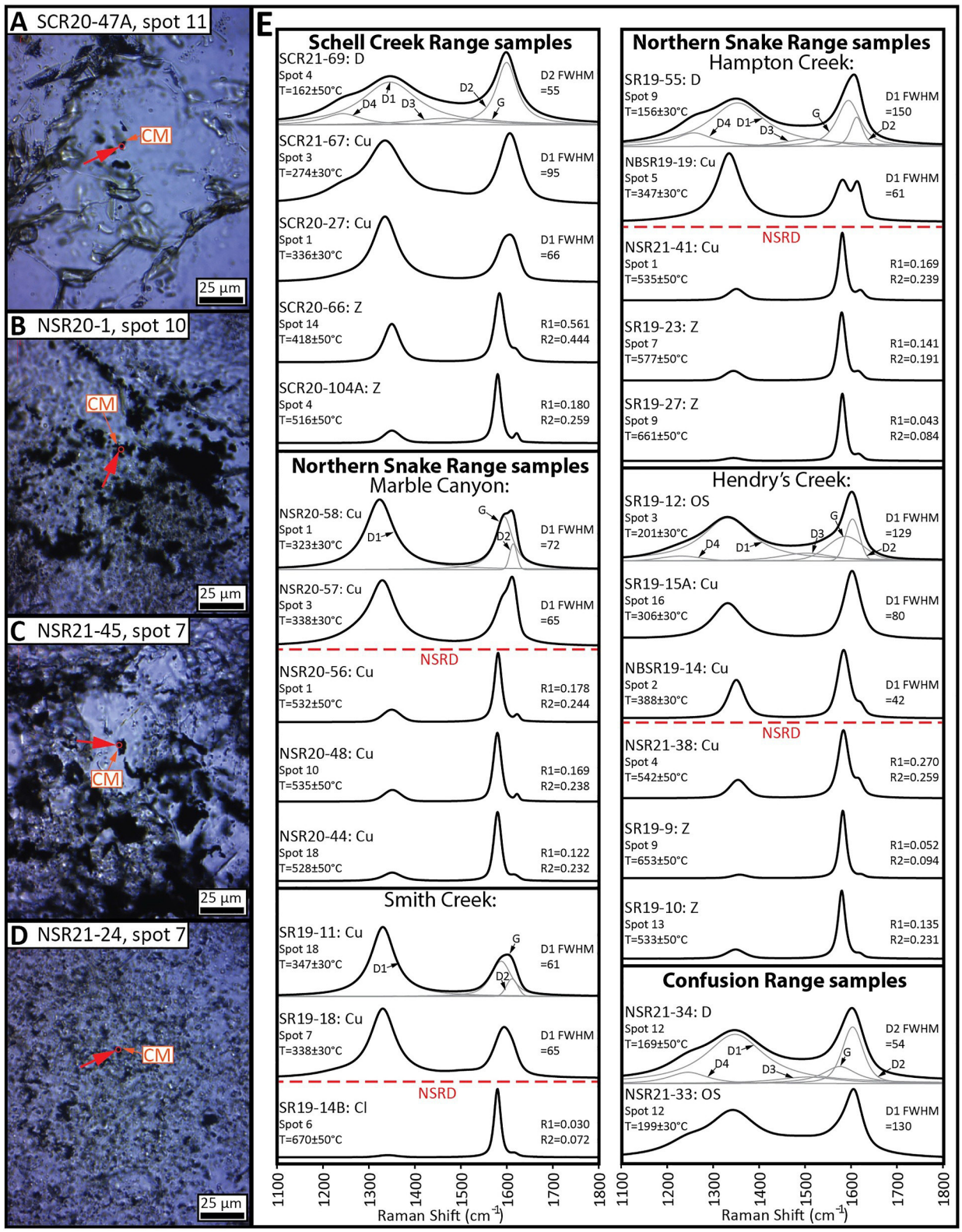

Figure 7.

($n = 6$) yielded temperatures that vary from ~310 to 380°C in the Egan and Deep Creek Ranges, to ~530°C in the Schell Creek Range, to ~420–670°C in the NSRD footwall (Figure 8d).

Neoproterozoic rocks in the Schell Creek Range ($n = 10$) yielded RSCM temperatures typically between ~470 and 525°C (502 ± 34°C average; Figures 8e and 8h). Neoproterozoic rocks in the Deep Creek Range ($n = 6$) yielded RSCM temperatures typically between ~575 and 625°C (586 ± 36°C average; Figures 8e and 8h). Neoproterozoic rocks in the NSRD footwall yielded overall similar temperatures between RSCM ($n = 6$) and thermobarometry ($n = 9$), with a total range between ~490 and 660°C (588 ± 61°C average; Figures 8e and 8h).

To quantify trends with depth, we graphed T_{peak} values against stratigraphic depth below the top of the Triassic section (Figure 9), using representative stratigraphic columns from specific ranges (see Figure 9 caption). These graphs yielded best-fit T_{peak} gradients of 57°C/km in the Schell Creek and Duck Creek Ranges (Figure 9a) (down to 12.5 km depth; $n = 36$), 49°C/km in the Deep Creek Range, Kern Mountains, and Antelope Range (Figure 9b) (down to 14.5 km depth; $n = 29$), and 53°C/km in the Confusion and House Ranges (Figure 9c) (down to 8.5 km depth; $n = 43$). In the Northern Snake Range, Cambrian to Permian rocks in the NSRD hanging wall yielded a best-fit T_{peak} gradient of 56°C/km (Figure 9d) (down to 8 km depth; $n = 45$). NSRD footwall rocks ($n = 60$), when graphed versus restored stratigraphic depth (i.e., after retro-deforming ductile strain; Figures 4b and 5b), exhibit T_{peak} values that largely overlap within error between ~6 and 13 km depth (Figure 9d). Middle-Upper Cambrian rocks in the NSRD footwall yielded consistent temperatures of ~500–600°C and Neoproterozoic rocks vary between ~500 and 650°C. Importantly, most Neoproterozoic samples in the NSRD footwall (including the majority of thermobarometry samples) fall close to the 56°C/km best-fit gradient defined by NSRD hanging wall rocks, and thus did not attain hotter conditions than predicted by this upper-crustal gradient (Figure 9d). Graphing all data from the NSRD hanging wall and surrounding ranges together ($n = 153$) defines an approximately linear downward-increasing trend to a pre-extensional depth of 14.5 km, which is best-fit by an average regional T_{peak} gradient of 56°C/km (Figure 9e). In contrast, projecting the T_{peak} values of the nine NSRD footwall thermobarometry samples to ~21–30 km lithostatic depths yields a much cooler (by a factor of 2.5) best-fit gradient of 22°C/km (Figure 9e). We acknowledge that this is an average T_{peak} gradient calculated between the surface and ~21–30 km depth, and therefore does not necessarily represent a true geotherm, which does not have to remain linear across such a large range of crustal depths.

We also graphed T_{peak} versus restored structural depth below the top of the Triassic section (Figure 10), as measured from our reconstructed cross sections in Figures 4c, 5c, and 6b. These graphs yielded best-fit T_{peak} gradients of 30°C/km for the Schell Creek and Duck Creek Ranges (Figure 10a) (down to 18.5 km depth; $n = 45$), 37°C/km for the Deep Creek Range, Kern Mountains, and Antelope Range (Figure 10b) (down to 20 km depth; $n = 29$), and 44°C/km for the Confusion and House Ranges (Figure 10c) (down to 12 km depth; $n = 43$). NSRD hanging wall samples yielded a best-fit gradient of 34°C/km (down to 10 km depth). Graphing all data from the NSRD hanging wall and surrounding ranges together (Figure 10e) yields an approximately linear trend that is best-fit by a regional T_{peak} gradient of 36°C/km, which is 1.6 times greater than the 22°C/km best-fit T_{peak} gradient predicted by projecting thermobarometry samples to lithostatic depths (Figure 10e).

In seven localities in the Northern Snake Range (Figure 2), spatially dense sampling transects constrain T_{peak} patterns as a function of present-day structural depth beneath the NSRD, as well as the upward decrease in T_{peak} across the NSRD (Figure 11). For five transects in the northern part of the range (the Western Marble Wash, Ryegrass Canyon, Marble Canyon, and Eastern Marble Wash sections of Long et al. (2023), and the Easternmost Marble Wash section of this study), T_{peak} in Middle-Upper Cambrian carbonates is largely invariant with structural depth below the NSRD, with similar mean T_{peak} values of 508 ± 57°C, 556 ± 25°C, 535 ± 34°C, 523 ± 31°C, and 502 ± 18°C, respectively (Figures 11a–11e). In the Hampton Creek and Hendry's Creek

Figure 7. (a–d): Photomicrographs of representative examples of analyzed grains of carbonaceous material (CM) from thin sections of (a) Schell Creek Range, (b and c) Northern Snake Range, and (d) Confusion Range samples (taken in plane-polarized light). Red circles represent the approximate area of the analyzed spot. (e) Examples of representative Raman spectra from single CM grain analyses of samples from the Schell Creek Range, Northern Snake Range (samples from four transects are shown; samples in each transect are ordered from structurally lowest at the bottom and structurally highest at the top), and Confusion Range. Unit abbreviations listed after sample numbers are as follows: "Z" = Neoproterozoic, "Cl" = lower Cambrian, "Cu" = middle-upper Cambrian, "OS" = Ordovician-Silurian, "D" = Devonian, NSRD = Northern Snake Range décollement. Positions of the graphite peak (G) and defect peaks (D1–D4) are labeled for the top sample in each sample group. R1 and R2 parameters are calculated after Rahl et al. (2005). FWHM = full width at half-maximum. Single grain analyses are listed with the external uncertainty of their corresponding calibration equation (see Table 1).

Table 2

Summary of Published RSCM Thermometry From the Egan Range, Schell Creek Range, Deep Creek Range, House Range, and Northern Snake Range, and Published Thermobarometry From the Northern Snake Range

Sample	Source publication	Latitude (°N)	Longitude (°W)	Transect	Structural position (m)[a]	Map unit	Formation	Lithology	Technique	Temperature calibration	T_{peak} (°C) Mean	T_{peak} (°C) Error[b]	*n*	Pressure calibration	Pressure (kbar)	Pressure error (kbar)[b]
ER19-13	Blackford et al. (2022)	39.73731	114.92717	Egan Range	–	D	Sevy Dolomite	Dolomite	RSCM	Kouketsu et al. (2014), Equation 2	154	19	13	–	–	–
ER19-18	Blackford et al. (2022)	39.72733	114.91086	Egan Range	–	Cu	Windfall Formation	Limestone	RSCM	Kouketsu et al. (2014) Equation 1	233	19	11	–	–	–
ER19-11	Blackford et al. (2022)	39.73433	114.86042	Egan Range	–	Cl	Pioche Shale	Shale	RSCM	Kouketsu et al. (2014) Equation 1	307	18	11	–	–	–
SCR18-13	Blackford et al. (2022)	39.47306	114.63667	Schell Creek Range, cross section B-B′	400	Cu	Windfall Formation	Limestone	RSCM	Kouketsu et al. (2014) Equation 1	278	20	10	–	–	–
SCR18-8	Blackford et al. (2022)	39.47278	114.61556	Schell Creek Range, cross section B-B′	−50	Cu	Eldorado Limestone	Limestone	RSCM	Kouketsu et al. (2014) Equation 1	338	19	11	–	–	–
SC16-6	Blackford et al. (2022)	39.42494	114.56092	Schell Creek Range, cross section B-B′	−2,510	Z	McCoy Creek Group, Unit C	Slate	RSCM	Rahl et al. (2005) Equation 3	472	36	11	–	–	–
SC16-5	Blackford et al. (2022)	39.42417	114.55325	Schell Creek Range, cross section B-B′	−2,990	Z	McCoy Creek Group, Unit F	Argillite	RSCM	Rahl et al. (2005) Equation 3	511	35	17	–	–	–
SC16-4	Blackford et al. (2022)	39.42731	114.54350	Schell Creek Range, cross section B-B′	−3,620	Z	McCoy Creek Group, Unit H	Phyllite	RSCM	Rahl et al. (2005) Equation 3	512	35	14	–	–	–
SC16-3	Blackford et al. (2022)	39.42928	114.54022	Schell Creek Range, cross section B-B′	−3,910	Z	McCoy Creek Group, Unit I	Marble	RSCM	Rahl et al. (2005) Equation 3	505	40	15	–	–	–
SC16-1	Blackford et al. (2022)	39.43225	114.53303	Schell Creek Range, cross section B-B′	−4,350	Z	McCoy Creek Group, Unit J	Marble	RSCM	Rahl et al. (2005) Equation 3	523	38	16	–	–	–
DCR17-20	Blackford et al. (2022)	39.76364	114.13639	Deep Creek Range	–	MIP	Chainman Shale	Limestone	RSCM	Kouketsu et al. (2014) Equation 2	130	32	12	–	–	–
DCR17-17	Blackford et al. (2022)	39.74503	114.12486	Deep Creek Range	–	D	Guilmette Formation	Dolomite	RSCM	Kouketsu et al. (2014) Equation 2	166	30	12	–	–	–
DCR17-15	Blackford et al. (2022)	39.73592	114.11942	Deep Creek Range	–	OS	Hanson Creek/Lone Mountain Dolomite	Dolomite	RSCM	Kouketsu et al. (2014) Equation 1	298	17	13	–	–	–
DCR17-13	Blackford et al. (2022)	39.73342	114.09233	Deep Creek Range	–	OS	Pogonip Group	Limestone	RSCM	Kouketsu et al. (2014) Equation 1	314	21	11	–	–	–
DCR17-11	Blackford et al. (2022)	39.73231	114.08158	Deep Creek Range	–	Cu	Mid-Upper Cambrian limestone, undiff.	Limestone	RSCM	Kouketsu et al. (2014) Equation 1	369	19	10	–	–	–

Tectonics
10.1029/2024TC008368

10.1029/2024TC008368

Table 2
Continued

Sample	Source publication	Latitude (°N)	Longitude (°W)	Transect	Structural position (m)[a]	Map unit	Formation	Lithology	Technique	Temperature calibration	T_{peak} (°C) Mean	T_{peak} (°C) Error[b]	*n*	Pressure calibration	Pressure (kbar)	Pressure error (kbar)[b]
DCR17-09	Blackford et al. (2022)	39.72844	114.07119	Deep Creek Range	–	Cu	Mid-Upper Cambrian limestone, undiff.	Limestone	RSCM	Kouketsu et al. (2014) Equation 1	361	20	10	–	–	–
DCR17-07	Blackford et al. (2022)	39.73181	114.06217	Deep Creek Range	–	Cu	Mid-Upper Cambrian limestone, undiff.	Limestone	RSCM	Kouketsu et al. (2014) Equation 1	372	19	10	–	–	–
DCR17-03	Blackford et al. (2022)	39.73506	114.04239	Deep Creek Range	–	Cl	Pioche Shale	Slate	RSCM	Kouketsu et al. (2014) Equation 1	381	13	13	–	–	–
DR-342J	Blackford et al. (2022)	39.72778	113.99861	Deep Creek Range	–	Z	McCoy Creek Group, Unit e	Slate	RSCM	Rahl et al. (2005) Equation 3	517	39	16	–	–	–
DR-329E	Blackford et al. (2022)	39.75556	113.88889	Deep Creek Range	–	Z	McCoy Creek Group, Unit b	Argillite	RSCM	Rahl et al. (2005) Equation 3	577	40	12	–	–	–
DR-338B	Blackford et al. (2022)	39.73611	113.90278	Deep Creek Range	–	Z	Trout Creek Formation, Unit 6	Slate	RSCM	Rahl et al. (2005) Equation 3	581	44	11	–	–	–
DR-336A4	Blackford et al. (2022)	39.71806	113.89028	Deep Creek Range	–	Z	Trout Creek Formation, Unit 5	Quartzite	RSCM	Rahl et al. (2005) Equation 3	621	32	13	–	–	–
DR-334E	Blackford et al. (2022)	39.75278	113.88611	Deep Creek Range	–	Z	Trout Creek Formation, Unit 3	Schist	RSCM	Rahl et al. (2005) Equation 3	624	39	8	–	–	–
DR-433G	Blackford et al. (2022)	39.74861	113.87222	Deep Creek Range	–	Z	Trout Creek Formation, Unit 1	Schist	RSCM	Rahl et al. (2005) Equation 3	597	43	13	–	–	–
HR19-5	Blackford et al. (2022)	39.01606	113.42181	House Range	–	OS	Laketown Dolomite	Dolomite	RSCM	Kouketsu et al. (2014) Equation 1	207	19	10	–	–	–
HR19-3	Blackford et al. (2022)	39.03389	113.34156	House Range	–	OS	Fillmore Formation	Shale	RSCM	Kouketsu et al. (2014) Equation 1	235	22	11	–	–	–
HR19-1	Blackford et al. (2022)	39.05936	113.26197	House Range	–	Cu	Notch Peak Formation	Limestone	RSCM	Kouketsu et al. (2014) Equation 1	267	19	11	–	–	–
HR19-13B	Blackford et al. (2022)	39.22114	113.37633	House Range	–	Cu	Weeks Limestone	Limestone	RSCM	Rahl et al. (2005) Equation 3	457	32	12	–	–	–
HR19-12	Blackford et al. (2022)	39.23006	113.37675	House Range	–	Cu	Marjum Formation	Limestone	RSCM	Kouketsu et al. (2014) Equation 1	329	20	10	–	–	–
FMW76	Cooper (2008)	39.44367	114.12631	Northern Snake Range, easternmost Marble Wash	−100	Cu	Raiff Limestone	Marble	RSCM	Aoya et al. (2010), Equation 3	479	54	10	–	–	–
16CH34	Hoiland et al. (2022)	39.46608	114.25099	Northern Snake Range, western Marble Wash	−10	OS	Pogonip Group	Marble	RSCM	Aoya et al. (2010), Equation 3	530	68	4	–	–	–

Table 2
Continued

Sample	Source publication	Latitude (°N)	Longitude (°W)	Transect	Structural position (m)[a]	Map unit	Formation	Lithology	Technique	Temperature calibration	T_{peak} (°C) Mean	T_{peak} (°C) Error[b]	*n*	Pressure calibration	Pressure (kbar)	Pressure error (kbar)[b]
16CH26	Hoiland et al. (2022)	39.44408	114.15074	Northern Snake Range, eastern Marble Wash	−100	Cu	Eldorado Limestone	Marble	RSCM	Aoya et al. (2010), Equation 3	539	51	30	–	–	–
16CH28	Hoiland et al. (2022)	39.44374	114.15074	Northern Snake Range, eastern Marble Wash	−109	Cu	Eldorado Limestone	Marble	RSCM	Aoya et al. (2010), Equation 3	569	53	12	–	–	–
16CH24a	Hoiland et al. (2022)	39.44409	114.15064	Northern Snake Range, eastern Marble Wash	−88	Cu	Monte Neva Formation	Marble?	RSCM	Aoya et al. (2010), Equation 3	496	52	30	–	–	–
16CH22	Hoiland et al. (2022)	39.44418	114.15048	Northern Snake Range, eastern Marble Wash	−69	Cu	Raiff Limestone	Marble	RSCM	Aoya et al. (2010), Equation 3	521	51	30	–	–	–
16CH14b	Hoiland et al. (2022)	39.44510	114.15013	Northern Snake Range, eastern Marble Wash	−18	Cu	Notch Peak Formation	Marble	RSCM	Aoya et al. (2010), Equation 3	475	51	20	–	–	–
16CH13	Hoiland et al. (2022)	39.44539	114.14985	Northern Snake Range, eastern Marble Wash	−3	Cu	Notch Peak Formation	Marble	RSCM	Aoya et al. (2010), Equation 3	532	53	16	–	–	–
16CH12a	Hoiland et al. (2022)	39.44571	114.14985	Northern Snake Range, eastern Marble Wash	7	Cu	Middle Cambrian limestone, undiff.	Limestone	RSCM	Kouketsu et al. (2014) Equation 1	315	51	12	–	–	–
16CH09b	Hoiland et al. (2022)	39.44825	114.14992	Northern Snake Range, eastern Marble Wash	~200	Cu	Middle Cambrian limestone, undiff.	Limestone	RSCM	Kouketsu et al. (2014) Equation 1	264	52	17	–	–	–
16CH07b	Hoiland et al. (2022)	39.44955	114.15028	Northern Snake Range, eastern Marble Wash	~260	Cu	Middle Cambrian limestone, undiff.	Limestone	RSCM	Kouketsu et al. (2014) Equation 1	293	59	4	–	–	–
16CH42	Hoiland et al. (2022)	39.47702	114.03873	Northern Snake Range, Spring Mountain	–	Cu	Dunderberg Shale	Marble?	RSCM	Kouketsu et al. (2014) Equation 1	325	52	15	–	–	–
16CH52	Hoiland et al. (2022)	39.49118	114.04197	Northern Snake Range, Spring Mountain	–	OS	Silurian-Ordovician dolomite, undiff.	Dolomite	RSCM	Kouketsu et al. (2014) Equation 1	251	51	7	–	–	–
16CH58	Hoiland et al. (2022)	39.40621	114.08143	Northern Snake Range, Pete's Knoll	70	D	Guilmette Formation	Dolomite	RSCM	Kouketsu et al. (2014) Equation 1	202	51	11	–	–	–
16CH56	Hoiland et al. (2022)	39.40614	114.08177	Northern Snake Range, Pete's Knoll	270	MIP	Joana Limestone	Limestone	RSCM	Kouketsu et al. (2014) Equation 2	193	50	6	–	–	–
1	Lewis et al. (1999)	39.24437	114.08482	Northern Snake Range, Hampton Creek	−200	Z	McCoy Creek Group, unit 2	Metapelite	*P-T*	GARB	660	140	–	GASP, GMBP	7.05	1.55
3	Lewis et al. (1999)	39.24682	114.10881	Northern Snake Range, Hampton Creek	−370	Z	McCoy Creek Group, unit 2	Metapelite	*P-T*	GARB	610	50	–	GASP, GMBP	8.1	0.7
FDC62	Cooper, Platt, Anczkiewicz, and Whitehouse (2010)	39.30479	114.21766	Northern Snake Range, Deadman Creek	~−400	Z	McCoy Creek Group, unit o	Metapelite	*P-T*	GARB	654	60	–	GMBP	8.2	0.9

Tectonics
10.1029/2024TC008368

Table 2
Continued

Sample	Source publication	Latitude (°N)	Longitude (°W)	Transect	Structural position (m)[a]	Map unit	Formation	Lithology	Technique	Temperature calibration	T_{peak} (°C) Mean	T_{peak} (°C) Error[b]	*n*	Pressure calibration	Pressure (kbar)	Pressure error (kbar)[b]
FDe178	Cooper, Platt, Anczkiewicz, and Whitehouse (2010)	39.32058	114.14078	Northern Snake Range, Smith Creek	~−480	Z	McCoy Creek Group, unit 2	Metapelite	*P-T*	GARB	650	67	–	GMBP	8.2	1.0
FHa49	Cooper, Platt, Anczkiewicz, and Whitehouse (2010)	39.24821	114.12369	Northern Snake Range, Hampton Creek	−390	Z	McCoy Creek Group, unit 2	Metapelite	*P-T*	GARB	578	58	–	GMBP	7.9	0.9
FHa270	Cooper, Platt, Anczkiewicz, and Whitehouse (2010)	39.24512	114.10765	Northern Snake Range, Hampton Creek	−360	Z	McCoy Creek Group, unit 2	Metapelite	*P-T*	GARB	568	57	–	GMBP	7.7	0.9
FHe9	Cooper, Platt, Anczkiewicz, and Whitehouse (2010)	39.20787	114.07891	Northern Snake Range, Hendry's Creek	−180	Z	McCoy Creek Group, unit 2	Metapelite	*P-T*	GARB	509	59	–	GMBP	5.7	0.9
FHe269	Cooper, Platt, Anczkiewicz, and Whitehouse (2010)	39.23590	114.16934	Northern Snake Range, Hendry's Creek	−450	Z	McCoy Creek Group, unit 2	Metapelite	*P-T*	GARB	505	46	–	GMBP	6.1	0.7
FSi18	Cooper, Platt, Anczkiewicz, and Whitehouse (2010)	39.18529	114.22828	Northern Snake Range, Silver Creek	~−280	Z	McCoy Creek Group, unit 2	Metapelite	*P-T*	GARB	548	69	–	GMBP	6.0	1.0

[a]Structural position was measured as foliation- or bedding-normal distance below or above the structurally lowest Schell Creek Range detachment fault for Duck Creek and Schell Creek Range samples, and foliation-normal distance below or detachment-normal distance above the NSRD for Northern Snake Range samples. [b]Errors for Blackford et al. (2022) data are listed at a two standard error of the mean level, which was calculated using an identical procedure to that described in footnote 3 of Table 1. Errors for Cooper (2008) and Hoiland et al. (2022) data are total errors. *P-T* data from Lewis et al. (1999) are final equilibration *P-T* values from their page 47. Errors listed for Lewis et al. (1999) data are the total error of the range of overlap of *P-T* fields from GARB, GMBP, and GASP from two thin sections per sample. *P-T* data from Cooper, Platt, Anczkiewicz, and Whitehouse (2010) are average peak *P* and *T* values from their Table 4. Errors listed for Cooper, Platt, Anczkiewicz, and Whitehouse (2010) data are reported at a two standard error or the mean level (from their Table 4).

Tectonics
10.1029/2024TC008368

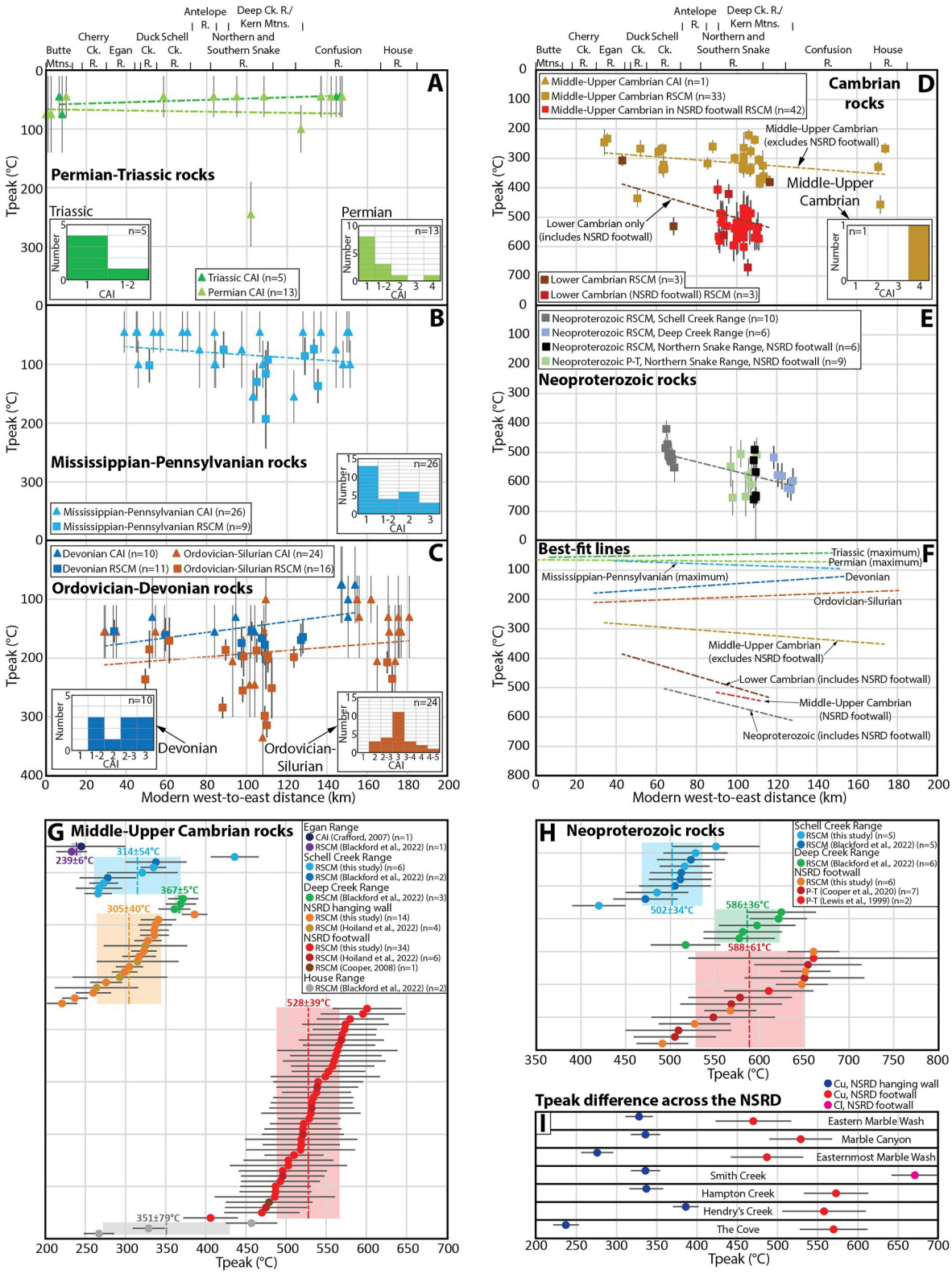

Figure 8.

drainages in the southeastern part of the range, T_{peak} values from Cambrian-Neoproterozoic rocks (which include thermobarometry and RSCM data) do not exhibit a trend with depth below the NSRD and yield mean T_{peak} values of 589 ± 53°C and 561 ± 55°C, respectively (Figures 11f and 11g). The upward temperature decrease across the NSRD will vary at any given locality, depending on the age of rocks in the overlying hanging wall klippen. When Middle-Upper Cambrian rocks are in the hanging wall, this upward temperature decrease is generally on the order of ~200°C, although it is locally as high as ~300°C (Figures 8i and 11c–11g).

4.4. Arguments Against Deep Structural Burial of the NSRD Footwall From the T_{peak} Data set

The T_{peak} data set for the Northern Snake Range and surrounding region supports several strong arguments against the deep structural burial of the NSRD footwall.

4.4.1. Regional T_{peak} Gradients Record Late Cretaceous Syn-Metamorphic/Magmatic Peak Crustal Thermal Conditions

Multiple geochronologic and thermochronologic studies in the Northern Snake, Schell Creek, and Deep Creek Ranges have documented Late Cretaceous (~73–91 Ma total range) peak metamorphism (Cooper, Platt, Anczkiewicz, & Whitehouse, 2010; Huggins & Wright, 1989; E. L. Miller et al., 1988; Rodgers, 1987), which was contemporaneous with Late Cretaceous (~101-75 Ma total range) granitic magmatism (Gottlieb et al., 2022; Kenney, 2013; E. L. Miller et al., 1988). Thermochronology from deeply exhumed portions of these ranges defines Late Cretaceous to Middle Eocene (~70-40 Ma), post-metamorphic/magmatic cooling, with no evidence of significant reheating during ≤~38 Ma extension (Armstrong, 1970; Best et al., 1974; Gébelin et al., 2011; Hoiland, 2019; D. E. Lee et al., 1980; J. Lee, 1995; J. Lee & Sutter, 1991; E. L. Miller et al., 1988; E. L. Miller, Dumitru, et al., 1999). Based on these data, many previous studies have concluded that peak thermal conditions in this region were attained during the Late Cretaceous (Barton, 1990; Barton et al., 1988; Blackford et al., 2022; Hoiland et al., 2022; C. F. Miller & Bradfish, 1980; E. L. Miller & Gans, 1989; E. L. Miller et al., 1988), which is consistent with recent interpretations from other areas of eastern Nevada (Long & Soignard, 2016; Vlaha et al., 2024; Zuza et al., 2020, 2022). Based on the geo- and thermo-chronologic data summarized above, we interpret that the average regional T_{peak} gradients that we calculate (Figures 9e and 10e) record the peak thermal conditions of the middle-upper crust that were attained during Late Cretaceous metamorphism and magmatism.

4.4.2. No Stratigraphic Overburden Above the Triassic Section

Permian-Triassic rocks yield T_{peak} values <50–80°C (Figures 8a and 8f) (Crafford, 2007; Harris et al., 1980), and their cumulative preserved thickness across this region is up to 2.1–2.5 km (Figure 9) (e.g., Stewart, 1980). Half of the Mississippian-Pennsylvanian samples yield T_{peak} values <50–80°C, with most of the rest yielding <140–150°C, and the restored base of the Mississippian section is as deep as 3.2–3.7 km across this region (Figure 9). These T_{peak} and depth constraints define a maximum T_{peak} gradient of 38–47°C/km through the Mississippian-Triassic section, which falls between the 36 and 56°C/km regional T_{peak} gradients that we calculated versus stratigraphic and structural depth, respectively (Figures 9e and 10e). Therefore, T_{peak} data rule out the existence of a thick package of overlying Mesozoic sedimentary rocks in eastern Nevada and western Utah, which has been hypothesized by Royse (1993), Bjerrum and Dorsey (1995), and Allen et al. (2000). Instead, T_{peak} data indicate that the top of the Triassic section approximated the surface prior to any syn-Cordilleran erosion (e.g., Long, 2012; Thorman et al., 2019). This rules out stratigraphic overburden as a mechanism to account for deep burial of NSRD footwall rocks.

Figure 8. (a–e) Graphs of T_{peak} vs. modern west-to-east distance for: (a) Permian-Triassic sedimentary rocks; (b) Mississippian-Pennsylvanian sedimentary rocks; (c) Ordovician-Devonian sedimentary rocks; (d) Cambrian sedimentary rocks; and (e) Neoproterozoic metasedimentary rocks. Frequency histograms of CAI values are shown for graphs (a–d). "Ck." = creek, "Mtns." = mountains. "R." = range. (f) Compilation of best-fit lines from graphs (a–e). (g) Graph of T_{peak} data from Middle-Upper Cambrian rocks in the Egan, Schell Creek, Deep Creek, Northern Snake, and House Ranges, with samples from each range ordered from low to high T_{peak} and corresponding mean T_{peak} values listed (with 1σ error range illustrated by the shaded area). (h) Graph of T_{peak} data from Neoproterozoic metasedimentary rocks in the Schell Creek, Deep Creek, and Northern Snake Ranges, with all samples from each range ordered from low to high T_{peak} and corresponding mean T_{peak} values listed (with 1σ error range illustrated by the shaded area). (i) Graph of the difference in T_{peak} across the Northern Snake Range décollement (NSRD) in seven localities in the Northern Snake Range (locations shown on Figure 2). Graphed data are from the structurally highest sample in the NSRD footwall and the structurally lowest sample in the NSRD hanging wall in each locality.

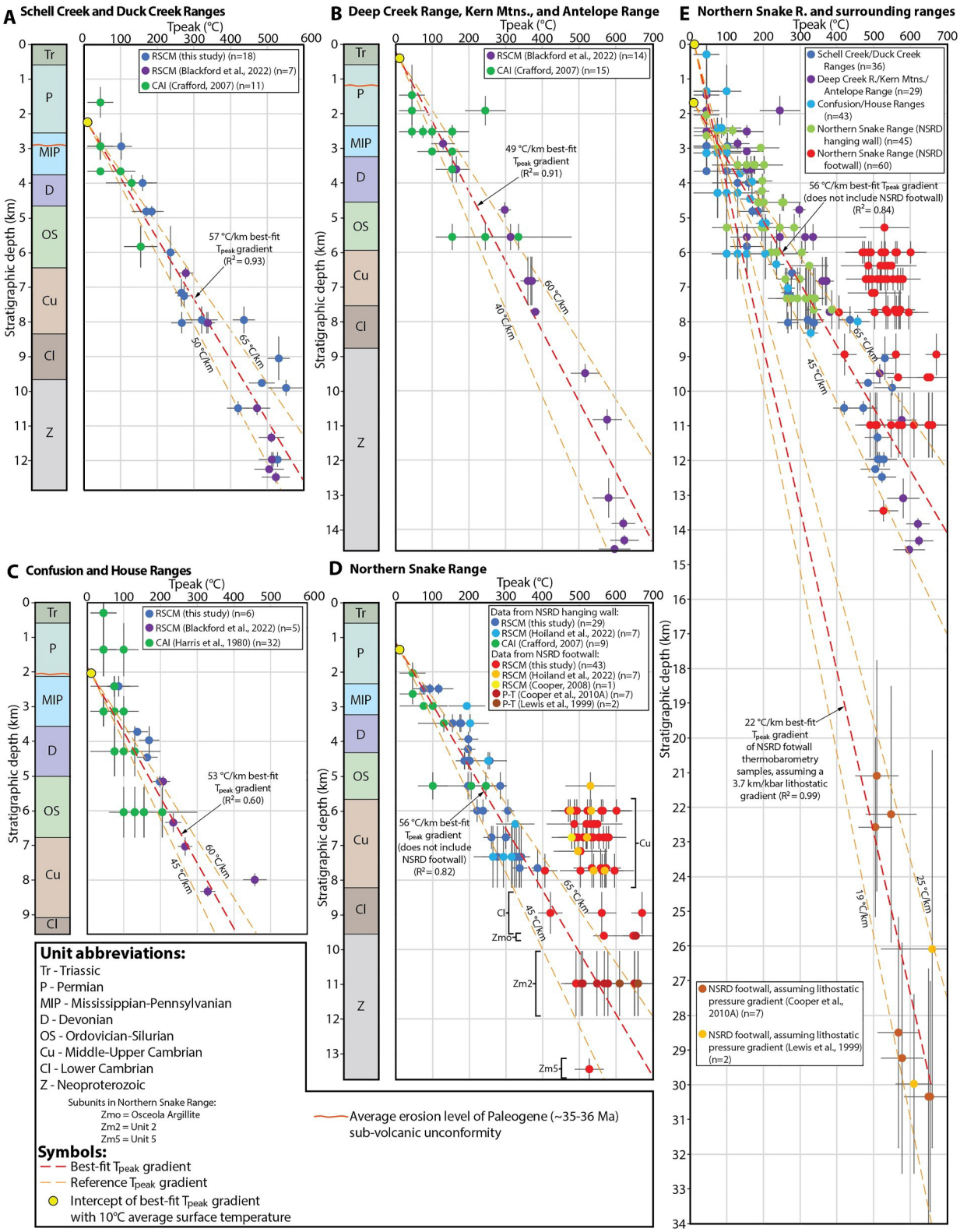

Figure 9.

4.4.3. T_{peak} Gradients Are Significantly Higher Than Predicted by Thermobarometry

The average regional T_{peak} gradient for all ranges (excluding data from the NSRD footwall) is 56°C/km to a depth of 14.5 km (when calculated vs. stratigraphic depth; Figure 9e) and 36°C/km to a depth of 19.5 km (when calculated vs. restored structural depth; Figure 10e). We interpret the stratigraphic depth T_{peak} gradient as a maximum possible constraint, as it is calculated assuming that no structural relief had been generated by thrust faults and folds before the Late Cretaceous attainment of peak temperatures. Accordingly, we interpret the structural depth T_{peak} gradient as a minimum possible constraint, as it takes into account all structural relief created by thrust faults and folds but was measured assuming that no erosion below the top of the Triassic section had taken place by the Late Cretaceous. The regional T_{peak} gradient (referred to from here onward as a center value with an error range, i.e., 46 ± 10°C/km), is 1.6–2.5 times greater than the 22°C/km average T_{peak} gradient implied by thermobarometry. Therefore, burial of NSRD footwall rocks to 21–30 km depths would necessitate that the steep upper-crustal T_{peak} gradient transitions abruptly downward to an isothermal middle crust that is at least 6-12 km-thick (Figure 10e) to 10-17 km-thick (Figure 9e), which we consider a highly unlikely thermal architecture. Instead, we argue that NSRD footwall rocks were never buried to such great depths, and that the steep upper-crustal T_{peak} gradient continued downward and eventually intersected a mid-crustal zone of partial melting (e.g., Blackford et al., 2022; Gottlieb et al., 2022; E. L. Miller & Gans, 1989). Downward projection of the steep T_{peak} gradient would result in temperatures above ~700–750°C at depths ≥14–15 km (Figure 9e) to ≥20–21 km (Figure 10e), which is above the dry solidus for pelitic rocks at ~4–6 kbar (e.g., Spear et al., 1999). No migmatitic textures have been documented anywhere in the NSRD footwall, despite widespread exposure of pelitic rocks (Gans, Miller, Huggins, & Lee, 1999; Gans, Miller, & Lee, 1999; J. Lee et al., 1999a, 1999b, 2023; J. Lee, Miller, et al., 1993; E. L. Miller & Gans, 1999; E. L. Miller, Gans, et al., 1999), which is a strong argument against deep footwall burial. Additionally, the 588 ± 61°C average T_{peak} of Neoproterozoic rocks in the NSRD footwall is virtually identical to the 586 ± 36°C average T_{peak} of Neoproterozoic rocks in the Deep Creek Range that restore to 9–14.5 km stratigraphic depths, and is only slightly hotter than the 502 ± 34°C average T_{peak} of Neoproterozoic rocks in the Schell Creek Range that restore to 10–12.5 km stratigraphic depths (Figure 8h), which provides another line of evidence against deep burial of NSRD footwall rocks.

4.4.4. T_{peak} Patterns in the NSRD Footwall Are Consistent With Enhanced Heating via Late Cretaceous Granitic Magmatism

T_{peak} values in the NSRD footwall are not systematic as a function of restored stratigraphic level or structural depth. T_{peak} values from Middle-Upper Cambrian rocks (average of 528 ± 39°C; $n = 41$) are ~160–260°C hotter than the best-fit stratigraphic depth T_{peak} gradient at their restored depth, T_{peak} values from the highest Neoproterozoic stratigraphic unit (Zmo; average 623 ± 39°C; $n = 3$) are an average of ~170°C hotter than the best-fit gradient, and T_{peak} values from the middle Neoproterozoic stratigraphic unit (Zm2; average 585 ± 63°C; $n = 11$) are an average of ~55°C hotter than the best-fit gradient (Figure 9d). We interpret the non-systematic T_{peak} distribution in the NSRD footwall as the consequence of enhanced heating proximal to Late Cretaceous granite intrusions, which is consistent with multiple studies that have argued that Late Cretaceous magmatism was the primary heat source for peak metamorphism in the Northern Snake Range and surrounding ranges (Barton, 1990; Barton et al., 1988; Blackford et al., 2022; Gottlieb et al., 2022; C. F. Miller & Bradfish, 1980; E. L. Miller & Gans, 1989; E. L. Miller et al., 1988). This interpretation is supported by T_{peak} values in the NSRD footwall that are the highest in the central part of the range, which contains the largest volume of Late Cretaceous granites (Figure 2). This portion of the range yielded the highest single T_{peak} sample (SR19-14B: 671°C; collected from an outcrop of interlayered pelitic rocks and granite), the highest two thermobarometric temperatures (FDC62: 654°C, FDe178: 650°C; collected within 0.2–0.5 km map distance of granite), and the Middle-Upper Cambrian

Figure 9. Stratigraphic thickness beneath the top of the Triassic section graphed versus T_{peak} for specific ranges (a–d) and for all ranges including and surrounding the Northern Snake Range (e). (a) Data from the Schell Creek and Duck Creek Ranges. Stratigraphic column from Long et al. (2022), with Permian unit thicknesses from Brokaw (1967) and Douglass (1960) and Triassic thickness from Greene (2014). (b) Data from the Deep Creek Range, Kern Mountains, and Antelope Range. Stratigraphic column from Rodgers (1987), with Permian unit thickness interpolated between thicknesses presented in Brokaw (1967) and Greene (2014), and Triassic thickness from Greene (2014). (c) Data from Confusion and House Ranges; stratigraphic column from Greene (2014). (d) Data from the Northern Snake Range; stratigraphic column from J. Lee, Miller, et al. (1993), with Permian unit thickness interpolated between thicknesses presented in Brokaw (1967) and Greene (2014), and Triassic thickness from Greene (2014). (e) All data from the Northern Snake Range and surrounding ranges.

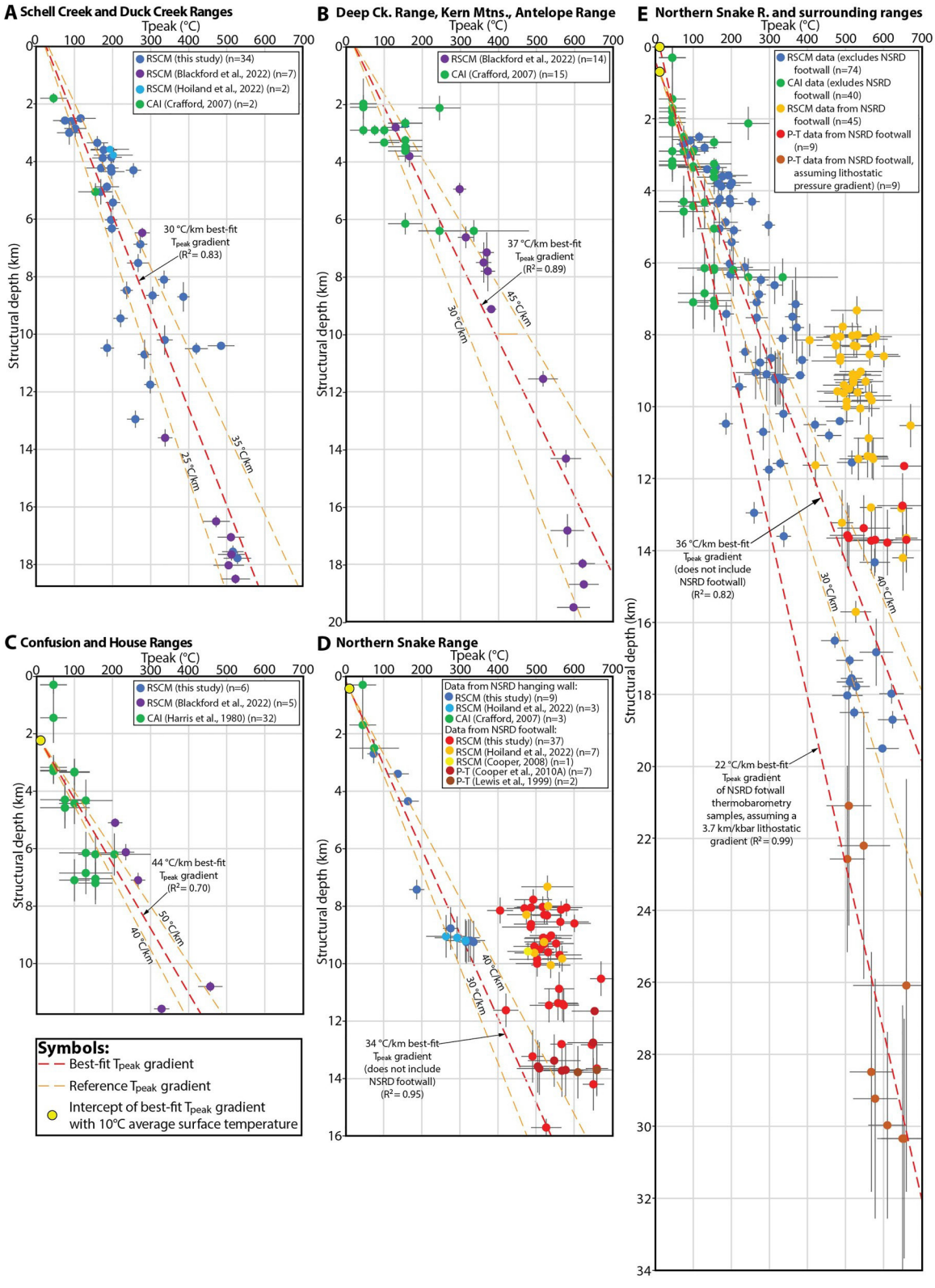

Figure 10.

carbonate section with the highest average T_{peak} (556 ± 25°C; Ryegrass Canyon section; collected within 0–2 km map distance of granite) (Figures 2 and 11b).

Contouring of T_{peak} values on the restored versions of our cross sections (Figure 12), which provides a detailed view of the Late Cretaceous crustal thermal architecture, clearly demonstrates high T_{peak} anomalies proximal to Late Cretaceous granites. Figures 12a–12c each illustrate the steep regional upper-crustal T_{peak} gradient in all ranges, which culminates downward in ~400–550°C background temperatures at sites of exposed of metasedimentary rocks in the SCRDS footwall in the Schell Creek/Duck Creek Ranges, Deep Creek Range, and NSRD footwall. Figures 12a–12c each exhibit high T_{peak} (~550–650°C) anomalies on the order of ~5 km east-west and ~2–4 km tall that are localized in the NSRD footwall and eastern Deep Creek Range. Each of these anomalies is spatially associated with Late Cretaceous granite intrusions. Figures 12b and 12c demonstrate that the 200–300°C upward decrease across the NSRD (Figure 8i) is the consequence of a lateral T_{peak} gradient, with eastward displacement on the NSRD placing Cambrian hanging wall rocks that attained ~250–350°C over Cambrian footwall rocks that experienced enhanced heating via Late Cretaceous granitic magmatism to ~475–650°C (Figure 8g).

5. Arguments Invalidating Published Structural Models for Deep NSRD Footwall Burial

Here, we explore the implications of our structural reconstructions and T_{peak} data set, as well as geophysical data and regional geologic field relationships, for testing the predictions of published structural models for high-magnitude burial and exhumation of the NSRD footwall.

5.1. Burial by Top-To-East Thrust Faulting

Bartley and Wernicke (1984) interpreted that NSRD footwall rocks were buried ~7 km beyond their stratigraphic depths via displacement on a hypothesized top-to-east thrust fault that places Neoproterozoic rocks over Devonian rocks (Figures 13a–13c). NSRD footwall rocks were then exhumed by 56 km of displacement on a 15–30° east-dipping (20° average) NSRD. In this model, the NSRD footwall represents a structural window into the underlying thrust sheet. The restored depth of Neoproterozoic rocks in the NSRD footwall on the Bartley and Wernicke (1984) model is 16–17 km (Figure 13a), which falls short of the 21–30 km depth range later interpreted by thermobarometry studies (Cooper, Platt, Anczkiewicz, & Whitehouse, 2010; Lewis et al., 1999). However, the Bartley and Wernicke (1984) model invokes a burial mechanism that is more plausible than other models, as Cordilleran contractional deformation was dominated by top-to-east thrust faulting (e.g., DeCelles & Coogan, 2006; Greene, 2014). In the following sections, we outline multiple lines of evidence that invalidate the thrust-related burial of NSRD footwall rocks to 21–30 km depths, as well as the extension magnitude necessary to exhume such deeply buried rocks.

5.1.1. Incompatibility With Regional Field Relationships and Cordilleran Deformation

Despite significant present-day structural relief, multiple-km-throw older-over-younger field relationships indicative of regional-scale thrust faults have not been mapped in this region of Nevada and Utah. The Deep Creek Range exposes a structurally intact package of Neoproterozoic-Permian rocks (Rodgers, 1987), which restore to structural depths as great as 20 km below the top of the Triassic section (Figures 6 and 10b). Rocks in this package restore as much as ~8 km deeper than the hypothesized thrust on Figure 13a, yet lack evidence for thrust faults.

Burial of Neoproterozoic rocks in the NSRD footwall to the high end of the 21–30 km depth range implied by thermobarometry would require structural duplication of the entire 14.5 km-thick Neoproterozoic-Triassic section, or alternatively would require two (or more) thrust sheets that duplicated significant portions of this section. This would have profound implications for the magnitude of crustal shortening accomplished during Cordilleran

Figure 10. Graphs of restored structural depth beneath the top of the Triassic section (measured from Figures 4c, 5c, and 6b) versus T_{peak} for specific ranges (a–d) and for all ranges (e). (a) Data from the Schell Creek and Duck Creek Ranges; includes data from all samples that restore to the west of the western limit of Northern Snake Range dècollement (NSRD) footwall exposure on Figures 4c and 5c. (b) Data from the Deep Creek Range, Kern Mountains, and Antelope Range. (c) Data from the Confusion and House Ranges; includes data from all samples that restore to the east of the eastern limit of NSRD footwall exposure on Figures 4c and 5c. (d) Data from the Northern Snake Range; includes all NSRD footwall samples and all samples that restore between the restored western and eastern limits of NSRD footwall exposure on Figures 4c and 5c. (e) All data from the Northern Snake Range and surrounding ranges.

10.1029/2024TC008368

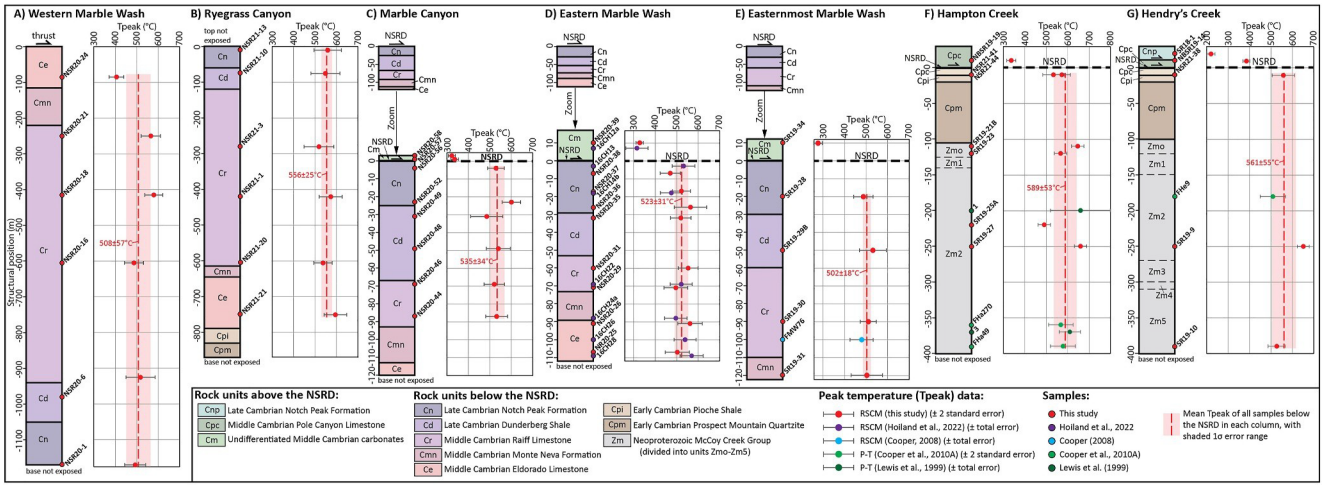

Figure 11. T_{peak} graphed vs. present-day structural position beneath the Northern Snake Range dècollement (NSRD). (a–e) Structural thickness columns of Middle-Late Cambrian rock units in the northern part of the Northern Snake Range, including the: (a) Western Marble Wash, (b) Ryegrass Canyon, (c) Marble Canyon, (d) Eastern Marble Wash, and (e) Easternmost Marble Wash transects (sample locations shown on Figure 2; columns (a–d) are modified from Long et al. (2023)). Rocks in column (a) are in the overturned limb of the O'Neill Peak recumbent syncline. Columns (c–e) are shown at the top of the figure with the same vertical scale as columns (a–b), which illustrates the dramatic eastward increase in ductile thinning across the range. (f–g) T_{peak} vs. structural thickness for Neoproterozoic-Cambrian rocks in the NSRD footwall in the southeastern part of the range, in the (f) Hampton Creek and (g) Hendry's Creek drainages (shown at a different vertical scale than columns (a–e)).

orogenesis. The hypothesized top-to-east thrust fault on Figure 13a adds at least 94 km of shortening to the Sevier fold-thrust system, and this could double or even triple if additional thrust sheets were emplaced at depth. This would generate strain incompatibility along-strike in the Sevier fold-thrust belt. For example, the 220 km of shortening measured in the Sevier fold-thrust belt to the east of the Northern Snake Range (DeCelles & Coogan, 2006) is already 70 km greater than shortening measured 200 km to the north (Coogan, 1992), and adding > ~100 km of shortening at our studied latitude would greatly exacerbate this discrepancy.

The geometry shown on Figure 13a requires a downward step in structural level to the west at the point where the ~14 km-thick thrust sheet folds downward over the 8 km-tall trailing footwall ramp of the underlying thrust sheet. This is invalidated by the Paleogene unconformity, which defines ~3 km of total regional structural relief and no significant steps in structural level for at least an additional ~70 km to the west of Figure 13a (restored pre-extensional distance measured from Long (2019), Armstrong (1972), Gans and Miller (1983), and Long (2012, 2015, 2019)).

The Bartley and Wernicke (1984) model requires that Neoproterozoic-Cambrian rocks in the NSRD footwall restore far to the east (94 km at the minimum) of age-correlative rocks in surrounding ranges prior to thrusting. However, E. L. Miller, Dumitru, et al. (1999) presented several lines of evidence that Neoproterozoic-Cambrian rocks in the Southern Snake, Northern Snake, and Deep Creek Ranges were laterally continuous prior to extension, including distinct east-west facies changes in Neoproterozoic quartzite and Middle Cambrian limestone that can be correlated between these ranges, and similarity in the age of metamorphism and the age and composition of Jurassic and Late Cretaceous granites between these ranges.

5.1.2. Large NSRD Displacement Results in Spatial Overlap of Preserved Rocks

The geometry shown on Figures 13a–13c requires at least 70–100 km of displacement on the NSRD to exhume the thermobarometry samples to the surface. Similar to our Figures 4 and 5, such a high displacement magnitude is not possible, as it would result in the spatial overlap of Cambrian rocks preserved in the SCRDS footwall in the Schell Creek Range and in the NSRD hanging wall in the Confusion Range. These rocks are separated by an NSRD-parallel distance of 56 km today (points "A" and "B" on Figure 13c), which provides a firm upper limit on displacement.

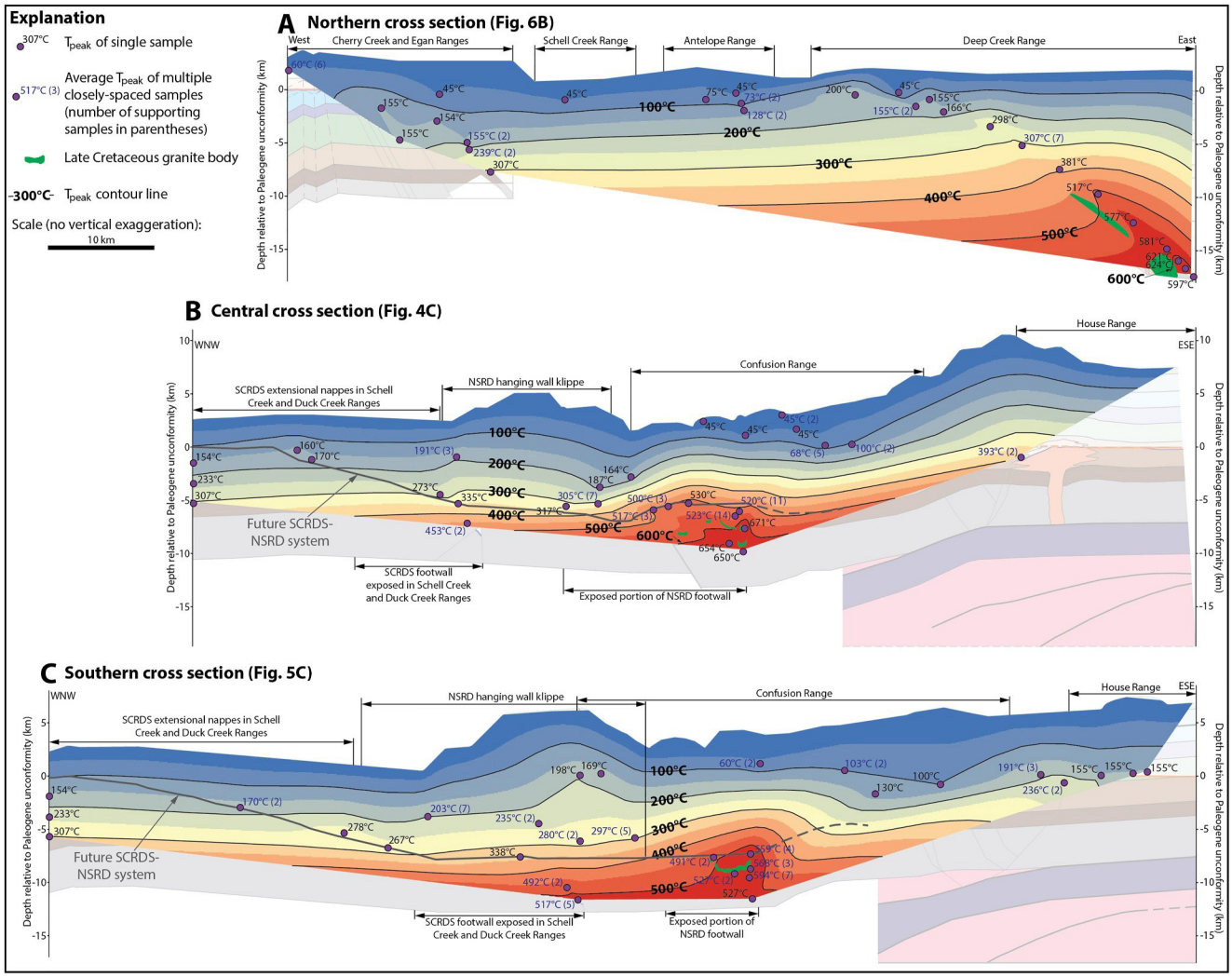

Figure 12. Late Cretaceous, pre-extensional crustal thermal architecture of eastern Nevada and western Utah, as illustrated with small-scale versions of the: (a) northern cross section (Figure 6b), (b) central cross section (Figure 4c) and (c) southern cross section (Figure 5c) that are contoured for T_{peak} values. The mean T_{peak} values of RSCM and thermobarometry samples and the center of the T_{peak} range of CAI values were contoured. In several places, a mean value of T_{peak} measurements from multiple closely spaced samples was calculated and contoured (the number of supporting samples for each average is listed in parentheses). Contouring was performed in ArcGIS using natural neighbor interpolation. The seven RSCM samples that yielded mean T_{peak} values <150°C were not utilized in contouring, as they fall below the minimum calibration temperature range from Equation 2 of Kouketsu et al. (2014). Panels (a–c) demonstrate the hot, regional background T_{peak} gradient in all ranges, which culminates downward in ~400–550°C T_{peak} values at sub-Paleogene unconformity depths of ~7–12 km in the SCRDS footwall in the Schell Creek and Duck Creek Ranges, the eastern Deep Creek Range, and the Northern Snake Range dècollement (NSRD) footwall, as well as km-scale, ~550–650°C T_{peak} anomalies that are localized proximal to Late Cretaceous granites in portions of the NSRD footwall and the eastern Deep Creek Range.

5.1.3. The NSRD Does Not Ramp Down-Section Eastward

The top-to-east thrust burial model requires the SCRDS-NSRD system to cut down-section eastward to 21–30 km depths at an average stratigraphic cutoff-angle of 20° (Figure 13a). The SCRDS does cut down-section eastward, at stratigraphic cutoff-angles of 4–11°, but it roots to a >13 km-long footwall flat at the top of the Lower Cambrian section (Figure 5) (Long et al., 2022). Across the southern half of the Northern Snake Range, the NSRD occupies a footwall flat at the top of the Lower Cambrian Prospect Mountain Quartzite (e.g., E. L. Miller et al., 1983), which can be traced for a restored (i.e., pre-footwall stretching) length of 8.7 km (Figure 5) (Long et al., 2022). Exposures of the overlying Pioche Shale are observed intermittently beneath the NSRD across the width of the range (J. Lee et al., 2023; J. Lee, Miller, et al., 1993; E. L. Miller & Gans, 1999; E. L. Miller, Gans, et al., 1999), which demonstrates that the NSRD does not cut downward to the east through the Prospect Mountain Quartzite. This invalidates the geometry of an eastward-ramping NSRD shown on Figures 13a–13c. To support

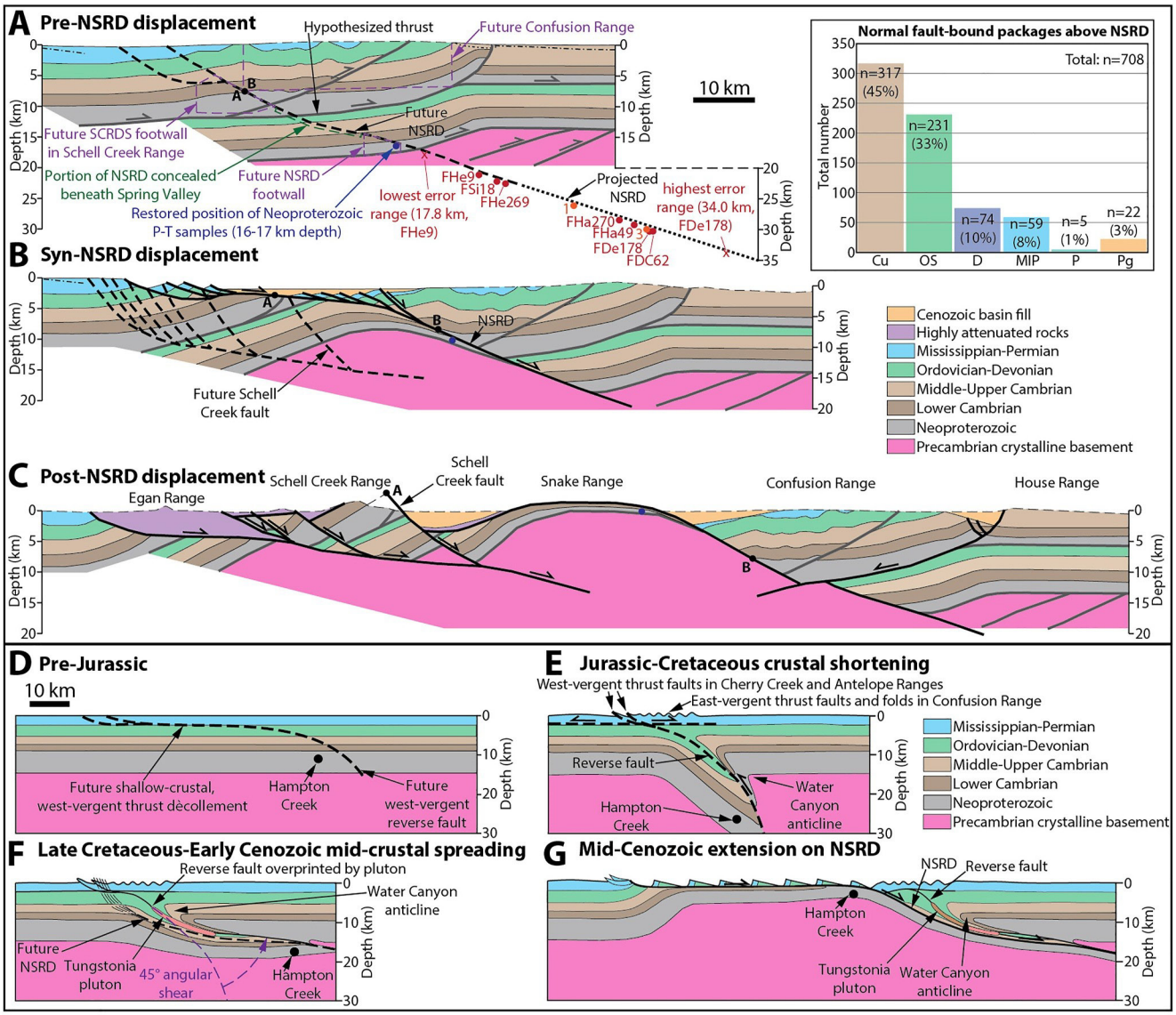

Figure 13. Published models for deep Northern Snake Range dècollement (NSRD) footwall burial via: (a–c) top-to-east thrust faulting, and (d–g) top-to-west reverse faulting. (a–c) Cross section diagrams modified from Figure 2 of Bartley and Wernicke (1984), showing their interpreted structural evolution. The positions of NSRD footwall thermobarometry samples (seven from Cooper, Platt, Anczkiewicz, and Whitehouse (2010) shown in red; two from Lewis et al. (1999) shown in orange) are projected to their peak depths beneath the NSRD (shown at the 20°E average dip angle measured from the deepest portions of the NSRD on Figure 2 of Bartley and Wernicke (1984)), assuming a lithostatic pressure gradient of 3.7 km/kbar. Inset on upper right shows a frequency histogram of the area-dominant geologic unit carried within each of the 708 normal fault-bound packages in the NSRD hanging wall (compiled from the geologic maps of Hose and Blake (1976), J. Lee et al. (1999a, 1999b, 2023), J. Lee, Miller, et al. (1993), Gans, Miller, Huggins, and Lee (1999), Gans, Miller, and Lee (1999), and Johnston (2000)). "Cu" = middle-upper Cambrian, "OS" = Ordovician-Silurian, "D" = Devonian, "MIP" = Mississippian-Pennsylvanian, "P" = Permian, "Pg" = Paleogene. (d–g) Cross section diagrams modified from Figure 6 of Lewis et al. (1999), showing their interpreted structural evolution. "Hampton Creek" corresponds with the projected locations of the Lewis et al. (1999) thermobarometry samples.

the top-to-east thrust burial model at the burial magnitudes implied by thermobarometry, the SCRDS-NSRD system would have to change geometry from a ~13 km-long flat in the Schell Creek Range to a footwall ramp that cuts sharply down-section through ~5.5–18.5 km of stratigraphy (which is now concealed beneath Spring Valley), and then switch back to a ~9 km-long flat within a lower thrust sheet in the Northern Snake Range. Not only is this geometry highly improbable, but it is geometrically impossible for the high end of the thermobarometry burial range, as exposures of the SCRDS and NSRD are separated by as little as 10 km east-west distance after restoration of post-SCRDS-NSRD normal faulting (Long et al., 2022).

5.1.4. No Klippe of Neoproterozoic-Lower Cambrian Rocks in the NSRD Hanging Wall

The top-to-east thrust burial model requires that the NSRD ramps downward to the east through at least 4.5 km of Neoproterozoic-Lower Cambrian rocks along the portion of the NSRD that is now concealed beneath Spring Valley (Figure 13a). If correct, this would be reflected by preservation of klippe of Neoproterozoic-Lower Cambrian rocks in the NSRD hanging wall. Using geologic maps of the Northern Snake Range (Gans, Miller, Huggins, & Lee, 1999; Gans, Miller, & Lee, 1999; Hose & Blake, 1976; J. Lee et al., 1999a, 1999b, 2023; J. Lee, Miller, et al., 1993; E. L. Miller & Gans, 1999; E. L. Miller, Dumitru, et al., 1999), we counted 708 total normal fault-bound rock packages in the NSRD hanging wall, and we documented the dominant age of rocks (by exposed area) in each of these packages (Figure 13 upper-right inset). All stratigraphic levels between Middle-Upper Cambrian and Permian are represented, with the relative proportion increasing stratigraphically downward. Not one klippe of Neoproterozoic-Lower Cambrian rocks is observed. This is strong evidence against the NSRD ramping downward through these rocks beneath Spring Valley, in particular as the Neoproterozoic-Lower Cambrian section is dominated by quartzite, which is commonly preserved as brecciated packages in normal fault zones. Instead, the age distribution of rocks in the NSRD hanging wall is consistent with the SCRDS and NSRD occupying the same 6–8 km deep footwall flat at the top of the Lower Cambrian section (e.g., Figures 4 and 5).

5.1.5. T_{peak} Arguments

Many of the same arguments derived above from the T_{peak} data set further invalidate the top-to-east thrust burial model. Most importantly, deep NSRD footwall burial would require the highly unlikely scenario of a 48 ± 10°C/km upper-crustal T_{peak} gradient that overlies a 6-17 km-thick interval of isothermal temperatures distributed across the hypothesized buried thrust sheets at depth. For example, the top-to-east thrust burial model would require Neoproterozoic rocks in the NSRD footwall that were buried to 21–30 km depths to have attained virtually the same average T_{peak} as Neoproterozoic rocks in the Schell Creek and Deep Creek Ranges that were never buried beyond half of these depths (Figure 8h).

5.2. Burial by Top-To-West Reverse Faulting

Lewis et al. (1999) presented a model for burial of Neoproterozoic rocks in the NSRD footwall to ~27 km depths via displacement on a hypothesized, steeply east-dipping (55° average), top-to-west, Jurassic-Cretaceous reverse fault (Figures 13d and 13e). The reverse fault is interpreted to have fed its ~25 km of total displacement into a thrust flat at the base of the Mississippian section at 2–3 km depth, with displacement transferred westward to emergent thrusts in the Cherry Creek and Antelope Ranges and eastward into folding in the Confusion Range (Figure 13e). Lewis et al. (1999) interpreted that the reverse fault is located in the Kern Mountains, but has been overprinted and concealed by a Late Cretaceous granitic pluton. Lewis et al. (1999) also interpreted that the reverse fault must be concealed beneath Snake Valley along the full ~65 km north-south length of the Northern Snake Range, to account for thermobarometry data that imply deep burial of the NSRD footwall in the south-eastern part of the range.

The reverse faulting model calls upon structures observed at different latitudes. The inspiration for a top-to-west reverse fault comes from the Water Canyon anticline, an overturned, west-vergent anticline exposed in the southern Deep Creek Range (Nelson, 1966, 1969; Rodgers, 1987) (Figures 1 and 6), which extends downward to restored structural depths of at least 14–20 km below the top of the Triassic section (Figure 6b) (Blackford et al., 2022). Lewis et al. (1999) interpreted the Water Canyon anticline as a drag fold that was constructed in the hanging wall of the reverse fault. However, no top-to-west reverse faults have been mapped associated with this fold (Rodgers, 1987), and no large-scale, top-to-west thrust or reverse faults have been mapped anywhere in this region of Nevada and Utah.

The reverse faulting model generates testable predictions that are invalidated by regional field relationships. First, the ~25 km of displacement on the reverse fault has to be accounted for by upper-crustal shortening distributed both eastward and westward (Figure 13e). To the east, Greene (2014) demonstrated that east-vergent folds and thrust faults in the Confusion Range account for ≤10 km of shortening. Lewis et al. (1999) called upon thrust faults in the Cherry Creek and Antelope Ranges mapped by Hose and Blake (1976) to distribute shortening westward, with a regional top-to-west thrust dècollement interpreted at the Mississippian-Devonian contact (Figure 13e). However, the "thrust faults" mapped in the Antelope, Schell Creek, Egan, and Cherry Creek Ranges

on Hose and Blake (1976) (which are compiled from the mapping of Young (1960), Avent (1962), Dechert (1967), and Fritz (1968)) all omit stratigraphy and have been reinterpreted in multiple studies as top-down-to-east normal faults (Blackford et al., 2022; Gans, 1982; Gans & Miller, 1983; Long et al., 2022; Wernicke, 1981; also see Figure 6). There is also no evidence for a regional thrust dècollement at the Mississippian-Devonian contact. For example, in the Egan, Cherry Creek, and Schell Creek Ranges, Fritz (1968), Young (1960), and Dechert (1967) mapped stratigraphic Mississippian-Devonian contacts in multiple places.

The Lewis et al. (1999) model suffers from the same T_{peak} arguments as other models, in that deep NSRD footwall burial would require an isothermal middle crust. For example, on Figure 13e, Neoproterozoic rocks in the footwall of the reverse fault (presently exposed in the NSRD footwall) were buried to ~25–30 km depths, while these same rocks in its hanging wall (presently exposed in the Deep Creek Range) only attained depths of ~9–14 km. However, these rocks record virtually identical average T_{peak} values (588 and 586°C, respectively; Figure 8h).

5.3. No Evidence for a "Late Cretaceous-Early Cenozoic Mid-Crustal Spreading" Event

Lewis et al. (1999) and Cooper, Platt, Anczkiewicz, and Whitehouse (2010) both interpreted that a pure shear-dominated, mid-crustal spreading event that post-dated Jurassic-Cretaceous thrust burial but pre-dated mid-Cenozoic extension on the NSRD accomplished approximately half (~10–15 km) of the total exhumation of NSRD footwall rocks (Figures 13e and 13f). Lewis et al. (1999) called upon mid-crustal spreading to flatten their hypothesized reverse fault from its 55°E average original dip to a significantly shallower 10°E average dip, corresponding to 45° of bulk angular shear (Figure 13f). Their proposed magnitude of exhumation and angular shear would require exceptionally high mid-crustal strains. For example, assuming that all rocks between 10 km and 25–30 km depth experienced homogeneous pure shear, it would require 100%–200% horizontal stretching to accomplish 10–15 km of exhumation and 285% stretching to accomplish 45° of angular shear.

Several lines of evidence rule out that such a pre-NSRD crustal spreading event occurred. First, U-Pb geochronology of deformed and undeformed dikes that intrude the NSRD footwall bracket the timing of ductile extensional shearing and related fabric development between ~38 and 22 Ma (J. Lee et al., 2017), which is contemporaneous with displacement on the NSRD (e.g., J. Lee, 1995; J. Lee & Sutter, 1991; J. Lee et al., 1987, 2017; E. L. Miller et al., 1983; E. L. Miller, Dumitru, et al., 1999). Second, there is no evidence for significant upper-crustal extension in this region prior to ~36-35 Ma volcanism. High-throw, regionally distributed, pre-volcanic normal faulting is ruled out by the minimal structural relief of the Paleogene subvolcanic unconformity (e.g., Armstrong, 1972; Gans & Miller, 1983; Long, 2012, 2015) and by field relationships described in myriad mapping- and cross section-based studies (e.g., Anderson et al., 1983; Blackford et al., 2022; Dechert, 1967; Drewes, 1967; Fritz, 1968; Gans, 1982; Gans & Miller, 1983; Greene, 2014; Hintze & Davis, 2002; Long, 2019; Long et al., 2022; Rodgers, 1987; Young, 1960). Thus, the hypothesized mid-crustal spreading would had to have been accomplished with complete decoupling between the middle and upper crust, which is incredibly unlikely given the lack of evidence for melt-related weakening down to restored depths of at least 15–20 km (Figure 10e).

Third, the northwestern part of the NSRD footwall did not experience *any* extensional ductile shearing (e.g., Gans et al., 1985; J. Lee et al., 1987). These rocks locally exhibit ductile fabrics with NNW-SSE-trending stretching and intersection lineations, which record low-magnitude strain generated during Late Cretaceous folding and thrusting (J. Lee et al., 1999a, 1999b, 2023; Long et al., 2023; Wrobel et al., 2021). However, this portion of the NSRD footwall lacks the strongly developed ductile fabrics that were generated during ~38–22 Ma, WNW-ESE-directed ductile extensional shearing of the NSRD footwall in the central and eastern parts of the range (Figure 2) (e.g., Gans, Miller, Huggins, & Lee, 1999; Gans, Miller, & Lee, 1999; J. Lee et al., 1999a, 2023; J. Lee, Miller, et al., 1993; E. L. Miller & Gans, 1999; E. L. Miller, Gans, et al., 1999).

Cambrian rocks in the NSRD footwall in the northwestern part of the range record an average T_{peak} of ~500°C (Figure 11a), which was likely attained during ~91-78 Ma peak metamorphism (Cooper, Platt, Anczkiewicz, & Whitehouse, 2010). Following this, these rocks cooled through ~425°C at ~55-50 Ma, through ~310–275°C at ~47–43 Ma, and through ~250°C at ~38 Ma (K-Ar muscovite and biotite, $^{40}Ar/^{39}Ar$ muscovite and K-feldspar; D. E. Lee et al., 1980; J. Lee, 1995; J. Lee & Sutter, 1991; Hoiland, 2019), defining a long-term cooling rate of ~4.5–6°C/Myr. We attribute this ~250°C of pre-extensional cooling to the gradual relaxation of the Late Cretaceous peak thermal regime, though we acknowledge that some of this cooling could be attributed to a portion

of the 2–4 km of total erosion above the Paleogene unconformity (Figures 4 and 5) being accomplished during this time interval. Importantly, this cooling history demonstrates that the western NSRD footwall had cooled below the ~300°C quartz crystal-plastic transition (e.g., Stipp et al., 2002) before the ~38 Ma initiation of NSRD displacement, and thus was residing at upper-crustal depths over the entire duration of extension (J. Lee, 1995). All of this cooling took place in the *absence* of extensional ductile shearing and normal faulting, which rules out *any* significant pre-NSRD extension-related exhumation, and thus provides another strong argument against deep footwall burial. This indicates that the western portion of the NSRD footwall was never at any point buried beyond upper-crustal depths (7.5–11 km depth below the top of the Triassic section, 5.5–8 km depth below the Paleogene unconformity; Figure 4c).

5.4. What if NSRD Footwall Rocks Were Initially East-Dipping?

Calcite-dolomite thermometry from the northeastern flank of the range (Cooper, Platt, Platzman, et al., 2010) defines a ~433°C deformation temperature in the NSRD footwall during ~38 Ma initial extensional ductile shearing, which is hotter than the ~250°C temperature of NSRD footwall rocks in the western part of the range at this time (J. Lee, 1995). This temperature difference could be the consequence of shear heating within the high-strain, eastern portion of the NSRD footwall (Long et al., 2023). Alternatively, it is possible that NSRD footwall rocks were dipping eastward at the onset of ductile extensional shearing (e.g., J. Lee, 1995; J. Lee & Sutter, 1991). We do not see evidence in our cross section reconstructions for an initial eastward dip of NSRD footwall rocks (Figures 4c and 5c), but we acknowledge that alternative geometries are possible.

However, restoration of ductile strain in the NSRD footwall (J. Lee et al., 1987; Long et al., 2022, 2023), combined with arguments discussed in the previous section that NSRD footwall rocks in the northwestern part of the range were never buried beyond depths of 7.5–11 km, provide another geometric argument against deep burial of the NSRD footwall. After restoration of ductile strain, the thermobarometry samples of Lewis et al. (1999) and Cooper, Platt, Anczkiewicz, and Whitehouse (2010) restore between 6.1 and 8.3 km NSRD-parallel distance eastward of the western limit of ductile fabrics (Figures 4c and 5c). Assuming that NSRD footwall rocks eastward of this point were tilted 40°E (e.g., J. Lee, 1995), this would yield maximum possible burial depths of 11.4–16.3 km for these samples, which are approximately half of the peak depths predicted by thermobarometry.

6. Discussion

The structural constraints, crustal thermal architecture, regional geologic field relationships, and seismic reflection interpretations discussed above, when viewed independently or together, do not allow for a viable scenario for burial of NSRD footwall rocks to the 21–30 km depths implied by thermobarometry. This makes the Northern Snake Range a critically important structural system that has implications for the global-scale issue of how pressure data are interpreted in orogenic settings. One possible scenario for reconciling this depth discrepancy is that NSRD footwall rocks have experienced non-lithostatic pressure (also known as tectonic overpressure) (e.g., Gerya, 2015; Luisier et al., 2019; Moulas et al., 2013; Petrini & Podladchikov, 2000; Schmalholz & Podladchikov, 2013; Schmalholz et al., 2014; Wheeler, 2014; Yamato & Brun, 2017). Though still a heavily debated topic, a growing number of studies over past 20 years have proposed mechanisms for achieving tectonic overpressure, including the influence of differential stress on metamorphic reactions (Wheeler, 2014, 2018), modeling of the deviatoric stress conditions experienced by rocks at depth (Gerya, 2015; Moulas et al., 2013, 2019; Petrini & Podladchikov, 2000; Schmalholz et al., 2014), the effects of variable rheology within ductile shear zones on deviatoric stress (Moulas et al., 2014, 2019; Schmalholz & Podladchikov, 2013), changes in deviatoric stress accompanying the switch from a contractional to an extensional stress regime (Yamato & Brun, 2017), and the effects of volume expansion and density reduction accompanying partial melting (Chu et al., 2017; Vrijmoed et al., 2009). With the exception of melting-related volume and density changes, all of these mechanisms are potentially applicable to NSRD footwall rocks.

Field-based studies that have argued for tectonic overpressure based on evaluation of relationships between barometry and restored depth include investigations in the Himalayas, Alps, and Appalachians (Chu et al., 2017; Luisier et al., 2019; Marques et al., 2018; Pleuger & Podladchikov, 2014). Recent studies have utilized structural reconstructions and T_{peak} gradients to argue for tectonic overpressure in the Ruby East-Humboldt metamorphic core complex in northeastern Nevada (Figure 1a) (Zuza et al., 2020, 2022), and the possibility of tectonic overpressure has recently been suggested for the Northern Snake Range (Hoiland et al., 2022). The multiple lines

of evidence that prohibit deep burial of the NSRD footwall make the Northern Snake Range one of a growing number of important case studies that necessitate a non-lithostatic interpretation of pressure data.

The results of this study have regional implications for limiting the magnitude of shortening and thickening accomplished in the Sevier hinterland region of westernmost Utah and eastern Nevada. Minimal upper-crustal shortening in east-central Nevada has long been supported by the 3 km total regional structural relief and lack of evidence for emergent thrust faults defined by the Paleogene subvolcanic unconformity (e.g., Armstrong, 1972; Gans & Miller, 1983; Long, 2012, 2015), as well as investigations of contractional structures that define low-magnitude (35–40 km total) shortening diffusely distributed across central Nevada, eastern Nevada, and western Utah (e.g., Blackford et al., 2022; Di Fiori et al., 2020, 2021; Greene, 2014; Long, 2019; Long et al., 2014; Taylor et al., 1993, 2000). The minimal upper-crustal shortening in the Sevier hinterland supports interpretations that underthrusting of the thick North American craton beneath eastern Nevada was the dominant thickening mechanism that constructed the ~50-60 km-thick crust of the Cordilleran retroarc plateau (Long, 2019, 2023).

Integrating the extension estimates from our central (Figure 4) and southern (Figure 5) cross sections with the province-wide cross section reconstruction of Long (2019) helps constrain the total extension across the Basin and Range Province and the pre-extensional crustal thickness of the Cordilleran retroarc plateau. Displacement on the NSRD was the largest single source of uncertainty in the Long (2019) reconstruction, accounting for ± 22 km of error in his 230 ± 42 km estimate of province-wide extension (46 ± 8%). Incorporating the results from our central (Figure 4) and southern cross sections (Figure 5, using the 50.0 km minimum and 64.6 km maximum NSRD displacement estimates as lower and upper bounds) yields 213 ± 14 km (41% ± 3%) and 229 ± 22 km (45% ± 4%) of province-wide extension, respectively. Additionally, Long (2019) documented that the Northern Snake Range and surrounding ranges lie within a domain of high-magnitude extension (137.5 ± 32.4 km extension; 66% ± 16%) that spans across eastern Nevada and westernmost Utah, which corresponds with the spatial extent of the ~2.75–3.5 km-elevation retroarc plateau (Cassel et al., 2018) and the thick underthrusted craton. Long (2019) incorporated present-day Moho depths (Gilbert, 2012) to calculate a 60 ± 11 km pre-extensional crustal thickness for this domain. Incorporating results from our Figures 4 and 5 into this reconstruction improves the pre-extensional crustal thickness estimate to 54 ± 3 km (120.3 ± 4.3 km extension; 53% ± 2%) and 58 ± 5 km (135.9 ± 12.2 km extension; 64% ± 6%), respectively.

7. Conclusions

1. The principal arguments that invalidate deep structural burial of the NSRD footwall are:
   a. Burial of Neoproterozoic-Cambrian NSRD footwall rocks to 21–30 km depths is incompatible with the 17–20 km depth of the top of Precambrian basement on the COCORP seismic line.
   b. Our two cross sections define 42 km and 50–65 km of displacement on the NSRD. It would require >66–94 km and >76–102 km of displacement, respectively, to exhume thermobarometry samples from 21 to 30 km depths, which is not possible without spatially overlapping Cambrian rocks preserved in the footwall and hanging wall of the SCRDS-NSRD system.
   c. CAI data define <50–80°C T_{peak} values for Permian-Triassic rocks, which rules out stratigraphic overburden above the Triassic section as a mechanism to bury the NSRD footwall.
   d. The 22°C/km T_{peak} gradient predicted by thermobarometry is incompatible with the regional Late Cretaceous T_{peak} gradient of 46 ± 10°C/km that we calculate down to 15–20 km depths.
2. A model for burial of the NSRD footwall by top-to-east thrust faulting is invalidated by:
   a. A lack of field evidence for large-displacement thrust faults in this region, down to pre-extensional depths of 20 km.
   b. Facies changes that demonstrate that Neoproterozoic-Cambrian rocks in the Southern Snake, Northern Snake and Deep Creek Ranges were laterally continuous prior to extension.
   c. This model requires the NSRD to ramp eastward to 21–30 km depths. However, the NSRD cannot be traced deeper than 8 km on the COCORP seismic line, and attempting to project it downward would result in its truncation at 15 km depth. Also, a lack of Neoproterozoic-Lower Cambrian rocks in NSRD hanging wall klippe indicates that the NSRD does not cut deeper than its 6-8 km-deep footwall flat at the top of the Lower Cambrian section.
3. A model for burial of the NSRD footwall by a top-to-west reverse fault, followed by 10–15 km of exhumation accommodated during a pre-NSRD mid-crustal spreading event, is invalidated by:

a. Geochronology that brackets extensional ductile shearing of the NSRD footwall between 38 and 22 Ma, which is contemporaneous with NSRD displacement.
b. Field relationships that do not allow for the 25 km of upper-crustal shortening that the model requires to have been distributed to the west and east of the hypothesized reverse fault.
c. The minimal regional structural relief of the 36-35 Ma sub-volcanic unconformity, which rules out any significant pre-NSRD upper-crustal extension.
d. The western part of the NSRD footwall never being buried beyond 7.5–11 km depth, based on a lack of pre- or syn-NSRD extensional ductile shearing.

4. T_{peak} distributions in the NSRD footwall are best explained by enhanced heating via Late Cretaceous granitic magmatism, as indicated by km-scale, 550–650°C T_{peak} anomalies spatially associated with granite bodies. The 200–300°C decrease across the NSRD results from a lateral T_{peak} gradient, with NSRD displacement placing Cambrian hanging wall rocks that attained 275–350°C over Cambrian footwall rocks that attained 475–650°C via magmatic heating.
5. Our cross sections reconstructions demonstrate that:
   a. NSRD footwall rocks restore to a maximum pre-extensional burial depth range of 7–16 km below the top of the Triassic section, and that the NSRD initiated at a depth of 6–8 km.
   b. The NSRD accomplished 42–65 km of top-down-to-ESE displacement, which progressively decreases eastward as a consequence of ductile stretching of the NSRD footwall.
   c. This region of the Sevier hinterland experienced minimal Jurassic-Cretaceous upper-crustal shortening and thickening.
6. The lack of deep burial of the NSRD footwall necessitates a non-lithostatic interpretation of barometry data. One possibility for reconciling this discrepancy is that NSRD footwall rocks experienced tectonic over-pressure. The outstanding structural and stratigraphic context of the Northern Snake Range make it a critical structural system for further investigation of this issue.

Data Availability Statement

All of the data used for this research are contained within the manuscript and Supporting Information S1. The data used for this research have been placed in the online data repository *MyGeohub* (https://mygeohub.org/projects/nsrdfootwallburial/files/browse, Long et al., 2024).

Acknowledgments
This work was supported by National Science Foundation Grants EAR-2022973 awarded to Sean Long and EAR-2022979 awarded to Jeffrey Lee. This work honors the pioneering research of Elizabeth Miller and Phil Gans, whose field work in the Northern Snake Range in the 1980s provided an enormous leap forward in our understanding of this outstanding structural system. We acknowledge the use of facilities within the Eyring Materials Center at Arizona State University, which is supported in part by NNCI-ECCS-2025490. We thank Thomas Hoisch and Andrew Zuza for reviews that improved this manuscript.

References

Allen, P. A., Verlander, J. E., Burgess, P. M., & Audet, D. M. (2000). Jurassic giant erg deposits, flexure of the United States continental interior, and timing of the onset of Cordilleran shortening. *Geology*, *28*(2), 159–162. https://doi.org/10.1130/0091-7613(2000)28<159:JGEDFO>2.0.CO;2

Allmendinger, R. W., Hauge, T. A., Potter, C. J., Klemperer, S. L., Nelson, K. D., Knuepfer, P., & Oliver, J. (1987). Overview of the COCORP 40°N transect, western United States: The fabric of an orogenic belt. *Geological Society of America Bulletin*, *98*(3), 308–319. https://doi.org/10.1130/0016-7606(1987)98%3C308:OOTCNT%3E2.0.CO;2

Allmendinger, R. W., Sharp, J. W., Von Tish, D., Serpa, L., Brown, L., Kaufman, S., et al. (1983). Cenozoic and Mesozoic structure of the eastern Basin and Range Province, Utah, from COCORP seismic-reflection data. *Geology*, *11*(9), 532–536. https://doi.org/10.1130/0091-7613(1983)11<532:CAMSOT>2.0.CO;2

Anderson, R. E., Zoback, M. L., & Thompson, G. A. (1983). Implications of selected subsurface data on the structural form and evolution of some basins in the northern Basin and Range Province, Nevada and Utah. *Geological Society of America Bulletin*, *94*(9), 1055–1072. https://doi.org/10.1130/0016-7606(1983)94%3C1055:IOSSDO%3E2.0.CO;2

Aoya, M., Kouketsu, Y., Endo, S., Shimizu, H., Mizukami, T., Nakamura, D., & Wallis, S. (2010). Extending the applicability of the Raman carbonaceous-material geothermometer using data from contact metamorphic rocks. *Journal of Metamorphic Geology*, *28*(9), 895–914. https://doi.org/10.1111/j.1525-1314.2010.00896.x

Armstrong, R. L. (1970). Geochronology of Tertiary igneous rocks, eastern Basin and Range Province, western Utah, eastern Nevada, and vicinity, USA. *Geochimica et Cosmochimica Acta*, *34*(1), 203–232. https://doi.org/10.1016/0016-7037(70)90007-4

Armstrong, R. L. (1972). Low-angle (denudation) faults, hinterland of the Sevier orogenic belt, eastern Nevada and western Utah. *Geological Society of America Bulletin*, *83*(6), 1729–1754. https://doi.org/10.1130/0016-7606(1972)83[1729:LDFHOT]2.0.CO;2

Avent, J. C. (1962). *Structure and stratigraphy of the Antelope Range, northeastern White Pine County, Nevada* [M.S. thesis]. University of Washington, Seattle. 2 plates.

Axen, G. J., Taylor, W. J., & Bartley, J. M. (1993). Space-time patterns and tectonic controls of Tertiary extension and magmatism in the Great Basin of the western United States. *Geological Society of America Bulletin*, *105*(1), 56–76. https://doi.org/10.1130/0016-7606(1993)105<0056:STPATC>2.3.CO;2

Bartley, J. M., & Wernicke, B. P. (1984). The Snake Range décollement interpreted as a major extensional shear zone. *Tectonics*, *3*(6), 647–657. https://doi.org/10.1029/TC003i006p00647

Barton, M., Battles, D., Debout, G., Capo, R., Christensen, J., Davies, S., et al. (1988). Mesozoic contact metamorphism in the western United States. In W. G. Ernst (Ed.), *Metamorphism and Crustal Evolution, Western United States, Rubey Volume VII* (pp. 111–178). Prentice-Hall.

Barton, M. D. (1990). Cretaceous magmatism, metamorphism, and metallogeny in the east-central Great Basin. In J. L. Anderson (Ed.), *The Nature and Origin of Cordilleran Magmatism* (Vol. 174, pp. 283–302). Geological Society of American Memoir. https://doi.org/10.1130/mem174-p283

Best, M. G., Armstrong, R. L., Graustein, W. C., Embree, G. F., & Ahlborn, R. C. (1974). Mica granites of the Kern Mountains pluton, eastern White Pine County, Nevada: Remobilized basement of the Cordilleran miogeosyncline? *Geological Society of America Bulletin*, *85*(8), 1277–1286. https://doi.org/10.1130/0016-7606(1974)85<1277:mgotkm>2.0.co;2

Beyssac, O., Goffé, B., Chopin, C., & Rouzaud, J. N. (2002). Raman spectra of carbonaceous material in metasediments: A new geothermometer. *Journal of Metamorphic Geology*, *20*(9), 859–871. https://doi.org/10.1046/j.1525-1314.2002.00408.x

Beyssac, O., Goffé, B., Petitet, J. P., Froigneux, E., Moreau, M., & Rouzaud, J. N. (2003). On the characterization of disordered and heterogeneous carbonaceous materials by Raman spectroscopy. *Spectrochimica Acta Part A: Molecular and Biomolecular Spectroscopy*, *59*(10), 2267–2276. https://doi.org/10.1016/S1386-1425(03)00070-2

Bjerrum, C. J., & Dorsey, R. J. (1995). Tectonic controls on deposition of Middle Jurassic strata in a retroarc foreland basin, Utah-Idaho trough, western interior, United States. *Tectonics*, *14*(4), 962–978. https://doi.org/10.1029/95TC01448

Blackford, N. R., Long, S. P., Stout, A. J., Rodgers, D. W., Cooper, C. M., Kramer, K., et al. (2022). Late Cretaceous upper-crustal thermal structure of the Sevier hinterland: Implications for the geodynamics of the Nevadaplano. *Geosphere*, *18*(1), 183–210. https://doi.org/10.1130/GES02386.1

Brokaw, A. L. (1967). Geologic map and sections of the Ely quadrangle, White Pine County, Nevada. *United States Geological Survey Geologic Quadrangle Map GQ-697, 1:24,000-scale, 1 plate*.

Burchfiel, B. C., Cowan, D. S., & Davis, G. A. (1992). Tectonic overview of the Cordilleran orogen in the western United States. In B. C. Burchfiel, P. W. Lipman, & M. L. Zoback (Eds.), *The Cordilleran Orogen conterminous US* (Vol. G-3, pp. 407–479). Geological Society of America. https://doi.org/10.1130/dnag-gna-g3.407

Camilleri, P. A., & Chamberlain, K. R. (1997). Mesozoic tectonics and metamorphism in the Pequop Mountains and Wood Hills region, northeast Nevada: Implications for the architecture and evolution of the Sevier orogen. *Geological Society of America Bulletin*, *109*(1), 74–94. https://doi.org/10.1130/0016-7606(1997)109<0074:MTAMIT>2.3.CO;2

Cassel, E. G., Smith, M. E., & Jicha, B. R. (2018). The impact of slab rollback on Earth's surface: Uplift and extension in the hinterland of the North American Cordillera. *Geophysical Research Letters*, *45*(20), 10996–11004. https://doi.org/10.1029/2018GL079887

Cassel, E. J., Breecker, D. O., Henry, C. D., Larson, T. E., & Stockli, D. F. (2014). Profile of a paleo-orogen: High topography across the present-day Basin and Range from 40 to 23 Ma. *Geology*, *42*(11), 1007–1010. https://doi.org/10.1130/G35924.1

Chapman, J. B., Ducea, M. N., DeCelles, P. G., & Profeta, L. (2015). Tracking changes in crustal thickness during orogenic evolution with Sr/Y: An example from the North American Cordillera. *Geology*, *43*(10), 919–922. https://doi.org/10.1130/G36996.1

Chu, X., Ague, J. J., Podladchikov, Y. Y., & Tian, M. (2017). Ultrafast eclogite formation via melting-induced overpressure. *Earth and Planetary Science Letters*, *479*, 1–17. https://doi.org/10.1016/j.epsl.2017.09.007

Coney, P. J. (1974). Structural analysis of the Snake Range décollement, east-central Nevada. *Geological Society of America Bulletin*, *85*(6), 973–978. https://doi.org/10.1130/0016-7606(1974)85%3C973:SAOTSR%3E2.0.CO;2

Coney, P. J., & Harms, T. J. (1984). Cordilleran metamorphic core complexes: Cenozoic extensional relics of Mesozoic compression. *Geology*, *12*(9), 550–554. https://doi.org/10.1130/0091-7613(1984)12<550:CMCCCE>2.0.CO;2

Coogan, J. C. (1992). *Thrust systems and displacement transfer in the Wyoming-Idaho-Utah thrust belt* [Ph.D. dissertation] (p. 240). University of Wyoming. 55 figures, 2 plates.

Cooper, F. J. (2008). *Structural and thermobarometric constraints on the exhumation of the Northern Snake Range metamorphic core complex, Nevada* [Ph.D. dissertation] (p. 185). University of Southern California.

Cooper, F. J., Hodges, K. V., & Adams, B. A. (2013). Metamorphic constraints on the character and displacement of the South Tibetan fault system, central Bhutanese Himalaya. *Lithosphere*, *5*(1), 67–81. https://doi.org/10.1130/L221.1

Cooper, F. J., Platt, J. P., Anczkiewicz, R., & Whitehouse, J. (2010). Footwall dip of a core complex detachment fault: Thermobarometric constraints from the northern Snake Range (Basin and Range, USA). *Journal of Metamorphic Geology*, *28*(9), 997–1020. https://doi.org/10.1111/j.1525-1314.2010.00907.x

Cooper, F. J., Platt, J. P., Platzman, E. S., Grove, M. J., & Seward, G. (2010). Opposing shear senses in a subdetachment mylonite zone: Implications for core complex mechanics. *Tectonics*, *29*(4), TC4019. https://doi.org/10.1029/2009TC002632

Crafford, A. E. J. (2007). *Geologic Map of Nevada*. *United States Geological Survey Data Series* (Vol. 249, p. 46). US Department of the Interior, US Geological Survey. https://doi.org/10.3133/ds249

Crittenden, M. D., Jr., Coney, P. J., & Davis, G. H. (Eds.) (1980)., *Cordilleran Metamorphic Core Complexes* (Vol. 153, p. 490). Geological Society of America Memoir.

DeCelles, P. G. (2004). Late Jurassic to Eocene evolution of the Cordilleran thrust belt and foreland basin system, western USA. *American Journal of Science*, *304*(2), 105–168. https://doi.org/10.2475/ajs.304.2.105

DeCelles, P. G., & Coogan, J. C. (2006). Regional structure and kinematic history of the Sevier fold-and-thrust belt, central Utah. *Geological Society of America Bulletin*, *118*(7–8), 841–864. https://doi.org/10.1130/B25759.1

Dechert, C. P. (1967). *Bedrock geology of the northern Schell Creek Range, White Pine County, Nevada* [Ph.D. dissertation] (p. 266). University of Washington, Seattle.

Dickinson, W. R. (2002). The Basin and Range province as a composite extensional domain. *International Geology Review*, *44*, 1–38. https://doi.org/10.2747/0020-6814.44.1.1

Dickinson, W. R. (2006). Geotectonic evolution of the Great Basin. *Geosphere*, *2*(7), 353–368. https://doi.org/10.1130/GES00054.1

Dickinson, W. R., & Snyder, W. S. (1978). Plate tectonics of the Laramide orogeny. In V. Mathews III (Ed.), *Laramide folding associated with basement block faulting in the Western United States* (Vol. 151, pp. 355–366). Geological Society of America Memoir. https://doi.org/10.1130/mem151-p355

Di Fiori, R. V., Long, S. P., Fetrow, A., Snell, K. E., Bonde, J. A., & Vervoort, J. D. (2020). Syn-contractional deposition of the Cretaceous Newark Canyon formation, Diamond Mountains, Nevada: Implications for strain partitioning within the U.S. Cordillera. *Geosphere*, *61*(2), 546–566. https://doi.org/10.1130/GES02168.1

Di Fiori, R. V., Long, S. P., Snell, K. E., Fetrow, A. C., Bonde, J. W., & Vervoort, J. D. (2021). The role of shortening in the Sevier hinterland within the U.S. Cordilleran retroarc thrust system: Insights from the Cretaceous Newark Canyon Formation in central Nevada. *Tectonics*, *40*(5), e2020TC006331. https://doi.org/10.1029/2020TC006331

Douglass, W. B., Jr. (1960). Geology of the southern Butte Mountains, White Pine County, Nevada. In J. W. Boettcher & W. W. Sloan Jr. (Eds.), *Guidebook to the Geology of East-Central Nevada: Intermountain Association of Petroleum Geologists, 11th Annual Field Conference* (pp. 181–185).

Drewes, H. (1967). Geology of the Connors Pass quadrangle, Schell Creek Range, east-central Nevada. *United States Geological Survey Professional Paper 557* (p. 97). scale 1:48,000, 1 sheet. https://doi.org/10.3133/pp557

Druschke, P., Hanson, A. D., & Wells, M. L. (2009). Structural, stratigraphic, and geochronologic evidence for extension predating Paleogene volcanism in the Sevier hinterland, east-central Nevada. *International Geology Review*, *51*(7–8), 743–775. https://doi.org/10.1080/00206810902917941

Druschke, P., Hanson, A. D., Wells, M. L., Gehrels, G. E., & Stockli, D. (2011). Paleogeographic isolation of the Cretaceous to Eocene Sevier hinterland, east-central Nevada: Insights from U-Pb and (U-Th)/He detrital zircon ages of hinterland strata. *Geological Society of America Bulletin*, *123*(5–6), 1141–1160. https://doi.org/10.1130/B30029.1

Epstein, A. G., Epstein, J. B., & Harris, L. D. (1977). Conodont color alteration - An index to organic metamorphism. *United States Geological Survey Professional Paper*, *995*, 27.

Evans, S. L., Styron, R. H., van Soest, M. C., Hodges, K. V., & Hanson, A. D. (2015). Zircon and apatite (U-Th)/He evidence for Paleogene and Neogene extension in the Southern Snake Range, Nevada, USA. *Tectonics*, *34*(10), 2142–2164. https://doi.org/10.1002/2015TC003913

Fritz, W. H. (1968). Geologic map and sections of the southern Cherry Creek and northern Egan Ranges, White Pine County, Nevada. *Nevada Bureau of Mines and Geology Map 35*. scale 1:62,500, 1 plate.

Gans, P. B. (1982). *Mid-tertiary magmatism and extensional faulting in the Hunter district, White Pine County, Nevada* [Ph.D. dissertation] (p. 179). Stanford University. 3 plates.

Gans, P. B., Mahood, G. A., & Schermer, E. (1989). Synextensional magmatism in the Basin and Range province: A case study from the eastern Great Basin. *Geological Society of America Special Paper*, *233*, 53.

Gans, P. B., & Miller, E. L. (1983). Style of mid-Tertiary extension in east-central Nevada. *Utah Geological and Mineral Survey Special Studies*, *59*, 107–160.

Gans, P. B., Miller, E. L., Huggins, C. C., & Lee, J. (1999). Geologic map of the Little Horse Canyon quadrangle, Nevada and Utah. *Nevada Bureau of Mines and Geology Field Studies Map FS-20* (p. 12). 1 sheet, 1:24,000-scale.

Gans, P. B., Miller, E. L., & Lee, J. (1999). Geologic map of the Spring Mountain quadrangle, Nevada and Utah. *Nevada Bureau of Mines and Geology Field Studies Map FS-18* (p. 12). 1 sheet, 1:24,000-scale.

Gans, P. B., Miller, E. L., McCarthy, J., & Oldcott, M. L. (1985). Tertiary extensional faulting and evolving ductile-brittle transition zones in the northern Snake Range and vicinity: New insights from seismic data. *Geology*, *13*(3), 189–193. https://doi.org/10.1130/0091-7613(1985)13%3C189:TEFAED%3E2.0.CO;2

Gans, P. B., Seedorff, E., Fahey, P. L., Hasler, R. W., Maher, D. J., Jeanne, R. A., & Shaver, S. A. (2001). Rapid Eocene extension in the Robinson District, White Pine County, Nevada: Constraints from $^{40}Ar/^{39}Ar$ dating. *Geology*, *29*(6), 475–478. https://doi.org/10.1130/0091-7613(2001)029<0475:REEITR>2.0.CO;2

Gébelin, A., Mulch, A., Teyssier, C., Heizler, M., Vennemann, T., & Seaton, N. C. A. (2011). Oligo-Miocene extensional tectonics and fluid flow across the northern Snake Range detachment system, Nevada. *Tectonics*, *30*(5), TC5010. https://doi.org/10.1029/2010TC002797

Gébelin, A., Teyssier, C., Heizler, M., & Mulch, A. (2015). Meteoric water circulation in a rolling-hinge detachment system (northern Snake Range core complex, Nevada). *Geological Society of America Bulletin*, *127*(1–2), 149–161. https://doi.org/10.1130/B31063.1

Gerya, T. (2015). Tectonic overpressure and underpressure in lithospheric tectonics and metamorphism. *Journal of Metamorphic Geology*, *33*(8), 785–800. https://doi.org/10.1111/jmg.12144

Gilbert, H. (2012). Crustal structure and signatures of recent tectonism as influenced by ancient terranes in the western United States. *Geosphere*, *8*(1), 141–157. https://doi.org/10.1130/GES00720.1

Gottlieb, E. S., Miller, E. L., Valley, J. W., Premo, W. R., Fisher, C. M., Vervoort, J. D., & Kitajima, K. (2022). Zircon petrochronology of Cretaceous Cordilleran interior granites of the Snake Range and Kern Mountains, Nevada, USA. In J. P. Craddock, D. H. Malone, B. Z. Foreman, & A. Konstantinou (Eds.), *Tectonic Evolution of the Sevier-Laramide Hinterland, Thrust Belt, and Foreland, and Postorogenic Slab Rollback (180–20 Ma)* (Vol. 555, pp. 21–65). Geological Society of America Special Paper. https://doi.org/10.1130/2022.2555(02)

Greene, D. C. (2014). The Confusion Range, west-central Utah: Fold-thrust deformation and a western Utah thrust belt in the Sevier hinterland. *Geosphere*, *10*(1), 148–169. https://doi.org/10.1130/GES00972.1

Hallett, B. W., & Spear, F. S. (2014). The *P-T* history of anatectic pelites of the Northern East Humboldt Range, Nevada: Evidence for tectonic loading, decompression, and anatexis. *Journal of Petrology*, *55*(1), 3–36. https://doi.org/10.1093/petrology/egt057

Harris, A. G., Wardlaw, B. R., Rust, C. C., & Merrill, G. K. (1980). Maps for assessing thermal maturity (conodont color alteration index maps) in Ordovician through Triassic rocks in Nevada and Utah and adjacent parts of Idaho and California. *United States Geological Survey Miscellaneous Investigation Series* (Vol. *I-1249*). 2 sheets.

Harris, H. D. (1959). A late Mesozoic positive area in western Utah. *American Association of Petroleum Geologists Bulletin*, *43*, 2636–2652. https://doi.org/10.1306/0BDA5F39-16BD-11D7-8645000102C1865D

Henry, C. D., & John, D. A. (2013). Magmatism, ash-flow tuffs, and calderas of the ignimbrite flareup in the western Nevada volcanic field, Great Basin, USA. *Geosphere*, *9*(4), 951–1008. https://doi.org/10.1130/GES00867.1

Henry, C. D., McGrew, A. J., Colgan, J. P., Snoke, A. W., & Brueseke, M. E. (2011). Timing, distribution, amount, and style of Cenozoic extension in the northern Great Basin. In J. Lee & J. P. Evans (Eds.), *Geologic Field Trips to the Basin and Range, Rocky Mountains, Snake River Plain, and Terranes of the U.S. Cordillera* (Vol. 21, pp. 27–66). Geological Society of America Field Guide. https://doi.org/10.1130/2011.0021(02)

Hintze, L. F. (1974a). Preliminary geologic map of the Conger Mountain quadrangle, Millard County, Utah. *United States Geological Survey Miscellaneous Field Studies*. Map MF-634, 1:48,000-scale, 2 sheets.

Hintze, L. F. (1974b). Preliminary geologic map of the Notch Peak quadrangle, Millard County, Utah. *United States Geological Survey Miscellaneous Field Studies*. Map MF-636, 1:48,000-scale, 2 sheets.

Hintze, L. F., & Davis, F. D. (2002). Geologic map of the Tule Valley 30′ x 60′ quadrangle and Parts of the Ely, Fish Springs, and Kern Mountains 30′ × 60′ quadrangles, northwest Millard County, Utah. *Utah Geological Survey Map 186*. 1:100,000-scale.

Hintze, L. F., & Davis, F. D. (2003). *Geology of Millard Country, Utah* (Vol. 133, p. 305). Utah Geological Survey.

Hodges, K. V., & Walker, J. D. (1992). Extension in the Cretaceous Sevier orogen, North American Cordillera. *Geological Society of America Bulletin*, *104*(5), 560–569. https://doi.org/10.1130/0016-7606(1992)104<0560:EITCSO>2.3.CO;2

Hoiland, C. W. (2019). *Extracting tectonic histories from metamorphic rocks in mountain belts: Insights from the Snake Range metamorphic cores complex, Nevada, and the Brooks Range, Alaska* [Ph.D. dissertation] (p. 388). Stanford University.

Hoiland, C. W., Hourigan, J., & Miller, E. L. (2022). Evidence for large departures from lithostatic pressure during Late Cretaceous metamorphism in the northern Snake Range metamorphic core complex, Nevada. In J. P. Craddock, D. H. Malone, B. Z. Foreman, & A. Konstantinou (Eds.), *Tectonic Evolution of the Sevier-Laramide Hinterland, Thrust Belt, and Foreland, and Postorogenic Slab Rollback (180–20 Ma)* (Vol. 555, pp. 27–219). Geological Society of America Special Paper. https://doi.org/10.1130/2021.2555(07)

Hose, R. K. (1965). *Geologic map and sections of the Conger Range NE quadrangle and adjacent area, Confusion Range, Millard County, Utah*. United States Geological Survey Miscellaneous Geologic Investigations. Map I-436, 1:24,000-scale, 1 sheet.

Hose, R. K. (1974). *Geologic map of the Trout Creek SE Quadrangle, Juab and Millard Counties, Utah*. United States Geological Survey Miscellaneous Geologic Investigations. Map I-827, 1:24,000-scale, 1 sheet.

Hose, R. K., & Blake, M. C., Jr. (1976). *Geology and mineral resources of White Pine County, Nevada* (Vol. 85, p. 32). Nevada Bureau of Mines and Geology Bulletin. 1:250,000-scale.

Huggins, C. C., & Wright, J. E. (1989). Superimposed Cretaceous and Tertiary metamorphism in the northern Snake Range, Nevada. *Geological Society of America Abstracts with Programs*, *21*, A95.

Humphreys, E. D. (1995). Post-Laramide removal of the Farallon slab, western United States. *Geology*, *23*(11), 987–990. https://doi.org/10.1130/0091-7613(1995)023<0987:PLROTF>2.3.CO;2

Hurlow, H. (2014). Chapter 3: Gravity Study. In H. Hurlow (Ed.), *Hydrogeologic studies and groundwater monitoring in Snake Valley and adjacent hydrographic areas, west-central Utah and east-central Nevada* (Vol. 135, pp. 29–55). Utah Geological Survey Bulletin.

Johnston, S. M. (2000). *Normal faulting in the upper plate of a metamorphic core complex, northern Snake Range, Nevada* [M.S. thesis] (p. 60). Stanford University.

Kenney, M. (2013). Intrusive and deformational histories of the footwall rocks in the central part of the northern Snake Range, Nevada. In R. J. Varga (Ed.), *Proceedings of the 26th Annual Keck Research Symposium in Geology, Keck Geology Consortium, Pomona College, California* (Vol. 26, pp. 201–206).

Königshof, P. (2003). Conodont deformation patterns and textural alteration in Paleozoic conodonts: Examples from Germany and France. *Senckenbergiana Lethaea*, *83*(1), 149–156. https://doi.org/10.1007/BF03043310

Kouketsu, Y., Mizukami, T., Mori, H., Endo, S., Aoya, M., Hara, H., & Wallis, S. (2014). A new approach to develop the Raman carbonaceous material geothermometer for low-grade metamorphism using peak width. *Island Arc*, *23*(1), 33–50. https://doi.org/10.1111/iar.12057

Lee, D. E., Friedman, I., & Gleason, J. D. (1984). Modification of delta D values in eastern Nevada granitoid rocks spatially related to thrust faults. *Contributions to Mineralogy and Petrology*, *88*(3), 288–298. https://doi.org/10.1007/BF00380174

Lee, D. E., Marvin, R. F., & Mehnert, H. H. (1980). A radiometric age study of Mesozoic-Cenozoic metamorphism is eastern White Pine County, Nevada and nearby Utah. *United States Geological Survey Professional Paper 1158-C* (pp. 17–28).

Lee, D. E., Stacey, J. S. D., & Fisher, L. (1986). Muscovite-phenocrystic two-mica granites of NE Nevada are Late Cretaceous in age. In *Shorter contributions to isotope research* (Vol. 1622, pp. 31–39). United States Geological Survey Bulletin.

Lee, J. (1990). *Structural geology and $^{40}Ar/^{39}Ar$ thermochronology in the northern Snake Range metamorphic core complex, Nevada* [PhD dissertation] (p. 184). Stanford University.

Lee, J. (1995). Rapid uplift and rotation of mylonitic rocks from beneath a detachment fault: Insights from potassium feldspar $^{40}Ar/^{39}Ar$ thermochronology, northern Snake Range, Nevada. *Tectonics*, *14*(1), 54–77. https://doi.org/10.1029/94TC01508

Lee, J., Blackburn, T., & Johnston, S. (2017). Timing of mid-crustal ductile extension in the northern Snake Range metamorphic core complex, Nevada: Evidence from U/Pb zircon ages. *Geosphere*, *13*(2), 439–459. https://doi.org/10.1130/GES01429.1

Lee, J., Gans, P. B., & Miller, E. L. (1999a). Geologic map of the Mormon Jack Pass quadrangle, Nevada. *Nevada Bureau of Mines and Geology Field Studies Map 17*. 1 sheet, 1:24,000-scale.

Lee, J., Gans, P. B., & Miller, E. L. (1999b). Geologic map of the Third Butte East Quadrangle, Nevada. *Nevada Bureau of Mines and Geology Field Studies Map 16* (p. 12). 1:24,000-scale, 1 plate.

Lee, J., Johnston, S., & Miller, E. L. (2023). Geologic map of the Sixmile Canyon quadrangle, White Pine County, Nevada. *Nevada Bureau of Mines and Geology Open-File Report 2023-08* (p. 8). scale 1:24,000.

Lee, J., Miller, E. L., Gans, P. B., & Huggins, C. C. (1999). Geologic map of the Mount Moriah Quadrangle, Nevada. *Nevada Bureau of Mines and Geology Field Studies Map 19* (p. 12). 1:24,000-scale, 1 plate.

Lee, J., Miller, E. L., & Sutter, J. F. (1987). Ductile strain and metamorphism in an extensional tectonic setting: A case study from the northern Snake Range, Nevada, U.S.A. In M. P. Coward, J. F. Dewey, & P. L. Hancock (Eds.), *Continental extensional tectonics* (Vol. 28, pp. 267–298). Geological Society of London Special Publication. https://doi.org/10.1144/gsl.sp.1987.028.01.18

Lee, J., & Sutter, J. F. (1991). Incremental $^{40}Ar/^{39}Ar$ thermochronology of mylonitic rocks from the northern Snake Range, Nevada. *Tectonics*, *10*(1), 77–100. https://doi.org/10.1029/90TC01931

Lewis, C. J., Wernicke, B. P., Selverstone, J., & Bartley, J. M. (1999). Deep burial of the footwall of the northern Snake Range decollement, Nevada. *Geological Society of America Bulletin*, *111*, 39–51. https://doi.org/10.1130/0016-7606(1999)111%3C0039:DBOTFO%3E2.3.CO;2

Long, S. P. (2012). Magnitudes and spatial patterns of erosional exhumation in the Sevier hinterland, eastern Nevada and western Utah, USA: Insights from a Paleogene paleogeologic map. *Geosphere*, *8*(4), 881–901. https://doi.org/10.1130/GES00783.1

Long, S. P. (2015). An upper-crustal fold province in the hinterland of the Sevier orogenic belt, eastern Nevada, U.S.A.: A Cordilleran Valley and Ridge in the Basin and Range. *Geosphere*, *11*(2), 404–424. https://doi.org/10.1130/GES01102.1

Long, S. P. (2019). Geometry and magnitude of extension in the Basin and Range Province (39°N), California, Nevada, and Utah, U.S.A: Constraints from a province-scale cross section. *Geological Society of America Bulletin*, *131*(1–2), 99–119. https://doi.org/10.1130/B31974.1

Long, S. P. (2023). Westward underthrusting of thick North American crust: The dominant thickening process that built the Cordilleran orogenic plateau. *Geology*, *51*(12), 1111–1116. https://doi.org/10.1130/G51339.1

Long, S. P., Blackford, N. R., Lee, J., & Soignard, E. (2024). Crustal thermal architecture, structural reconstructions, field relationships and geophysical data rule out deep structural burial of the footwall of the Northern Snake Range metamorphic core complex (Nevada, USA) [Dataset]. *MyGeohub*. https://mygeohub.org/projects/nsrdfootwallburial/files

Long, S. P., Henry, C. D., Muntean, J. L., Edmondo, G. P., & Cassel, E. J. (2014). Early cretaceous construction of a structural culmination, Eureka, Nevada, U.S.A.: Implications for out-of-sequence deformation in the Sevier hinterland. *Geosphere*, *10*(3), 564–584. https://doi.org/10.1130/GES00997.1

Long, S. P., Lee, J., & Blackford, N. R. (2022). The low-angle breakaway system for the Northern Snake Range décollement in the Schell Creek and Duck Creek Ranges, eastern Nevada, USA: Implications for displacement magnitude. *Geosphere*, *18*(4), 1194–1222. https://doi.org/10.1130/GES02482.1

Long, S. P., Lee, J., & Blackford, N. R. (2023). Extreme ductile thinning of Cambrian marbles in the Northern Snake Range metamorphic core complex, Nevada, USA: Implications for extension magnitude and structural evolution. *Journal of Structural Geology*, *173*, 104912. https://doi.org/10.1016/j.jsg.2023

Long, S. P., & Soignard, E. (2016). Shallow-crustal metamorphism during Late Cretaceous anatexis in the Sevier hinterland plateau: Peak temperature conditions from the Grant Range, eastern Nevada, U.S.A. *Lithosphere*, *8*(2), 150–164. https://doi.org/10.1130/L501.1

Luisier, C., Baumgartner, L., Schmalholz, S. M., Siron, G., & Vennemann, T. (2019). Metamorphic pressure variation in a coherent Alpine nappe challenges lithostatic pressure paradigm. *Nature Communications*, *10*, 1–11. https://doi.org/10.1038/s41467-019-12727-z

Lund-Snee, J. E., & Miller, E. L. (2022). Magmatism, migrating topography, and the transition from Sevier shortening to Basin and Range extension, western United States. In J. P. Craddock, D. H. Malone, B. Z. Foreman, & A. Konstantinou (Eds.), *Tectonic Evolution of the Sevier-Laramide Hinterland, Thrust Belt, and Foreland, and Postorogenic Slab Rollback (180–20 Ma)* (Vol. 555, p. 23). Geological Society of America Special Paper. https://doi.org/10.1130/2021.2555(13)

Lünsdorf, N. K., Dunkl, I., Schmidt, B. C., Rantitsch, G., & von Eynatten, H. (2017). Towards a higher comparability of geothermometric data obtained by Raman spectroscopy of carbonaceous material. Part 2: A revised geothermometer. *Geostandards and Geoanalytical Research*, *41*(4), 593–612. https://doi.org/10.1111/ggr.12178

Marques, F. O., Ranalli, G., & Mandal, N. (2018). Tectonic overpressure at shallow depth in the lithosphere: The effects of boundary conditions. *Tectonophysics*, *746*, 702–715. https://doi.org/10.1016/j.tecto.2018.03.022

Martinez, C. M., Miller, E. L., & Stockli, D. F. (1998). Miocene age rock avalanche deposits of the Sacramento Pass Basin, Basin and Range Province, Nevada. *Geological Society of America Abstracts with Programs*, *30*(5), 53.

McGrew, A. J. (1993). The origin and evolution of the southern Snake Range Decollement, east central Nevada. *Tectonics*, *12*, 21–34. https://doi.org/10.1029/92TC01713

McGrew, A. J., Peters, M. T., & Wright, J. E. (2000). Thermobarometric constraints on the tectonothermal evolution of the East Humboldt Range metamorphic core complex, Nevada. *Geological Society of America Bulletin*, *112*(1), 45–60. https://doi.org/10.1130/0016-7606(2000)112<45:TCOTTE>2.0.CO;2

Miller, C. F., & Bradfish, L. J. (1980). An inner Cordilleran belt of muscovite-bearing plutons. *Geology*, *8*(9), 412–416. https://doi.org/10.1130/0091-7613(1980)8%3C412:AICBOM%3E2.0.CO;2

Miller, E. L., Dumitru, T. A., Brown, R. W., & Gans, P. B. (1999). Rapid Miocene slip on the Snake Range–Deep Creek Range fault system, east-central Nevada. *Geological Society of America Bulletin*, *111*(6), 886–905. https://doi.org/10.1130/0016-7606(1999)111<0886:RMSOTS>2.3.CO;2

Miller, E. L., & Gans, P. B. (1989). Cretaceous crustal structure and metamorphism in the hinterland of the Sevier thrust belt, western U.S. Cordillera. *Geology*, *17*(1), 59–62. https://doi.org/10.1130/0091-7613(1989)017<0059:CCSAMI>2.3.CO;2

Miller, E. L., & Gans, P. B. (1999). Geologic map of the Cove quadrangle, Nevada and Utah. *Nevada Bureau of Mines and Geology Field Studies Map 22* (p. 12). 1:24,000-scale, 1 sheet.

Miller, E. L., Gans, P. B., & Garing, J. (1983). The Snake Range décollement: An exhumed mid-Tertiary ductile-brittle transition. *Tectonics*, *2*(3), 239–263. https://doi.org/10.1029/TC002i003p00239

Miller, E. L., Gans, P. B., Grier, S. P., Huggins, C. C., & Lee, J. (1999). Geologic map of the Old Man's Canyon quadrangle, Nevada. *Nevada Bureau of Mines and Geology Field Studies Map 21* (p. 12). 1:24,000-scale, 1 sheet.

Miller, E. L., Gans, P. B., Wright, J. E., & Sutter, J. F. (1988). Metamorphic history of the east central Basin and Range Province: Tectonic setting and relationship to magmatism. In W. G. Ernst (Ed.), *Metamorphism and Crustal Evolution, Western United States, Rubey Volume VII* (pp. 649–682). Prentice-Hall.

Moulas, E., Burg, J. P., & Podladchikov, Y. (2014). Stress field associated with elliptical inclusions in a deforming matrix: Mathematical model and implications for tectonic overpressure in the lithosphere. *Tectonophysics*, *631*, 37–49. https://doi.org/10.1016/j.tecto.2014.05.004

Moulas, E., Podladchikov, Y. Y., Aranovich, L. Y., & Kostopoulos, D. (2013). The problem of depth in geology: When pressure does not translate into depth. *Petrology*, *21*(6), 527–538. https://doi.org/10.1134/s0869591113060052

Moulas, E., Schmalholz, S. M., Podladchikov, Y., Tajčmanová, L., Kostopoulos, D., & Baumgartner, L. (2019). Relation between mean stress, thermodynamic, and lithostatic pressure. *Journal of Metamorphic Geology*, *37*, 1–14. https://doi.org/10.1111/jmg.12446

Nelson, R. B. (1966). Structural development of the northernmost Snake Range, Kern Mountains, and Deep Creek Range, Nevada and Utah. *American Association of Petroleum Geologists Bulletin*, *50*(5), 921–951. https://doi.org/10.1306/5d25b605-16c1-11d7-8645000102c1865d

Nelson, R. B. (1969). Relation and history of structures in a sedimentary succession with deeper metamorphic structures, eastern Great Basin. *American Association of Petroleum Geologists Bulletin*, *53*, 307–339. https://doi.org/10.1306/5d25c60f-16c1-11d7-8645000102c1865d

Petrini, K., & Podladchikov, Y. (2000). Lithospheric pressure-depth relationship in compressive regions of thickened crust. *Journal of Metamorphic Geology*, *18*(1), 67–77. https://doi.org/10.1046/j.1525-1314.2000.00240.x

Platt, J. P., Behr, W. M., & Cooper, F. J. (2015). Metamorphic core complexes: Windows into the mechanics and rheology of the crust. *Journal of the Geological Society of London*, *172*(1), 9–27. https://doi.org/10.1144/jgs2014-036

Pleuger, J., & Podladchikov, Y. Y. (2014). A purely structural restoration of the NFP20-East cross section and potential tectonic overpressure in the Adula nappe (central Alps). *Tectonics*, *33*(5), 656–685. https://doi.org/10.1002/2013TC003409

Poole, F. G., Stewart, J. H., Palmer, A. R., Sandberg, C. A., Madrid, R. J., Ross, R. J., Jr., et al. (1992). Latest Precambrian to latest Devonian time; development of a continental margin. In B. C. Burchfiel, P. W. Lipman, & M. L. Zoback (Eds.), *The Cordilleran Orogen: Conterminous U.S* (pp. 9–56). Geological Society of America, The Geology of North America, G-3. https://doi.org/10.1130/DNAG-GNA-G3.9

Rahl, J. M., Anderson, K. M., Brandon, M. T., & Fassoulas, C. (2005). Raman spectroscopic carbonaceous material thermometry of low-grade metamorphic rocks: Calibration and application to tectonic exhumation in Crete, Greece. *Earth and Planetary Science Letters*, *240*(2), 339–354. https://doi.org/10.1016/j.epsl.2005.09.055

Rodgers, D. W. (1987). *Thermal and structural evolution of the southern Deep Creek Range, west central Utah and east central Nevada* [Ph.D. dissertation] (p. 149). Stanford University. 5 plates.

Royse, F., Jr. (1993). Case of the phantom foredeep: Early Cretaceous in west-central Utah. *Geology*, *21*(2), 133–136. https://doi.org/10.1130/0091-7613(1993)021%3C0133:COTPFE%3E2.3.CO;2

Schmalholz, S. M., Medvedev, S., Lechmann, S. M., & Podladchikov, Y. (2014). Relationship between tectonic overpressure, deviatoric stress, driving force, isostasy and gravitational potential energy. *Geophysical Journal International*, *197*(2), 680–696. https://doi.org/10.1093/gji/ggu040

Schmalholz, S. M., & Podladchikov, Y. Y. (2013). Tectonic overpressure in weak crustal-scale shear zones and implications for the exhumation of high-pressure rocks. *Geophysical Research Letters*, *40*(10), 1984–1988. https://doi.org/10.1002/grl.50417

Smith, M. E., Carroll, A. R., Jicha, B. R., Cassel, E. J., & Scott, J. J. (2014). Paleogeographic record of Eocene Farallon slab rollback beneath western North America. *Geology*, *42*(12), 1039–1042. https://doi.org/10.1130/G36025.1

Snell, K. E., Koch, P. L., Druschke, P., Foreman, B. Z., & Eiler, J. M. (2014). High elevation of the 'Nevadaplano' during the Late Cretaceous. *Earth and Planetary Science Letters*, *386*, 52–63. https://doi.org/10.1016/j.epsl.2013.10.046

Spear, F. S., Kohn, M. J., & Cheney, J. T. (1999). *P-T* paths from anatectic pelites. *Contributions to Mineralogy and Petrology*, *134*(1), 17–32. https://doi.org/10.1007/s004100050466

Stewart, J. H. (1980). Geology of Nevada: A discussion to accompany the Geologic Map of Nevada. *Nevada Bureau of Mines and Geology Special Publication* (Vol. *4*, p. 136).

Stewart, J. H., & Poole, F. G. (1974). Lower Paleozoic and uppermost Precambrian Cordilleran miogeocline, Great Basin, Western United States. In W. R. Dickinson (Ed.), *Tectonics and Sedimentation* (Vol. 22, pp. 28–57). Society of Economic Paleontologists and Mineralogists Special Publication. https://doi.org/10.2110/pec.74.22.0028

Stipp, M., Stünitz, H., Heilbronner, R., & Schmid, S. M. (2002). The eastern Tonale fault zone: A "natural laboratory" for crystal plastic deformation of quartz over a temperature range from 250 to 700°C. *Journal of Structural Geology*, *24*(12), 1861–1884. https://doi.org/10.1016/S0191-8141(02)00035-4

Stockli, D. F. (1999). *Regional timing and spatial distribution of Miocene extension in the Northern Basin and Range Province* [Ph.D. dissertation] (p. 239). Stanford University.

Taylor, W. J., Bartley, J. M., Fryxell, J. E., Schmitt, J., & Vandervoort, D. S. (1993). Mesozoic central Nevada thrust belt. In M. M. Lahren, J. H. Trexler Jr., & C. Spinosa (Eds.), *Crustal evolution of the Great Basin and the Sierra Nevada: Geological Society of America Cordilleran/Rocky Mountain Sections Field Trip Guidebook* (pp. 57–96). University of Nevada Mackay School of Mines.

Taylor, W. J., Bartley, J. M., Martin, M. W., Geissman, J. W., Walker, J. D., Armstrong, P. A., & Fryxell, J. E. (2000). Relations between hinterland and foreland shortening: Sevier orogeny, central North American Cordillera. *Tectonics*, *19*(6), 1124–1143. https://doi.org/10.1029/1999TC001141

Thorman, C. H., Ketner, K. B., Brooks, W. E., Snee, L. W., Zimmerman, R. A., & Raines, G. L. (1991). Late Mesozoic-Cenozoic tectonics in northeastern Nevada. In *Geology and ore deposits of the Great Basin, Symposium Proceedings* (pp. 25–45). Geological Society of Nevada.

Thorman, C. H., Sandberg, C. A., Henry, C. D., Zuza, A. V., & Ressel, M. W. (2019). Regional tectonics and conodont CAIs indicate normal burial depths, not Mesozoic thickening, in the Pequop Mountains, NE Nevada. In *Geological Society of America Abstracts with Programs* (Vol. 51). https://doi.org/10.1130/abs/2019cd-329504

Vlaha, D. R., Zuza, A. V., Chen, L., & Harlaux, M. (2024). Hot Cordilleran hinterland promoted lower crust mobility and decoupling of Laramide deformation. *Nature Communications*, *15*(1), 3750. https://doi.org/10.1038/s41467-024-48182-8

Vrijmoed, J. C., Podladchikov, Y. Y., Andersen, T. B., & Hartz, E. H. (2009). An alternative model for ultra-high pressure in the Svartberget Fe-Ti garnet-peridotite, Western Gneiss Region, Norway. *European Journal of Mineralogy*, *21*(6), 1119–1133. https://doi.org/10.1127/0935-1221/2009/0021-1985

Wernicke, B. (1981). Low-angle normal faults in the Basin and Range Province: Nappe tectonics in an extending orogen. *Nature*, *291*(5817), 645–648. https://doi.org/10.1038/291645a0

Wheeler, J. (2014). Dramatic effects of stress on metamorphic reactions. *Geology*, *42*(8), 647–650. https://doi.org/10.1130/G35718.1

Wheeler, J. (2018). The effects of stress on reactions in the Earth: Sometimes rather mean, usually normal, always important. *Journal of Metamorphic Geology*, *36*(4), 439–461. https://doi.org/10.1111/jmg.12299

Whitebread, D. H. (1969). Geologic map of the Wheeler Peak and Garrison quadrangles, Nevada and Utah. *United States Geological Survey Miscellaneous Geologic Investigations Map I-578*. 1:48,000-scale, 1 sheet.

Whitney, D. L., Teyssier, C., Rey, P., & Buck, R. W. (2013). Continental and oceanic core complexes. *Geological Society of America Bulletin*, *125*(3–4), 273–298. https://doi.org/10.1130/B30754.1

Womer, J. B. (2017). *Late Mesozoic shortening structures in the western portion of the northern Snake Range metamorphic core complex, White Pine County, Nevada* [M.S. Thesis] (p. 47). University of California.

Wrobel, A. J., Gans, P. B., & Womer, J. B. (2021). Late Cretaceous crustal shortening in the Northern Snake Range metamorphic core complex: Constraints on the structural geometry and magnitude of pre-extensional footwall burial. *Tectonics*, *40*(8), e2020TC006460. https://doi.org/10.1029/2020TC006460

Yamato, P., & Brun, J. P. (2017). Metamorphic record of catastrophic pressure drops in subduction zones. *Nature Geoscience*, *10*(1), 46–50. https://doi.org/10.1038/ngeo2852

Yonkee, W. A., Dehler, C. D., Link, K., Balgord, E. A., Keeley, J. A., Hayes, D. S., et al. (2014). Tectono-stratigraphic framework of Neoproterozoic to Cambrian strata, west-central U.S.: Protracted rifting, glaciation, and evolution of the North American Cordilleran margin. *Earth-Science Reviews*, *136*, 59–95. https://doi.org/10.1016/j.earscirev.2014.05.004

Yonkee, W. A., Eleogram, B., Wells, M. L., Stockli, D. F., Kelley, S., & Barber, D. E. (2019). Fault slip and exhumation history of the Willard thrust sheet, Sevier fold-thrust belt, Utah: Relations to wedge propagation, hinterland uplift, and foreland basin sedimentation. *Tectonics*, *38*(8), 2850–2893. https://doi.org/10.1029/2018TC005444

Yonkee, W. A., & Weil, A. B. (2015). Tectonic evolution of the Sevier and Laramide belts within the North American Cordillera orogenic system. *Earth-Science Reviews*, *150*, 531–593. https://doi.org/10.1016/j.earscirev.2015.08.001

Young, J. C. (1960). *Structure and stratigraphy in the north-central Schell Creek Range, eastern Nevada* [Ph.D. dissertation] (p. 207). Princeton University. 3 plates.

Zuza, A. V., Levy, D. A., & Mulligan, S. (2022). Geologic field evidence for non-lithostatic overpressure recorded in the North American Cordillera hinterland, northeast Nevada. *Geoscience Frontiers*, *13*(2), 101099. https://doi.org/10.1016/j.gsf.2020.10.006

Zuza, A. V., Thorman, C., Henry, C., Levy, D., Dee, S., Long, S., et al. (2020). Pulsed mesozoic deformation in the Cordilleran hinterland and evolution of the Nevadaplano: Insights from the Pequop Mountains, NE Nevada. *Lithosphere*, *2020*, 1–24. https://doi.org/10.2113/2020/8850336